



Design and Fabrication of Biomedical Platform Technologies for Improved Diagnostic Performance

A thesis submitted to Dublin City University for the Degree of Master of
Science in the Faculty of Science and Health

By

Brian O'Reilly BEng

Supervisors:

Prof. Collete McDonagh, *School of Physical Sciences, DCU*

Dr. Paul Leonard, *Vaccinogen Inc.*

Biomedical Diagnostics Institute, Dublin City University

Dublin City University

May 2016

Declaration

I hereby certify that this material, which I now submit for assessment on the programme of study leading to the award of Master of Science is entirely my own work, and that I have exercised reasonable care to ensure that the work is original, and does not to the best of my knowledge breach any law of copyright, and has not been taken from the work of others save and to the extent that such work has been cited and acknowledged within the text of my work.

Signed:

(Candidate) ID Number:

Date:

Acknowledgements

I owe sincere thanks and appreciation to the following people for their contribution to this work:

My supervisors, Prof. Colette McDonagh and Dr. Paul Leonard, for their guidance, mentorship, perseverance and motivation throughout the process.

To all in the BDI for the great support throughout my time there. A special mention for Dr. Valerie Fitzgerald, Dr. Gemma Keegan, Martin Somers, Brian Manning and Barry O'Donnell who were great mentors and collaborators along the way.

To past and present directors of the BDI, who facilitated the projects and encouraged this work at all stages. To Celine Heffernan for helping at every turn and Dr Conor Burke for all your advice.

The Umbrella Office, Maurice, Barry, Stephen, Lorcan, Nigel and Mick for making my time in DCU so enjoyable and entertaining, thank you for your friendships.

To my parents, Christy and Patricia, for your never ending support, patience and love. To my siblings also who are always there, you have always been a great support in every way.

And to Helena, thank you for all your love, support and belief that has taken me to this point.

Publications

1. **Development of a High Sensitivity Rapid Sandwich ELISA Procedure and Its Comparison with the Conventional Approach**, Chandra Kumar Dixit, Sandeep Kumar Vashist, Feidhlim T. O'Neill, Brian O'Reilly, Brian D.MacCraith, and Richard O'Kennedy. *Analytical Chemistry* 2010 82 (16), 7049-7052
2. **Simple and Efficient Microfluidic Tool for Facile Assessment of Adsorption of Biomolecules on Substrates used in Biomedical Devices**
Vladimir Gubala, Jonathan Siegrist, Ruairi Monaghan, Brian O'Reilly, Ram Prasad Gandhiraman, Stephen Daniels, David E. Williams, Jens Ducr  e.
Analytica Chimica Acta, Volume 760, 14 January 2013, Pages 75–82
3. **Exploiting Highly Ordered Subnanoliter Volume Microcapillaries as Microtools for the Analysis of Antibody Producing Cells**
Valerie Fitzgerald, Brian Manning, Barry O'Donnell, Brian O'Reilly, Dermot O'Sullivan, Richard O'Kennedy, Paul Leonard. *Analytical Chemistry*, 5th December, 2014
4. **Cicada Wing Surface Topography: An Investigation into the Bactericidal Properties of Nanostructural Features**
Kelleher, S. M., Habimana, O., Lawler, J., O'Reilly, B., Daniels, S., Casey, E., & Cowley, A. *ACS Applied Materials & Interfaces*, 9th November 2015, DOI: 10.1021/acsami.5b08309 (2015)

Table of Contents

DECLARATION.....	II
ACKNOWLEDGEMENTS.....	III
PUBLICATIONS.....	IV
TABLE OF CONTENTS.....	V
LIST OF FIGURES	VIII
LIST OF TABLES	X
ABSTRACT	XI
CHAPTER I: INTRODUCTION AND BACKGROUND.....	1
1.1 INTRODUCTION.....	2
1.2 ANTIBODY GENERATION.....	3
1.2.1 Antibody Structure.....	3
1.2.2 Types of Antibodies	4
1.3 TARGETED ANTIBODY THERAPEUTICS.....	4
1.4 ANTIBODY ANALYSIS AND SELECTION TECHNOLOGIES.....	5
1.4.1 Current Selection Technologies	6
1.5 SINGLE CELL ANALYSIS.....	8
1.6 INFLAMMATION	9
1.6.1 C-Reactive Protein.....	10
1.7 POINT OF CARE.....	11
1.7.1 Assays.....	11
1.7.2 Point of Care Technology	12
1.7.3 Microfluidics and Point Of Care.....	12
CHAPTER II: METHODS.....	14
2.1 ANTIBODY SELECTION TOOL	15
2.1.1 Micro-capillary Array Preparation.....	15
2.1.1.1 Photolithography Mask Fabrication.....	15
2.1.1.2 Gold Sputtering.....	15
2.1.1.3 Laser ablation	15
2.1.1.4 Polymer Mask Fabrication	16
2.1.1.5 Photoresist Application.....	17
2.1.2 Alignment Patterning.....	18
2.1.2.1 PDMS preparation and Alignment Transfer Procedure.....	18

2.1.2.2	PDMS Scanning and Analysis	18
2.2	MICRO-AIR JET FABRICATION	19
2.2.1	Experimental Rigs	20
2.2.1.1	3D Printing	20
2.3	MICRO-LIQUID JET FABRICATION	21
2.3.1	Glass Capillaries	21
2.3.2	Aluminium Sleeve	22
2.4	BLOOD SEPARATION PLATFORM.....	23
2.4.1	Microfluidic Chip Fabrication.....	23
2.4.2	Soft Lithography.....	24
2.4.3	Trench Fabrication.....	25
2.4.4	Chip Preparation	26
2.4.4	Image and Video Capture	27
2.4.5	Blood Handling and Collection	27
2.5	IMMUNOASSAY	28
2.5.1	On-Plate Assays	28
2.5.2	Microfluidic Assay	29
2.5.2.1	Glass preparation	29
2.5.2.2	CRP/ α CRP Solution Preparation.....	30
CHAPTER III: ENABLING DEVELOPMENT OF AN ANTIBODY SCREENING AND RECOVERY PLATFORM FOR SINGLE CELL MANIPULATION WITHIN A MICRO-CAPILLARY ARRAY.....		31
3.1	INTRODUCTION	32
3.1.1	Hypothesis	32
3.1.2	Rationale.....	32
3.1.3	Challenges	34
3.2	ALIGNING PATTERN ON PDMS SURFACE TO MICRO-CAPILLARY ARRAY	35
3.2.1	Concept Design and Considerations.....	37
3.2.2	Experimental Approach.....	39
3.2.2.1	Photolithographic Masking.....	39
3.2.2.2	Polymer Masking.....	42
3.2.3	Results	44
3.2.4	Discussion	46
3.3	CAPILLARY RECOVERY CHALLENGE	48
3.3.1	Micro-Air Jet.....	49
3.3.1.1	Design and Fabrication.....	49

3.3.1.2	Proof of Concept Experimental Setup	51
3.3.1.3	Results.....	51
3.3.2	Experimental Setup for Improved Control/ Accuracy	52
3.3.2.1	Results:	55
3.3.3	Discussion	62
3.4	MICRO-LIQUID JET.....	63
3.4.1	Proof of Concept.....	66
3.4.2	HRP Recovery to Investigate Efficiency	68
3.4.3	Glass Capillary Cell Recoveries.....	72
3.5	DISCUSSION	74
CHAPTER IV: WHOLE BLOOD CELLULAR FRACTION EXTRACTION WITH ACTIVE TRAPPING (CLEAR)		76
4.1	INTRODUCTION	77
4.2	SIMBAS EXPLAINED	77
4.2.1	Trench Filter Operation	78
4.2.2	Limitations of SIMBAS.....	78
4.3	CLEAR RATIONALE AND IMPLEMENTATION	79
4.3.1	Proof of Concept: Active Trapping of Beads Suspended in a Liquid Sample.....	80
4.3.2	Trench Modifications and Redesign	81
4.4	CLEAR DUAL-LAYER FABRICATION	82
4.4.1	Preparing the Master	83
4.4.1.1	Pouring the Mould	83
4.5	OPTIMISATION OF FLOW RATE AND TRENCH DIMENSIONS	84
4.5.1	Trench Design	84
4.5.2	Degassed Pumped Section Considerations	85
4.6	QUANTIFICATION OF RBC SEPARATION	87
4.7	MICROFLUIDIC ASSAY APPLICATION.....	89
4.7.1	2-Step “Static” Sandwich Assay	89
4.7.2	Single Step “Static” Sandwich Assay	90
4.7.3	Assay by Degas-Driven Flow – 1 Step Sandwich Assay	91
4.7.4	Possible Causes of Decreased Signal or “Hook Effect”	92
4.7.5	Integrated 1 Step Microfluidic Assay.....	93
4.7.5.1	Re-suspension of Lyophilised Reagents	94
4.8	DISCUSSION	95
4.9	SUMMARY.....	95
CHAPTER V: CONCLUSION AND FUTURE WORK		96
BIBLIOGRAPHY		I

List of Figures

Figure 1.1 Phage display diagram	6
Figure 2.1 Air-jet schematic.....	19
Figure 2.2 Stratasys UPrint SE 3D printer.....	21
Figure 2.3 Liquid Jet schematic	22
Figure 2.4 HPLC assembly detail.....	23
Figure 2.5 Double sided mold diagram	24
Figure 2.6 Zing CO ₂ laser.....	25
Figure 2.7 Trench configuration and schematic.....	26
Figure 3.1 DiCAST explained	33
Figure 3.2 Graphical representation of the DiCAST process	35
Figure 3.3 Alignment process.....	37
Figure 3.4 Reference alignment marks	38
Figure 3.5 An example of an early design used to pattern arrays.....	38
Figure 3.6 Photolithography process steps	40
Figure 3.7 Results from photolithographic approach	41
Figure 3.8 Positive fluorescent masking and resulting fluorescent transfer upon PDMS surface.	42
Figure 3.9 Negative fluorescent masking with resulting fluorescent transfer upon PDMS surface	43
Figure 3.10 Final alignment design.....	44
Figure 3.11 Array under microscope	45
Figure 3.12 Reproducibility and stability data of alignment experiments	46
Figure 3.13 Laser ablation recovery method explained.....	48
Figure 3.14 Demonstration of air jet removing contents of an individual micro-capillary.....	49
Figure 3.15 Micro air-jet design.	50
Figure 3.16 Experimental rig 1	51
Figure 3.17 Rig 1 results.....	52
Figure 3.18 Experimental rig 2.....	53
Figure 3.19 Rig 2 results.....	54
Figure 3.20 Experimental rig 3	55
Figure 3.21 Air-jet bacteria cell recoveries 1.....	56
Figure 3.22 Air-jet bacteria cell recoveries 2.....	57

Figure 3.23 Air-jet bacteria cell recoveries 3.....	58
Figure 3.24 Air-jet bacteria cell recoveries 4.....	58
Figure 3.25 Air-jet HRP recovery 1.....	59
Figure 3.26 Air-jet HRP recovery 2	60
Figure 3.27 Air-jet HRP recovery 3.....	61
Figure 3.28 Air-jet HRP recovery 4.....	61
Figure 3.29 Liquid-jet concept.....	63
Figure 3.30 Liquid-jet proof of concept rig 1.....	66
Figure 3.31 Liquid-jet proof of concept rig 2.....	67
Figure 3.32 Liquid-jet rig 2 results.....	68
Figure 3.33 Liquid-jet HRP recoveries	69
Figure 3.34 3D models describing liquid-jet assembly	70
Figure 3.35 Images of liquid jet assembly.....	71
Figure 3.36 Liquid-jet cell recovery experiment 1	72
Figure 3.37 Liquid-jet cell recovery experiment 2	73
Figure 4.1 SIMBAS explained.....	78
Figure 4.2 Limitations of SIMBAS	79
Figure 4.3 Potentail pitfall of CLEAR with current SIMBAS configuration.....	80
Figure 4.4 Detailed schematic illustration of micro-fluidic chip implementing the CLEAR proof of concept.....	81
Figure 4.5 Modified trench schematic	82
Figure 4.6 Schematic representation of the moulding process.....	83
Figure 4. 7 Illustration of the redesigned trench.....	85
Figure 4.8 Three different channel dimensions used for the plasma extraction channel.....	86
Figure 4. 9 CLEAR in operation.....	86
Figure 4. 10 Image of chip post-separation	87
Figure 4. 11 Seaparation efficiency of CLEAR.....	88
Figure 4.12 Two-step sandwich assay.....	90
Figure 4.13 One-step sandwich assay, with hook effect.....	91
Figure 4.14 One-step sandwich FLISA, carried out under flow	92
Figure 4.15 Possible cause of hook effect explained.....	92
Figure 4.16 Initial test using a straight channel	94
Figure 4. 17 Schematic of the channel with increased channel length and mixing region	94

List of Tables

Table 1.1 Laser parameters used for ablating gold layer on glass.....	16
Table 1.2 Laser parameters used for ablating Scotch tape on glass.....	17
Table 3.1.Failure modes and effects analysis (FMEA) of potential liquid recovery configurations.....	65

Abstract

Design and Fabrication of Biomedical Platform Technologies for Improved Diagnostic Performance

Brian O'Reilly

Point-of-care diagnostics and therapeutics have the potential to radically change and improve the way disease and illness are detected and managed. This can be achieved by empowering the patient with rapid, real time information. Point of care testing also has the potential to alleviate some of the burden on crippled health care systems worldwide. Furthermore, personalised point-of-care testing can give more tailored and specific feedback to the end user. In this body of work, a novel single cell analysis system for antibody discovery and an integrated personalised point-of-care platform is presented.

In the first instance key challenges in the development of a novel single cell analysis antibody selection platform were addressed. This Direct Clone Analysis and Selection (DiCAST) Technology incorporates a highly ordered array of glass micro-capillaries of 20 μm diameter. The first key challenge was to identify a single target micro-capillary of interest, containing the single antibody secreting cell of interest, among $\approx 1,000,000$ other identical capillaries and cells. To achieve this, the ability to map assay patterns from the micro-capillary array to the master array containing the target cell was critical. Similar to where X marks the spot on a treasure map, micro-capillaries in a predefined pattern and orientation were blocked permanently using photolithography providing a reference stamp for alignment. These blocked capillaries provided a reference point upon the array, giving both spatial reference and orientation, allowing the cell recovery hardware to locate the micro-capillaries required to be evacuated.

Following the successful mapping of the array of micro capillaries the recovery of the contents of the micro-capillaries proved elusive. Here a system for the recovery of single cells from a micro-capillary was developed. Initially investigated was a method whereby a micro-jet of air, passed through a nozzle equal in diameter to the micro-capillary, for the removal of its contents. With limited success it was demonstrated that, while single micro-capillaries could be interrogated and the contents removed, the successful and controlled recovery of the contents was inconclusive. Subsequently, a liquid recovery system was investigated. By coupling both ends of the micro-capillary with a glass capillary of similar internal diameter, and by flowing a buffer solution through the capillary, recovery of the contents of a single micro-capillary was demonstrated.

In a second body of work, a method for cellular fraction extraction using an active trapping (CLEAR) approach was developed. CLEAR separates plasma from a whole blood sample in <10 min by removing the red and white blood cells to give improved signal to noise ratio during a subsequent fluorescence measurement of the on chip assay. Designed for point-of-care applications, CLEAR requires no external actuation relying on degas driven flow, together with cell gravitational sedimentation in a trench to separate the sample, removing the need for pumps, tubing, extra power sources etc. CLEAR removes the likelihood of cell re-suspension by actively sequestering those cells to a separate reservoir on chip. As a result, CLEAR could be used to analyse the cellular constituents post separation, to screen

for e.g. cell health or cell counting. The CLEAR concept was demonstrated using a fluorescence-based sandwich assay for the cardiac marker C-reactive protein (CRP).

The research presented in this thesis describes the initial development of two key biomedical platforms that if combined has the potential for improved point of care testing. Using the research described herein as a corner stone for future follow on development and validation, it is envisaged that best in class antibodies selected using the novel DiCAST antibody discovery platform could be applied in a fluorescence-based assay on a whole blood sample using the CLEAR microfluidic chip platform for improved cardiac diagnosis at the point of patient need.

Chapter I

Introduction and Background

1.1 Introduction

More recent developments in Point of Care Diagnostics (POC) means that remote monitoring and maintenance of disease states is enabled, thus, providing the patient with rapid, near-patient test results. Removing the skilled laboratory worker and using samples that require little or no preparation by the user or patient, point-of-care can provide relief for overcrowded healthcare systems in developed countries and lead to early detection of certain biomarkers linked to various non-communicable disease states. This may allow for early detection and treatment and therefore prevention of disease progression while removing costly laboratory based tests. With advances in wireless communications, results obtained remotely can quickly be delivered to a physician to be interpreted. Frequency of testing may also be improved providing better trend analysis, resulting in better understanding of disease progression or dosage effects in the case of therapeutics. Together with advances in manufacturing, where disposable test kits can be manufactured at low cost, point of care diagnostics has potential to revolutionise the way health care is delivered.

Split into two strands, this work contributed to two Enterprise Ireland/Science Foundation Ireland commercialisation projects carried out in DCU. Led by Dr Paul Leonard, the first section of this work relates to the development of a novel single cell antibody selection tool (Fitzgerald et al. 2015). By segregating individual antibody secreting cells and screening each cell for a specific antigen, this new technology aims to provide a high throughput, highly selective antibody selection tool. Part of this work describes some of the roadblocks encountered in developing this technology and the solutions realised using microfabrication techniques.

The second body of work describes the development of an integrated microfluidic platform for separation of blood into its cellular components and plasma while also performing fluorescence based assay that could be used for a wide range of diagnostic applications from detection of cardiac markers to infectious disease. Building on work previously developed at the Biomedical Diagnostic Institute (BDI) (Dimov et al. 2011), an improved platform is described where cellular components are removed from a whole blood sample and the resulting biomarker rich plasma is screened for particular indicators of inflammation or disease. As part of an Enterprise Ireland commercialisation fund, the platform described was designed to be incorporated into a smart phone based point-of-care device for monitoring biomarkers of inflammation.

1.2 Antibody Generation

There are an abundance of micro-organisms, or proteins known as pathogens, present in our environments and humans are exposed to them constantly. Pathogens fall into four general categories: viruses, bacteria, fungi and parasites. Once these pathogens are detected in our bodies, an individual with a well-functioning and strong immune system, will illicit an immune response to the particular pathogen (Murphy et al. 2008). Plasma cells of the immune system, upon detection of “foreign” proteins, generate the antibodies that bind these proteins and recruit other cells and molecules to destroy them. The proteins which bind to the antibody are known as antigens, which stimulate antibody generation, hence their name (Murphy et al. 2008). This process forms the adaptive immune response and is responsible for longer term immunity. It differs from the innate immune response which is non-specific and is the immediate response to any pathogens present (Conroy et al. 2009). Once presented with a pathogen, the naïve T cell becomes activated and transforms into an effector T cell. As a result, T cells proliferate and differentiate, and cytokines are released. The released cytokines activate naïve B cells, which then differentiate into plasma cells and memory B cells. Memory B cells produce the antigen specific antibody which is used in any subsequent immune response (Murphy et al. 2008).

1.2.1 Antibody Structure

Antibodies are a large protein molecule (150kDa) oriented roughly in a Y-shape. The Y-shape is made up of a stem, and two branches which are equal in size with all three sections connected by flexible disulphide bonds (Murphy, Kenneth; Janeway, Charles; Walport, Mark; Travers 2012). The structure can be further broken into heavy (50 kDa) and light (25 kDa) chains, with each heavy chain consisting of three constant regions and one variable region. The light chain is made up with one constant and one variable region.(Buss et al. 2012) The variable region is located at the top of the Y branches comprising of the top heavy and light chains which binds the specific antigens (Zeng et al. 2012; Conroy et al. 2009). Due to the Y-shaped structure, antibodies have the ability to bind two antigens at once, which increases the antibodies avidity (Murphy et al. 2008). The antibody can then be further subdivided into two fragments. The Fab region consists of the branches of the Y-shape structure. The Fab is the antigen binding portion of the antibody, or Fragment Antigen Binding (Fab). This portion can be cleaved from the antibody, with its smaller size (25 kDa) proving useful for penetration

into tissue. The Fc region or Fragment Crystalizable region is cleaved from the stem of the Y-structure. The Fc region is responsible for effector function of the antibody. Single chain variable fragments or ScFv are also a common useful form of antibody. The ScFv is comprised of the both branches of the antibody but just includes the variable heavy and variable light chains of the antigen binding site. The two branches are bound together with a peptide linker.

1.2.2 Types of Antibodies

Antibodies are available in three as monoclonal, polyclonal and recombinant. Monoclonal (MAbs) and polyclonal (PABs) antibodies are produced by eliciting an immune response in a host animal with a specific antigen. When fused with a myeloma cell, MAbs become homogenous and monospecific to that myeloma resulting in MAbs being extremely valuable research tools (Tansey & Catterall 1994). In contrast PABs are heterogenous in nature and may bind to multiple epitopes of the antigen. This can result in lower specificity but less susceptible to antigen conformational change and changes in pH (Lipman et al. 2005). Recombinant antibodies are engineered in-vitro following the development of DNA technology. By engineering the antibody it has been possible to reduce its size, “arm” the antibody with a toxic payload which it would deliver to the antigen cell of interest and even fuse radio isotopes to the antibody for tracking treatment (Carter 2001; Hudson & Souriau 2003).

1.3 Targeted Antibody Therapeutics

Over 100 years has passed since Paul Ehrlich suggested that one day there would be a “magic bullet” solution to specifically target disease causing pathogens (Weiner et al. 2010; Adams & Weiner 2005). It is only since the discovery of monoclonal antibodies in 1975, by Kohler and Milstein, that the real value of targeted therapies has been realized (KÖHLER & MILSTEIN 1975). Even with this breakthrough, development of products for human therapeutics was not fully realized until the late 1980’s. This was due to the murine origin of these MAbs, which were immunogenic in human subjects, inducing an immune response as a result (Weiner et al. 2010; Buss et al. 2012). In more recent years, MAbs are established as targeted therapies for many applications e.g. malignancies, autoimmune disease and transplant rejection (Lu et al. 2012; Hansel et al. 2010).

1.4 Antibody Analysis and Selection Technologies

Over the past 35 years, hybridoma technology has enhanced our ability to detect and quantify target molecules in cells using monoclonal antibodies (Bradbury, Sidhu et al. 2011). Since then, other methods have been developed to replicate the immune response (Love, Ronan et al. 2006, Jin, Ozawa et al. 2009, Reddy, Ge et al. 2010) which allow us to screen increasing numbers of antibody producing cells. In vitro display technologies have also been refined and show great promise in their ability to permit more control over the nature of the derived antibody in comparison to immunization. In fact, many of the antibodies derived using in vitro display methods have properties that would be difficult to obtain using animal immunization (Bradbury, Sidhu et al. 2011). Current selection technologies try to mimic or replicate a similar response to that of the immune system, where a library of antibodies is exposed to the antigen of interest. The antibodies then compete to bind with that antigen. The competitive nature of such techniques relies upon the affinity of the antigen/antibody interaction and can limit the specificity of selection (Mao, Graziano et al. 2010). As further developments in animal immunization techniques are expected to be minimal, in vitro methods have the unique potential to improve antibody screening. Importantly, a body of the literature suggests that a high proportion of commercially available antibodies demonstrate poor specificity and some even fail to recognize their targets at all (Spicer, Spivey et al. 1994, Saper 2005, Pozner-Moulis, Cregger et al. 2007, Grimsey, Goodfellow et al. 2008, Jensen, Swigart et al. 2009, Jositsch, Papadakis et al. 2009, Bordeaux, Welsh et al. 2010). Considering modern biology depends on the quality and fidelity of commercially available antibodies, this highlights the need for robust techniques to improve antibody quality (Bradbury, Sidhu et al. 2011). In vitro display technologies, best represented by phage and yeast display, have the capability of synthesizing tailor-made antibodies which can be used to acquire the desired affinity of binding and specificity for both in vitro and in vivo diagnosis and immunotherapy for human disease (Hoogenboom, de Bruine et al. 1998).

Current selection technologies try to mimic or replicate a similar response to that of the immune system, where a library of antibodies is exposed to the antigen of interest. The antibodies then compete to bind with that antigen. The competitive nature of such techniques relies upon the affinity of the antigen/antibody interaction and can limit the specificity of selection (Mao et al. 2010).

1.4.1 Current Selection Technologies

Phage display allows the identification of antibodies targeting a certain antigen from a large antibody repertoire or library. Phage display has been reported since 1985 and involves the binding of an antibody to a filamentous bacteriophage (George P. Smith 1985). Libraries with millions or potentially billions of antibodies may be screened by attaching to a phage molecule. The bound ligand or protein is presented on the surface of the phage, while its genetic material is stored within the phage. When presented to the target, suitable proteins on the surface of the phage bind to the target. Unbound or nonspecific protein and phage are washed away, while the bound phage is retained and analysed for specificity and affinity. This cycle is repeated until the most suitable antibody remains (Hoogenboom et al. 1998).

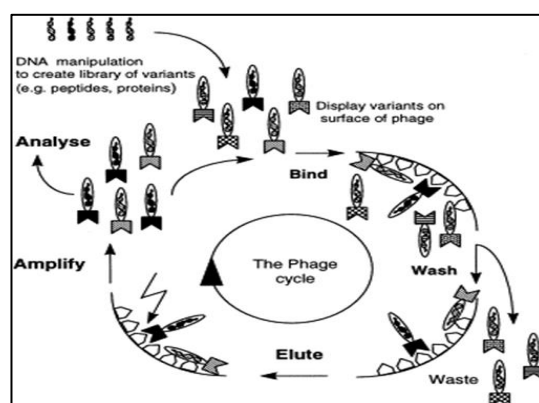


Figure 1.1 Phage display diagram (Hoogenboom et al. 1998)

Despite its continuing popularity antibody phage display is a very complex and time consuming technique. Due to the screening of $\sim 10^8$ antibodies from large libraries some lower affinity antibodies can be overlooked (Hammers & Stanley 2014)

Using a similar technique to phage display, yeast display is another popular method for screening large antibody libraries. First reported in 1997 by Boder and Wittrup, yeast display promised some improvements over the older phage technology (Boder & Wittrup 1997). The yeast host is a eukaryotic cell and as a result can mimic the way the antibody is displayed as it might be with a mammalian cell (Sheehan & Marasco 2015). Yeast display has been reported to increase affinity and specificity as a result of the eukaryotic host (Gai & Wittrup 2007). Fluorescence activated cell sorting (FACS), used in conjunction with yeast display, and offers a big advantage over phage display. FACS can rapidly sort cells tagged with a fluorescent label from a large library of cells. Upon identifying the fluorescent label, the cell stream is subjected to a high voltage which deflects the cell of interest to a different collection vessel.

Direct Clone Analysis and Selection technology (DiCAST) is a patented antibody discovery technology that is applicable to screening both bacterial and mammalian antibody secreting cells (ASCs). The development of DiCAST was driven by the need for optimal antibody detection technology reducing time and cost for their discovery as monoclonal antibodies are now the largest class of biological drug with up to 30 monoclonal antibody drugs approved by the FDA (Morrow Jr and Das 2013). An obvious obstacle in monoclonal drug development is how to find the monoclonal antibody with targeted and therapeutic properties from such diverse libraries of billions of potential candidates (Fitzgerald, Manning et al. 2014). Many microtools have demonstrated the discovery of antigen-specific ASCs. Such methods include micro engraving of miniature wells (Love, Ronan et al. 2006, Ogunniyi, Story et al. 2009), etched fibres (Biran and Walt 2002), homogenous cell spot assay (Jin, Ozawa et al. 2009) and microfluidic cell sorting (Wheeler, Thronset et al. 2003, Singhal, Haynes et al. 2010, Ryan, Ren et al. 2011, El Debs, Utharala et al. 2012). However, these methods pose certain limitations. They are generally not applicable to both bacterial and mammalian screening. They offer limited multiplexed capabilities and relating to spatially addressed techniques they are limited in cell number capacity (10^5 cells per experiment) (Fitzgerald, Manning et al. 2014). DiCAST, however, is a new and novel microtool built for the identification of antigen specific monoclonal antibodies from millions of individual bacterial and mammalian cells in picolitre to nanolitre bioincubation chambers.

DiCAST is a new microtool developed to identify antigen specific monoclonal antibodies from millions of individual bacterial and mammalian cells in picolitre to nanolitre bioincubation chambers using commercially available capillary plates of densely packed micro-capillary flow-through arrays. These flow-through plates are advantageous in that they utilize an advanced glass drawing technology in order to produce hollow arrays in a range of cross sections, pore sizes and lengths providing over 0.95 million assay chambers when using densely packed 40 μ M diameter hollow capillaries placed on a chip the size of a standard microscope slide. Another unique aspect of these capillaries is that they possess an open top and bottom which allows for the dual detection surfaces for antigen specific monoclonal antibodies can bind. This process allows us to analyze cells captured and cultured in micro capillaries which are sealed at one or both ends by an antigen coated plate, which in itself is a removable assay surface for each capillary. These surfaces can be washed and if any specific antibody is bound to the antigen surface, it can be detected using fluorescence. The

fluorescent spots which correspond to a positive signal can then be mapped to the micro-capillary array which contains the ASC which is required to be cloned. The image pixel coordinates allows for specific identification of the capillary that contains the single cell producing the antibody to the target of interest. Individual cells are recovered into 384 well microtiter plates using high precision alignment whereby the contents of the capillary of interest are recovered by flowing nitrogen through a hole to simply blow out the contents into a well of a 384 well plate located just beneath the capillary array, recovering one cell every 3 seconds using the DiCAST custom LabView software (Fitzgerald, Manning et al. 2014).

The existing technologies are unable to directly screen libraries of antibody secreting cells consisting of millions to billions of individual cells. Therefore, it may prove beneficial to utilize selection rounds based on enrichment by biopanning or cloning by limiting dilution, prior to direct cell analysis. With this in mind, DiCAST provides us with a direct cell screening and analysis platform of both bacterial and mammalian libraries with little need for enrichment on the antibody discovery phase. Therefore, it is suggested that a number of aspects of the DiCAST technology do have advantages over other more traditional methods with regard to monoclonal antibody discovery. For instances, the open ended and densely packed micro capillary array allows DiCAST to provide up to 10 – 1000 times more analysis chambers per chip compared in comparison to other well based assays (Love, Ronan et al. 2006, Ogunniyi, Story et al. 2009, Sendra, Lie et al. 2013). Another unique feature of this method is that it has two open ended assay surface allowing for a dual surface exposure and analysis. This open capillary system allows for precise and quick automated recovery of the capillary contents every three seconds using pneumatic based pressure. DiCAST is more dynamic in that it can identify antibody secreting cells from both mammalian and bacterial libraries which requires less time and less resources in comparison to current commonly used methods. Therefore, cell based screening using micro tools allows for real time characterization of individual antibody secreting cells. DiCAST is presented in this thesis as a novel and more advanced technology for single cell analysis.

1.5 Single Cell Analysis

Single cell analysis is a powerful tool that allows the differentiation of individual or select cells from heterogeneous populations. By analysing cells individually greatly reduces noise in the process, and allows for example the differentiation of cancer cells from a normal cell population by looking at mitochondrial mutations in DNA or in the

case of stem cell research, the differentiation of embryonic and adult stem cells (Wang & Bodovitz 2010).

Flow cytometry for example, is regarded as the mainstay for high throughput single cell analysis for many years. As a technology it is limited by instrumentation complexity and cost (Lecault et al. 2012) and by observing the cell in isolation, does not capture the innate cellular response. Recent advances in imaging technology are allowing real time observation of cell interactions in their natural environment, but these developments are limited in their throughput (Yin & Marshall 2012a). With imaging techniques, any subsequent manipulation of the cells identified may require the use of micro-tools such as a micromanipulator. Developed in the early 20th century micromanipulators have advanced hugely since but still require great skill and dexterity to operate while also being very low throughput (Barer & Saunders-Singer 1948). Optical tweezers are emerging as a useful tool for manipulating object in a precise and non-contact fashion. First reported in 1986 as purely a method of manipulating of small dielectric particles in water, optical tweezers have been developed to trap, manipulate, detect and measure biochemical materials (Moffitt et al. 2008; Burger et al. 2015). Again this technique is limited instrumentation complexity, cost and low throughput. It seems microfluidics possible applications are limitless, with single cell analysis emerging as a leading application. Described as “total analysis”, microfluidics promises to be able to deliver analysis from the cell live state to cell death on one platform. However, this requires the complex fabrication of micron scale geometries typically in a polymer substrate, delivery of, and possibly incorporation of reagents within the channels along with a detection method to obtain a result. All those considerations need to be addressed before the recovery of the single cell that has just been analysed is recovered (Yin & Marshall 2012b).

1.6 Inflammation

The inflammatory process plays an important role in the development and pathogenesis of many chronic diseases such as cardiovascular disease (CVD), type 2 diabetes, rheumatoid arthritis and metabolic syndrome. Early identification of metabolic biomarkers may be of great importance in order to halt the progression of such non-communicable diseases. Serum C-Reactive Protein (CRP) is a widely tested inflammatory marker. In fact, it has been widely debated whether CRP should be used as a predictor of first cardiovascular event. In 2010, the American College of Cardiology Foundation AHA Task Force on practice guidelines suggested that CRP assessment was

reasonable for individuals at intermediate risk of a cardiovascular risk (Greenland, Alpert et al. 2010) where intermediate risk qualified as having at least two cardiovascular risk factors. To support this, an analysis of 52 prospective cohort studies that included 246,669 individuals with no history of CVD, investigated the value of adding CRP assessment to the conventional risk factors for the prediction of a cardiovascular event. It was reported that adding CRP screening in people at intermediate risk could help prevent one additional event in every 400 out of 500 people to be screened over a 10 year period (Collaboration 2012). The literature supports the early measurement and monitoring of inflammatory states and in particular C-reactive protein.

1.6.1 C-Reactive Protein

CRP was first detected in 1930 by Tillett and Francis. They identified the substance in serum of patients with acute infections like pneumonia (Tillett and Francis 1930) which indicated that the body had a chemical response to inflammatory states. This led to the characterization of “acute phase proteins” (Abernethy and Avery 1941). An acute phase protein exists in the blood and is rapidly increased or decreased in response to injury or trauma such as a heart attack, infection, burns or inflammation. CRP is the classical acute phase reactant, the circulating concentration of which increases rapidly in response to tissue injury and inflammation (Thompson, Pepys et al. 1999). CRP increases in order to enhance the inflammatory function of leucocytes that are responsible for removing the invading bacteria or virus. It does so by attaching to the invading agent inducing white blood cells or other leucocytes to attack the agent. Under normal conditions, CRP concentrations in blood are 10 mg/L. However, upon injury, it has been reported that the concentration can increase up to 1000 fold (Clyne and Olshaker 1999) reaching a peak concentration of 350 – 400 mg/L within 48 hours of injury (Clyne and Olshaker 1999). CRP elevation is stimulated by cytokines, particularly IL-6, IL-1 and tumor necrosis factor (Kolb-Bachofen 1991, Jupe 1996) and is synthesized by hepatocytes. It is a pentameric protein made up of five noncovalently bonded identical subunits with a molecular weight of 118 KDa. It has been suggested that CRP has the capacity to activate complement through the classic complement pathway and to modulate the actions of phagocytic cells lending to its role in opsonisation of infectious agents and damaged cells (Kolb-Bachofen 1991). For this reason, measurement of CRP has been found useful for monitoring exacerbations in chronic inflammatory conditions such as rheumatoid arthritis (Young, Gleeson et al. 1991). The early quantification of CRP using point of care diagnostics could be a useful

tool in order for medical staff to risk assess patients and indeed for patients to monitor this biomarker themselves independently using microfluidic electrophoretic immuneassays integrated with sample preconcentration and mixing of analytes with fluorescently labelled antibodies (Meagher, Hatch et al. 2008).

1.7 Point Of Care

1.7.1 Assays

Point-of-care (POC) testing has been defined by the College of American Pathologists as analytical testing performed outside the laboratory using devices that are easily transported to the vicinity of the patient (Pathologists 2001). By obtaining human biological samples such as saliva, blood urine or other bodily fluids, POC testing can quantify analytical targets such as proteins. The ease of obtaining a sample with little or no pre-preparation allows the care giver in a hospital setting or a person at home to easily and efficiently apply the sample and obtain an “answer” within seconds to hours (Meagher, Hatch et al. 2008). The more conventional bench top techniques such as enzymatic activity assay or ELISA are limited by expense, labour demands, time and the need for highly trained personnel (Meagher, Hatch et al. 2008). However, with the development of point of care testing, these hand held devices require uncomplicated instructions for use. Additionally, interpretation of test results may be as simple as viewing a colour change on a strip or a polymer. Another positive aspect of POC is the relative low cost in comparison to more conventional methods. The reading instruments are smaller and infact more specialized than laboratory devices. Additionally, the biological sample never makes contact with the instrument; hence there is no need for a self-cleaning system. The sample is placed on a chip or cartridge that is not designed for reuse. With POC testing, sample mislabelling or mishandling is less likely as results are provided instantly, again lowering the medical cost of sample processing. The time taken to administer the test and obtain the result is instant. However, the literature clearly suggests that speed of obtaining results must never be traded for accuracy or reliability (Gubala, Harris et al. 2011). While POC testing is often administered by a medical professional, it can also be self-administered, giving patients independence and forcing them to become more responsible about the management of their disease state and indeed more compliant to the their treatment plan. However, this does raise a concern regarding the lack of professional medical input and monitoring. It is therefore imperative that patients receive reliable devices and adequate training to learn how to use the device.

1.7.2 Point of Care Technology

Optical detection is the leading method by which blood is analysed, dictating the removal of the large cellular components when trying to identify protein biomarkers. With the larger cellular components removed, the remaining clear plasma provides a better medium for detection with less noise, light scattering and non-specific binding(Dimov et al. 2011). The larger red blood cells, due to their shape, size and density have certain behaviours that can be harnessed to aid their removal. Due to their flat disc shape, RBC's have been reported to tumble randomly within the flow(Shi et al. 2012; Kersaudy-Kerhoas et al. 2009), migrate away from the vessel walls towards the centre of the vessel and over time sediment under their density and weight(Sun et al. 2012; Bernate et al. 2013). Individually or collectively these characteristics can be exploited by microfluidic platforms to effectively separate the cellular components from a whole blood sample.

The devices used should be inexpensive disposable chips which have a microfluidic feature to control sample preparation, flow rate, mixing with reagents, reaction time associated with binding of antibodies and filtration of the samples which obtaining an effective measurement (Gubala, Harris et al. 2011).

1.7.3 Microfluidics and Point Of Care

From its origins in gas-phase (GC) and high-pressure liquid (HPLC) chromatography, microfluidics has many different application areas as alluded to earlier in this thesis. Driven also by advances in the semiconductor industry, photolithography and silicon were seen as an ideal platform to achieve the scale of features require to realise the microfluidic concept (Whitesides 2006). One of the main motivations for microfluidics is that of point-of- care. While accessible in the developed world, rapid and accurate diagnostics are not readily available in the developing world and it is thought that microfluidics will assist in the deployment of cheap alternatives to these impoverished areas. The WHO recommendation is the diagnostics for the developing world should be ASSURED: affordable, sensitive, specific, user-friendly, rapid and robust, equipment free and deliverable to end-users (Martinez et al. 2010). Microfluidics is also seen as a way to alleviate the already overburdened health care systems in the developed world by shifting ownership of testing and monitoring to either the general practitioner or the patient in the home (Yager et al. 2008).

Many pumping techniques exist for delivering the sample through the microfluidic channel network. Capillary force is the dominant force at the micro scale and can be harnessed to propel a liquid through a microchannel (Sackmann et al. 2014). Capillary forces are used in most lateral flow assays such as home pregnancy kits and can use porous materials like paper or high density micro-pillars to transport the sample through a device (Jönsson et al. 2008; Godino et al. 2012). Capillary force flow is seen as an ideal method for pumping owing to its simplicity, low cost, and no requirement for external power (Gubala et al. 2012). Pressure driven flow by means of peristaltic or syringe pumps is common in point of care research settings. Ideal for the benchtop in terms of programmability and control, the technique is limited by its complexity, size and external power requirement (Haeberle & Mark 2012). Centrifugal microfluidics have been reported for some time and are based on the original centrifuge technology (Haeberle & Mark 2012). By fabricating channels radially from the centre of a disc, the resulting force upon the contents of the channels force the contents towards the outer edge of the disc. The technology lends itself well to cell separation, capturing and assaying but is ultimately limited by the need for a device on which to spin the disc (Burger et al. 2012). Electrokinetic driven flow has been investigated as a mode of transport for in microfluidics since the early 1990's, and involves inducing a large voltage to an electrolytic solution to propel the sample along the channel (Harrison et al. 1992). Electroosmosis and electrophoresis use a DC voltage source and can require a large voltage, up to hundreds of volts, which can adversely affect delicate samples such as DNA (Sin et al. 2011). AC voltages typically require <10 V and can be used as an alternative. AC driven flow can also perform operations such as making it more attractive as point of care option (Gubala et al. 2012).

Chapter II

Methods

2.1 Antibody Selection Tool

2.1.1 Micro-capillary Array Preparation

In this section, processes and materials used to implement the novel antibody selection tool is described. The capillary arrays described in all the following work were sourced from INCOM (www.incomusa.com). All arrays used consisted of 40 μm diameter x 1 mm length capillaries, bundled together in a 23x23 mm form. This equated to $\sim 260,000$ capillaries within that footprint.

2.1.1.1 Photolithography Mask Fabrication

All masks used were fabricated in-house. This process involved the sputtering of a layer of gold onto a standard glass slide. The gold layer was then ablated using an excimer laser to generate the desired pattern.

2.1.1.2 Gold Sputtering

Using a Quorum K650X sputter coater (www.quorumtech.com), a 100 nm layer was deposited onto the surface of a standard glass slide. The layer thickness was controlled by the voltage applied to the target and the time allowed. The chamber was purged of ambient air and reduced to 1×10^{-3} mbar in order for the plasma to form on the gold electrode. The plasma allowed the transfer of gold from the target to the glass surface.

2.1.1.3 Laser ablation

The gold sputtered glass slides were then patterned by ablating a design realised using AutoCAD 2014, in the gold layer. Ablating a portion of the gold layer allowed the transmission of light.

The sputtered glass slide was placed on the XY translation stage of the excimer laser. The AutoCAD 2014 trace file was transferred to the PC connected to the laser. By following the path of the trace file, the laser ablated the desired pattern. The focal point of the laser was set by adjusting the laser head in the z-plane. To set the focal point the top surface of the gold layer was viewed and once it was in sharp focus the laser was focused. The work piece was viewed through the laser optics using a through the lens (TTL) system. This also allowed the laser to be aligned to specific points on the work piece. A 300 μm diameter aperture was used, which controls the

diameter of the beam applied to the surface of the work piece. By applying a 10 % demagnification, the resulting feature ablated on the work piece is 30 μm .

Laser ablation was carried out using the Optec MicroMaster Excimer laser (www.optec.be). The excimer laser uses a 248 nm Krypton-Fluoride (KrF) laser source.

The following settings were used for ablating the deposited gold layer:

Table 1.1 *Laser parameters used for ablating gold layer on glass*

Frequency	300 Hz
No. of Shots	250
% Transmission	70 %
Power	10 mJ
Speed (function of freq. vs no. of shots)	120 $\mu\text{m}/\text{sec}$
Energy Density	875 mJ/cm^2

2.1.1.4 Polymer Mask Fabrication

The array was covered with Scotch® Easy Tear Clear Tape. The covered array was then placed on the translation stage of the excimer laser. An AutoCad 2014 trace file was transferred to the PC connected to the laser. By following the path of the trace file, the laser ablated the desired pattern. Before starting to ablate a single pore was aligned with the laser by means of the through the lens (TTL) vision system. This allowed the user to view the focal point of the laser for both alignments on focal length relative to the workpiece. The focal point was adjusted by moving the laser head in the z plane until the top surface of the work piece i.e. the scotch tape upon the array was in sharp focus.

Ablating the Scotch tape however required different laser parameters, as detailed in Table 1.2 below. More power was required to ablate $\sim 50\mu\text{m}$ thick polymer scotch tape compared to the 100 nm gold layer. In this case the aperture used was 750 μm in diameter, resulting in 75 μm features ablated on the surface.

Table 1.2 *Laser parameters used for ablating Scotch tape on glass*

Frequency	300 Hz
No. of Shots	400
% Transmission	80 %
Power	20 mJ (max)
Speed (function of freq. vs no. of shots)	56 $\mu\text{m}/\text{sec}$
Energy Density	2715 mJ/cm^2

The extra energy, shots and % transmission produce an overall greater energy density to ablate the thicker layer.

2.1.1.5 Photoresist Application

The photo resist used for this application was SU8 3010 by MicroChem Corp., USA. SU8 3010 is specified for features of 10–20 μm . It's low viscosity allowed penetration into the 40 μm capillaries. SU8 3010 is a negative photoresist, where UV exposure cures the epoxy bonding it to the glass surface with which it is contact.

Before applying the photoresist to the array, the array was sealed to a slab of PDMS. The PDMS was degassed prior to the array being applied. The PDMS was utilised to draw the photoresist into the micro-capillaries and also while sealing the bottom side of the array; prevent photoresist from leaking onto the underside of the array.

Once sealed to the PDMS, photoresist was applied to the array in each of the four corners. For the photo mask approach, the photoresist was applied to the positions that corresponded to the mask. With the polymer mask the location was defined by where the scotch tape was ablated.

Photomask:

Here the photomask was applied directly to the uncured SU8 upon the array. As a consequence of the contact with the uncured SU8, the masks were not reusable. The photo mask made contact with the array to reduce the divergence of the UV light as it passed through the mask.

Polymer Mask:

The scotch tape mask covered the entire array except the portion above the capillaries that were required to be modified. Holes were ablated in the tape as described above to allow the photoresist penetrate the capillaries required.

2.1.2 Alignment Patterning

The following procedure describes the steps involved in transferring the patterns applied to the array in Section 2.1.1 to a PDMS surface for analysis. For this, firstly the PDMS surface is coated with the hIgG antigen. Following incubation and blocking steps, fluorescently labelled α -hIgG is added to the array around the alignment marks. If the marks were successfully applied the α -hIgG will not penetrate the capillaries intended to be blocked and transfer that pattern to the PDMS surface.

2.1.2.1 PDMS preparation and Alignment Transfer Procedure

A 5 mm slab of PDMS was prepared using a 10:1 mixture ratio of polymer to curing agent by placing a thin PDMS layer (what company) onto a thick PDMS slab. This thicker slab provides more suction to draw liquid through the array. The surface of the thin PDMS was covered with 5 μ g/ml hIgG in 2 ml 1xPBS and incubated at room temperature for 1 hour. Using a Gilson pipette, the hIgG was carefully removed. The surface was incubated in a blocking solution using 3% BSA in 1x PBS and incubated for 1 hour at room temperature. The surface was then gently washed using 1X PBS and allowed to air dry. Any air bubbles present were removed following 30-60 minutes of vacuum degassing. 7.5 μ l of α -hIgG (1:6000 dilution in 3% BSA) was applied to each alignment mark and entered the capillaries. In one fluid motion, the array was then sealed to the PDMS. A change in colour of the array/PDMS contact surface was noted and ensured the array was sealed. After 1 hour incubation at room temperature, the array was removed from the PDMS. The PDMS was washed with 1X PBS and allowed to air dry.

2.1.2.2 PDMS Scanning and Analysis

Once the PDMS has been allowed to dry it was scanned to image the transferred pattern. The thin PDMS layer was removed from the thicker PDMS slab. The thin layer was then applied to a glass coverslip. Another glass coverslip was applied on top of the patterned surface, sandwiching the PDMS between them. The coverslips

provide a rigid support for the PDMS and its introduction into the Perkin Elmer ScanArray GX.

The Perkin Elmer scans the surface of the PDMS by traversing the 25 mm width of the PDMS in 5 μm increments. This increment produces a 5 μm resolution image of PDMS surface.

2.2 Micro-Air Jet Fabrication

The micro-air jet concept was realised by casting PDMS around a tungsten wire. The tungsten wire (Goodfellow Cambridge Ltd., part # W005130) was 25 μm in diameters and formed the inner diameter of the micro-air jet.

An outer housing was fabricated using a lathe. The housing was formed using 20 mm aluminium bar. Using the design described in Figure 2.1, the aluminium bar was machined to the dimensions described. Once the lathe machining was complete the 5.5 mm diameter opening at one end of the housing was threaded to R 1/4 UNF thread. This thread was used to couple a 6 mm pneumatic push fitting with a R 1/4 male thread.

Either end of the machined aluminium housing was sealed with custom made caps with centred guide holes for suspending the 25 μm tungsten wire. With the caps in place and the wire suspended through the centre of the aluminium housing, PDMS was poured into the housing and baked at 65° C for 6 hours.

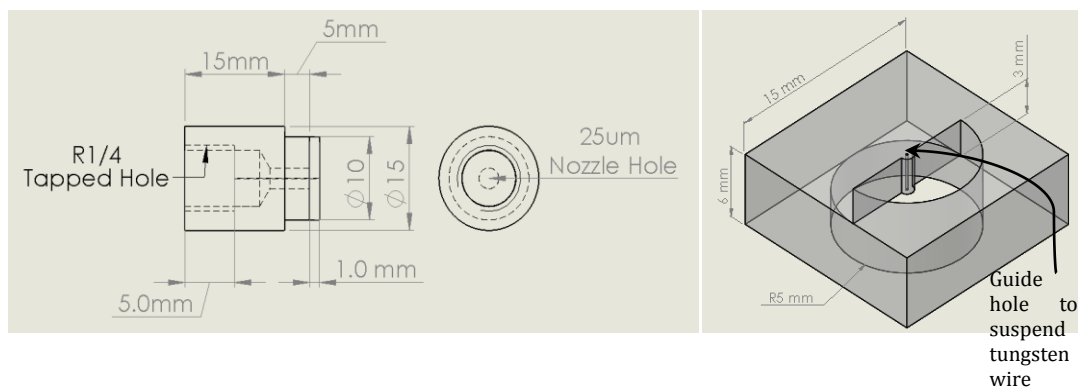


Figure 2.1 Air Jet mechanical drawing. Cap used to align tungsten wire within centre of aluminium sleeve also show. All dimensions in mm except thread described.

Once cured the caps were removed. The tungsten wire was then withdrawn from the cured PDMS which maintained the 25 μm inner diameter.

The 6mm pneumatic push fitting was then applied to the R 1/4" threaded hole. 6 mm tubing could then be coupled from the regulator in the lab to the micro-air jet.

2.2.1 Experimental Rigs

The experimental rigs were setup using standard optical tables allowing flexibility to modify and change the layout of the experimental components as required. Optical posts were used to mount parts upon. The 25 mm pitch allowed the components to be arranged in a modular fashion and modified easily.

2.2.1.1 3D Printing

As a rapid prototyping method, 3D printing was used to fabricate components which would otherwise be difficult and expensive to fabricate. Using this method allowed the in-house design and fabrication of these parts where otherwise would be outsourced to a third party.

All parts were fabricated using a Stratasys UPrint SE (Stratasys Ltd., MN, USA) fused deposition modelling instrument. The parts were initially modelled using SolidWorks 2014 3D modelling software. The 3D models were converted from a ".prt" file to a ".stl" file. This conversion divided the model into multiple thin horizontal slices which were then printed one by one on top of each other. Each layer had a resolution of 254 μm which ultimately restricted the minimum feature size that could be printed. The ABS material was heated to 300 °C allowing it to be extruded and bond to the previous layer. The printing chamber was maintained at 70 °C to prevent the previous layers from fully setting before the subsequent layers were allowed to bond.

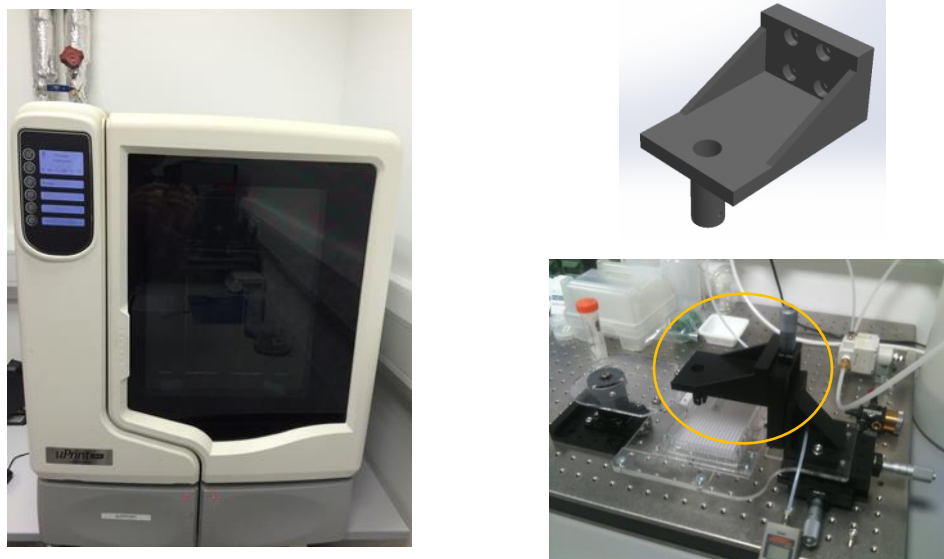


Figure 2.2 Stratasys UPrint SE with a 3D model of a part with the resulting printed part as part of the experimental assembly.

Once printed the part was immersed in a caustic detergent solution to dissolve any support material used in the process. The caustic detergent solution was also supplied by Stratasys Ltd. Once all support material was removed the part was rinsed with deionised water and was ready for use.

2.3 Micro-Liquid Jet Fabrication

The micro-liquid jet was designed by coupling a thick walled glass capillary to an aluminium sleeve. The capillary was coupled via the aluminium sleeve to HPLC tubing and a gas tight syringe.

2.3.1 Glass Capillaries

Thick walled glass capillaries were sourced from Vitrocom Inc., NJ, USA via CM Scientific Ltd., UK. 3mm outer diameter capillary with inner diameters of 25, 75, 125, and 200 μm was cut into 20 mm sections using a diamond blade cutter. The machine held the capillary in a y clamp which aided cutting the capillary as square as possible.

After cutting the cut face was polished either end of the 20mm section. The first polish used a 250 μm grade polishing pad followed by a 25 μm polishing sheet. A small block of 10 mm thick acrylic was drilled with a 3mm hole with a friction tolerance to that of the outer diameter of the capillary. The capillary was held in the acrylic block and passed over the polishing pad to achieve a flat surface finish.

2.3.2 Aluminium Sleeve

The aluminium sleeve was designed as a means to hold the fragile glass capillary and to couple the capillary to the gas tight syringe via HPLC tubing.

The sleeve was machined manually using a lathe. The through hole for the capillary was machined to a friction fit tolerance. A thin layer of epoxy glue (Araldite) was applied to the outer surface of the capillary before it was inserted into the sleeve. With the tight tolerance a strong bond was formed with the capillary and the aluminium sleeve. The sleeve could then be clamped in position reducing the risk of breaking the glass capillary. A collar was machined on the sleeve as a means to position it in the experimental rig and restrict its movement.

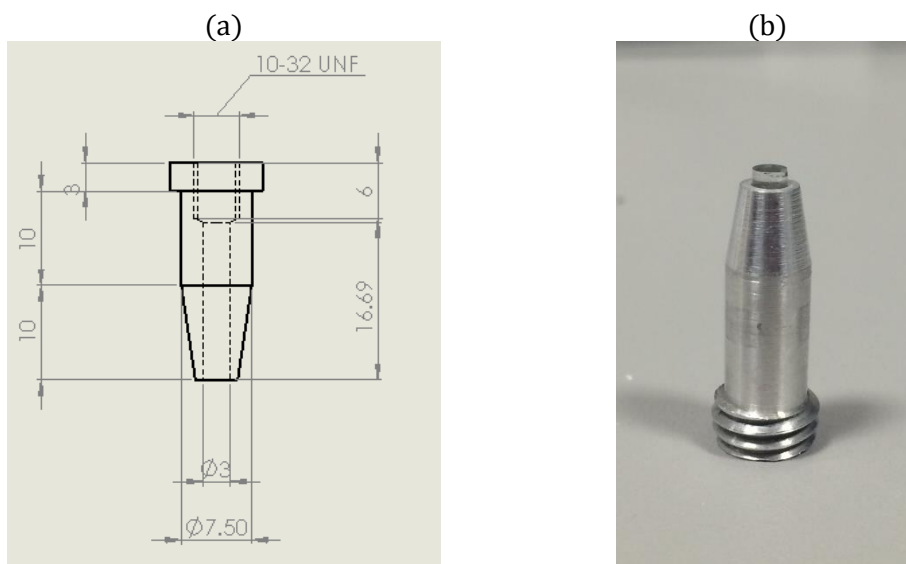


Figure 2.3 Aluminium Sleeve for liquid jet. (a) Mechanical drawing of the sleeve with physical part shown in image (b)

The sleeve was threaded at one end. This allowed the HPLC fitting to connect to the capillary. The HPLC tubing, which is clamped using a ferrule, forms a high pressure seal to the glass capillary.

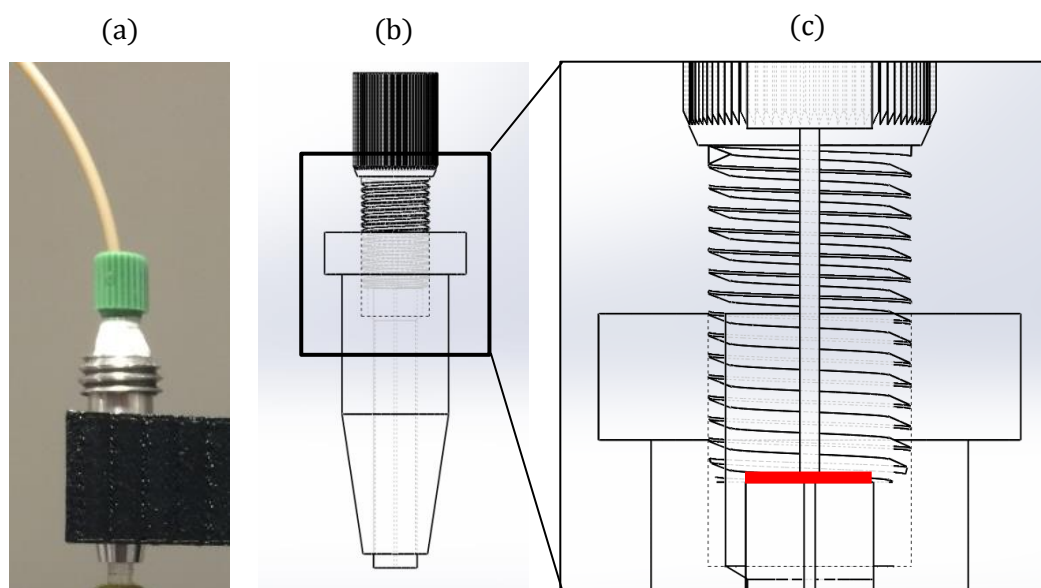


Figure 2.4 HPLC assembly detail. (a) shows the aluminium sleeve with green HPLC fitting in place. (b) CAD schematic of the assembly with (c) showing the contact point between the glass capillary and the HPLC tubing. The red line in (c) highlights the two surfaces in contact where the seal is formed with the inner diameters of both the capillary and tube aligned. (Tube and capillary inner diameters not drawn to scale)

The HPLC PEEK tubing with 1/16" outer diameter and 0.010" inner diameter from IDEX Corp., US is coupled to the capillary using HPLC flanged fittings. The flange clamps and seal the tubing forming a high pressure seal between the nut shown in Figure 2.4 (above in green) and the surface which the nut is tightening against. In this case the glass capillary is acting as the surface to which the HPLC flange is tightening. The flange and the nut maintain the tube in a concentric position within the threaded hole also, keeping it aligned with the inner diameter of the glass capillary.

2.4 Blood Separation Platform

Blood separation was carried out with in-house designed and fabricated microfluidic platforms.

2.4.1 Microfluidic Chip Fabrication

The microfluidic chips were fabricated by using a double sided adhesive tape supplied by Ahesives Research Inc. The product, ARcare 92712 with dimensions 48 μm ($\pm 2 \mu\text{m}$) in height was cut using a Graphtec RoboMaster PRO. The Graphtec instrument is knife cutter from Graphtec GB. Designs drawn with AutoCAD 2014 were traced with the knife to produce the required channel features.

2.4.2 Soft Lithography

To create the master around which the Sylgard 183 PDMS was moulded to form the microfluidic structures, a layer of ARcare 92712 was applied to a polystyrene petri dish. ARcare 92712 is a double sided adhesive tape and is structured with two protective liners on either side of the double sided tape.

The top release liner and the double sided tape were cut only at this point. The bottom release liner was not cut, thus acted as a support for the features of < 1 mm which were cut. The tape was cut using a Graphtec RoboMaster PRO knife cutter from Graphtec GB, using designs drawn with AutoCAD.

To start the petri dish was wiped down using paper towel soaked in ethanol. The double sided tape was applied to the bottom of the petri dish. The trench, described in Section 2.4.3 was applied to the trench portion of the double sided tape. Pressure was applied to the trench to ensure adhesion to the tape.

The top plate to carry the upper channels of the microfluidic chip was also wiped clean with ethanol soaked paper towel. This top plate was cut from a 3 mm sheet of acrylic with a diameter of 130 mm, allowing it to fit with the petri dish. When prepared the double sided tape to make the top channel structure was applied to the top plate. The top plate was then inverted and again the trench, already in place on the petri dish, was aligned with the double sided tape on the top plate. Pressure was applied to the trench tape junction to ensure good adhesion. PDMS was then prepared and added to the dish, filling the void between the top plate and the bottom of the dish.

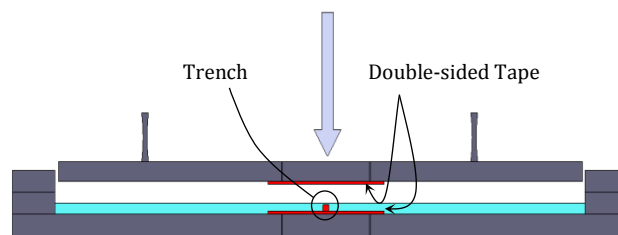


Figure 2.5 Double sided mold. The trench forms the height of the part and the via from the top features to the bottom features

40ml of PDMS was required for each petri dish. Sylgard 184 PDMS by Dow Corning was mixed with a 10:1 polymer to curing agent ratio. Once mixed the PDMS was poured into two 50 ml centrifuge tubes. The tubes were then spun at 3000rpm for 3 minutes to remove any air bubbles from the mixture.

The PDMS was then poured into the petri dish, taking care to fill gradually from one side of the dish to the next and not allowing air pockets to form under the top plate. If any air pockets were observed the dish was placed under vacuum in a desiccator and allowed sufficient time to remove the unwanted air.

With all air removed from the PDMS, and ensuring that there was sufficient PDMS in the dish to make contact with the entire top plate, the dish was placed in an oven and baked overnight at 65°C. Care was taken to ensure that the dish was placed level on the shelf of the oven to ensure uniform thickness post baking.

Following baking the parts were removed from the oven and cut to 75 x 35 mm, with the microfluidic channels centred roughly along the 75 mm length.

2.4.3 Trench Fabrication

The trench was fabricated by laser cutting acrylic sheet to the desired dimensions. Designs were once again drawn using AutoCAD 2014 and transferred to the EPILOG Zing CO₂ Laser.



Figure 2.6 CO₂ laser. Zing laser used to cut acrylic parts for trench.

The trench dimensions were adjusted according to the schematic in Figure 2.7 below. The 2 mm width was controlled by the thickness of the acrylic sheet with the remaining dimensions controlled by the AutoCAD design.

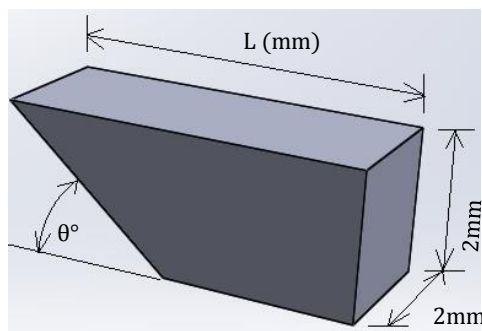


Figure 2.7 Trench configuration . Length and angle θ were adjusted.

The EPILOG laser system was controlled by setting the power applied to the laser, adjusting the focal height of the laser head and the write speed of the laser head. The output power of the 40 W CO₂ laser was expressed as a percentage and could be adjusted in 1 % increments. The speed was measured in mm/sec and could be adjusted by 0.1 mm/sec increments. The focal height from the laser head to the material was constant, but with different thickness of material, the machine bed required adjustment up and down to maintain that focal distance.

Once cut and reclaimed from the machine bed, the trench parts were cleaned with 95% ethanol, rinsed with deionised water and dried under a nitrogen stream.

2.4.4 Chip Preparation

After removal from the oven as described in Section 2.4.2, a strip of 250 μ m Zeonor polymer sheet was prepared to seal either side of the PDMS. The Zeonor sheet was supplied by Zeon Chemicals Europe Ltd., UK.

To prepare the strip, it was first cut to the same dimensions as the PDMS, 75 x 25 mm. The strips were then prepared by firstly washing in 2% Micro90 mixed with deionised water. The Zeonor was sonicated in 2% Micro90 for 15 minutes. The strips were removed and rinsed with deionised water to remove any residual Micro90 detergent. The strips were then placed in 95% ethanol, also diluted with deionised water, and sonicated for 15 minutes. Next, the strips of Zeonor were removed and rinsed with deionised water and placed in a bath of fresh deionised water and sonicated for a further 15 minutes. Once this step was completed, the strips were rinsed one final time and dried with a N₂ stream.

When fully dried the strips were then applied to the PDMS microfluidic chip. Care was taken to fully seal the channel structures with the Zeonor. The strip applied to

the top layer of the PDMS was placed so that the end of the inlet channel was accessible for the application of the sample during experimentation.

The microfluidic chips were then stored under vacuum in a desiccator until ready for use.

2.4.4 Image and Video Capture

All video footage of experiments was captured using a USB MicroViewer microscope camera. The picture was recorded in 640x480 pixels. The AVI footage was viewed and analysed using VLC media player.

Still images were all recorded with an iPhone 5S digital camera and recorded at 8-megapixels.

2.4.5 Blood Handling and Collection

Blood was collected for separation experiments at the DCU Student Health Centre by a trained nurse and phlebotomist. 10 ml Lithium Heparin coated glass tubes were used for collection. Lithium heparin tubes were chosen to limit the coagulation of the blood before experiments.

Samples were drawn and utilised in experiments, where possible, in less than 2 hours to reduce the effect of coagulation and natural sedimenting of the cellular portion of the sample.

Blood was only handled upon attendance at the mandatory blood handling and lab safety seminar provided by the BDI.

All blood was handled at designated biohazard areas within the lab with designated benches for use with bio-hazard material. Designated bio-hazard pipettes with filtered tips were also used when handling blood. A lab coat, gloves and safety glasses were worn at all times in line with PPE procedures when handling blood or other bio-hazard substances.

Any surplus blood sample and discarded pipette tips, consumables and microfluidic chips etc were initially soaked in 1% Virkon for > 12 hours before disposing. After soaking the Virkon solution was drained off and the waster disposed in a designated bio-hazard bin.

2.5 Immunoassay

The following sections describe the application of an immunoassay upon the microfluidic platform and its verification using the gold standard lab techniques which were carried out upon standard 96-well plates.

2.5.1 On-Plate Assays

The on plate assay was carried out in two ways. Initially it was performed as a standard ELISA protocol. The assay was carried out as follows:

- 100 μ L @ 5 μ g/mL of mouse anti-human CRP-C2 capture antibody was added to a Nunc Maxisorp 96 well micro-titre plate (3 rows of 10)
- The capture anti-body was incubated at 4°C overnight.
- The plate was washed with PBST/PBS three times.
- 200 μ L 3% BSA was added to the plate to block the portion of the surface that did not bind the capture antibody.
- Incubated at 37°C for 1 hour.
- After incubation the plate was washed with PBST, followed by a rinse with PBS three times.
- Starting with 40 mg/L CRP in PBS, a series of $1/4$ dilutions were applied to the plate in triplicate. (Dilutions – 40, 10, 2.5, 0.625, 0.15625, 0.0390625, 0.00976563, 0.0024414, 0.00061, 0.00015, 0)
- The plate was again incubated at 37°C, washing again with PBST/PBS three times.
- Finally the detection antibody, DY647- α CRP (2.5 μ g/mL) was applied to the plate,
- Incubated at 37°C for 1 hour.
- Finally, the plate was washed once again with PBST/PBS three times, and the fluorescence was measured on the Tecan Infinite 200 plate reader. The Tecan gave a fluorescence intensity measurement for the individual wells in a 96 well plate.

This standard assay was then modified to demonstrate what result might be expected if the assay were carried out using a microfluidic system where multiple washing and incubation steps were not feasible or possible. This single step protocol is described as follows:

- 100 μL @ 5 $\mu\text{g/mL}$ of mouse anti-human CRP-C2 capture antibody was added to a Nunc Maxisorp 96 well micro-titre plate (3 rows of 10)
- The capture antibody was incubated at 4°C overnight.
- The plate was washed with PBST, followed by rinse with PBS three times.
- 200 μL 3% BSA was added to the plate to block the portion of the surface that did not bind the capture antibody.
- Incubated at 37°C for 1 hour.
- After incubation the plate was washed with PBST, followed by a rinse with PBS three times.
- 300 μL CRP/DY647- αCRP solution was added in triplicate
- Incubated at 37°C for 1 hour, and finally washed before measuring the fluorescence in the Tecan Infinite 200.

2.5.2 Microfluidic Assay

Following the same principle as the single step assay described in the previous section, the assay was transferred to the microfluidic platform that was developed as part of this work.

2.5.2.1 Glass preparation

For this experiment the substrate used is a standard microscope glass slide. The surface is functionalised with amine groups to promote a covalent bond with the capture antibody and the glass surface.

- The glass was functionalised with a 3% APTES coating to generate amine groups on the surface. The amine groups allowed the capture antibody mixed with an oxidised dextran matrix to bind to the surface.
- Capture antibody, C2 anti-CRP @ 200 $\mu\text{g/mL}$, was deposited within the detection zone of the micro-fluidic chip using the Scienion S3 micro-arrayer. The Scienion S3, a non-contact piezo dispensing system, generates microarrays with high accuracy and control on deposition patterns and volumes.
- A 10 x 10 array, with a 500 μm pitch between each drop, was deposited within the channel of the chip. Each drop was ~ 500 pL, with the volume dictated by the 90 μm dispense capillary used.

Once deposited on the functionalised APTES surface, the capture antibody was allowed to incubate for 1 hour, at room temperature. Incubation was carried out in a humidity chamber to reduce the effect of evaporation and drying due to the small volumes deposited. After incubation, the surfaces were washed with PBS and blocked with 3% BSA for 1 hour at 37°C. The slides were washed again with PBS dried under a stream of compressed N₂ and stored in a desiccator until required for experiments.

2.5.2.2 CRP/ α CRP Solution Preparation

Off chip, the different concentrations of CRP (Millipore/BBI group.) were prepared in CRP free plasma (AssayPro). To generate the curve from Figure 4.12, concentrations of 0, 0.1, 0.2, 0.5, 2.0, 10.0 and 20 mg/L were prepared. 5 μ L of each concentration of CRP spiked plasma was mixed with 5 μ L of the DY647 labelled α -CRP (10 μ g/mL) detection antibody. A separate chip was used for each concentration of CRP spiked plasma, with individual drops of capture antibody within the deposited 10x10 array providing replicates.

10 μ L of the CRP/ α CRP solution was loaded onto the chip and allowed to flow over the detection zone. As the sample required \approx 10 minutes to flow through the chip, i.e. the incubation time is remarkably reduced from the usual 1 hour incubation at 37°C.

When the sample cleared the detection zone completely the PDMS portion of the chip was disassembled from the glass slide and disposed of. The glass slide was washed with PBST/PBS to remove any remaining CRP/ α CRP solution or unbound proteins that might have bound non-specifically and distort the final signal. The slide was then read using a Perkin Elmer ScanArrayGX.

Chapter III

Enabling Development of an Antibody Screening and Recovery Platform for Single Cell Manipulation within a Micro-capillary Array

3.1 Introduction

3.1.1 Hypothesis

At present, state of the art for screening of antigen specific antibodies involves multiple panning steps of a large antibody library. With each cycle of panning, the number of candidate antibodies available for selection is reduced until a more manageable number is available for more specific characterisation. With all candidates within the library competing against one another, potential candidates are often overlooked and washed out due to weaker affinity or binding but this weak binding does not always constitute a less specific antibody. By segregating each antibody secreting cell into an individual micro-capillary, the library can be screened on a single cell basis, allowing an unbiased and highly specific interaction for each cell. By combining numerous micro-capillaries into a densely packed array, a high throughput, highly selective antibody selection tool could be realised.

3.1.2 Rationale

With antibody libraries potentially containing billions of potential ASC's, identifying and retrieving the most antigen-specific using current technologies involve displaying the antibody on the surface of a phage (Bradbury et al. 2011) or cell (Horlick et al. 2013) and selecting the best candidates by affinity-based biopanning (Ehrlich et al. 2000) or fluorescence activated cell sorting (FACS) (Kruif et al. 1995). While techniques such as micro-engraving and microfluidic cell sorting have been developed for antibody discovery, they fall short in terms of their throughput, ability to screen both bacterial and mammalian cell and have limited multiplexing capability.

Herein this chapter describes a novel process for screening antibody libraries, using high density glass micro-capillary arrays. The micro-capillaries are available with diameters as small as 5 μm up to several hundred μm . The work presented here utilises an array with diameter 40 μm , with 1 mm height holding 1.2 nL. The micro-capillaries are bundled together in hexagonal groups with 45 μm pitch, centre to centre, and are open either end.

It is proposed, that by loading the array with the cell/media solution diluted to the appropriate concentration, each micro-capillary would contain one cell only. The

loaded array would then be reversibly bonded to an antigen coated PDMS substrate, with the open ended micro-capillary allowing the secreted antibody within, to interact with the PDMS surface.

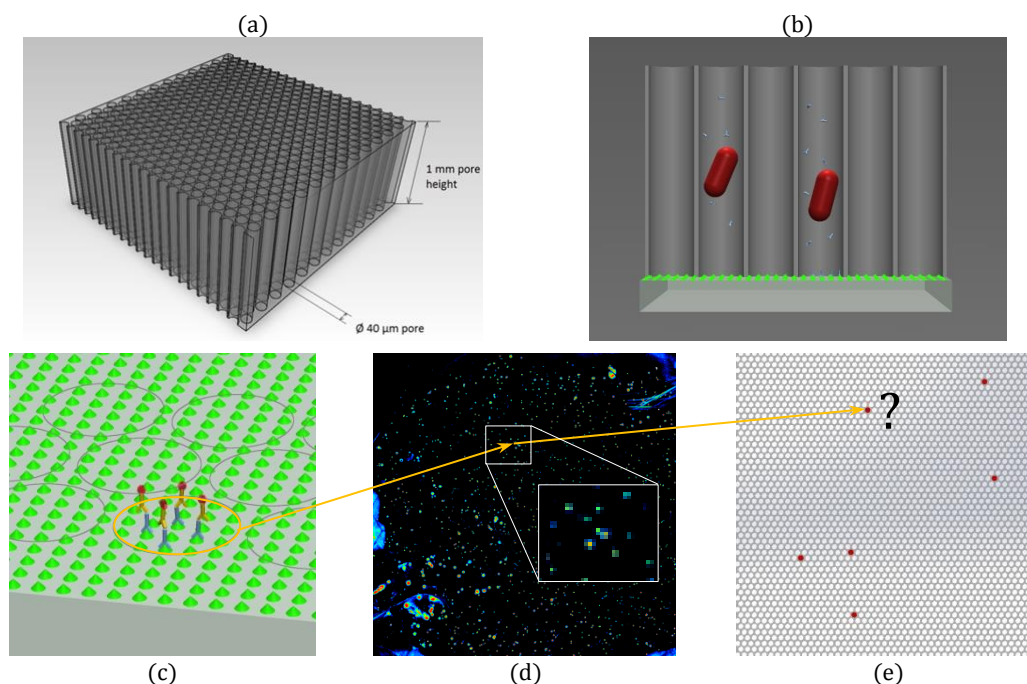
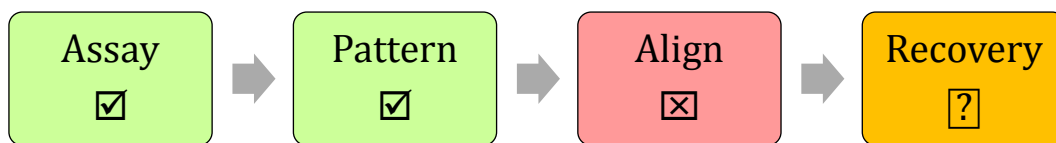


Figure 3.1 (a) 3D model of the micro-capillary array, not to scale. (b) Cross section model of an antibody secreting cell (ASC) with secreted antibody contained within a capillary, coupled to the PDMS surface. (c) Model of antibody/PDMS surface interaction with outline of micro-capillaries highlighted. (d) Scanned fluorescent image of the PDMS assay surface with each fluorescent dot representing the location of an ASC of interest. (e) Model with red dots highlighting the capillaries of interest and the randomness at which they happen. To translate or map (d) to (e) posed a significant challenge, with little indication of orientation relating the image to the array.

Once removed from the array, the PDMS surface would be coated with a fluorescently labelled secondary antibody, which when viewed under a fluorescent microscope would reveal where the specific ASC's from the array interacted with the PDMS surface. The resulting image of the fluorescent dots upon the PDMS surface, would essential provide a map of the corresponding micro-capillary within the array. The contents of each micro-capillary would then be retrieved into a standard microtiter plate for further analysis.

3.1.3 Challenges



To realise the potential of this new technology, two key challenges within the process were identified to enable its development and will be discussed in this chapter.

1. The initial challenge in the process was to align the assay pattern from the PDMS surface with the micro-capillary array, providing a map of the locations of the ASC's of interest within the physical array.
2. With the locations of the ASC's now mapped to the micro-capillary array, a method of retrieving the extremely small volumes from a single micro-capillary was the next challenge addressed.

By addressing the challenges above, the technology would be able to progress towards a high throughput antibody screening process as describes in Figure 3.2 below.

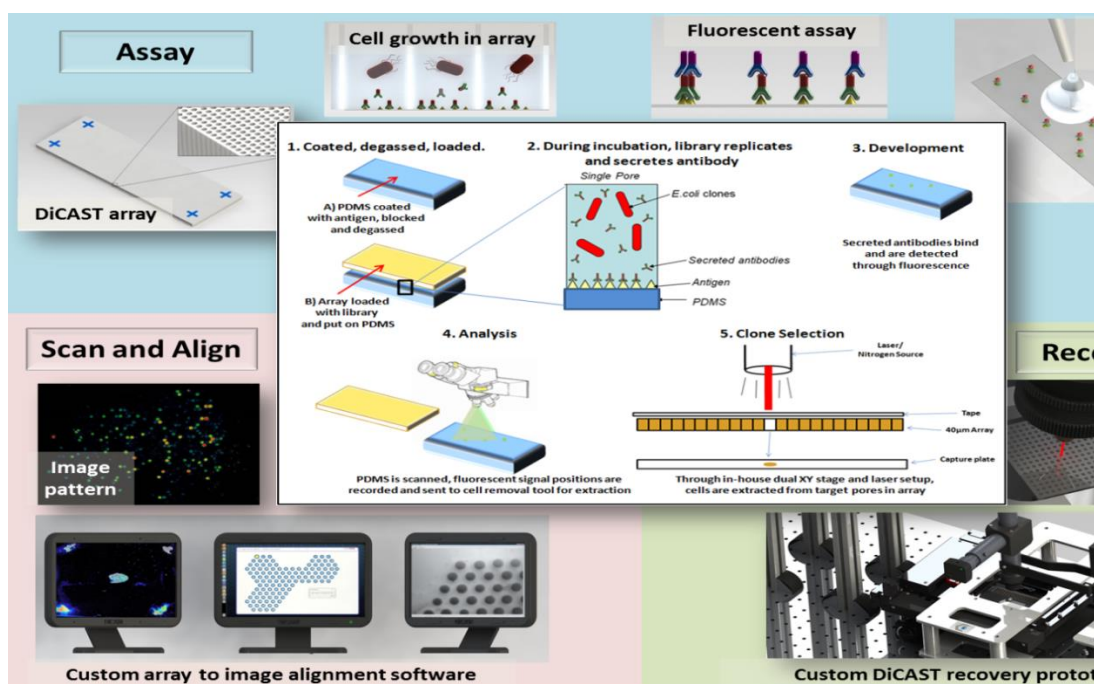


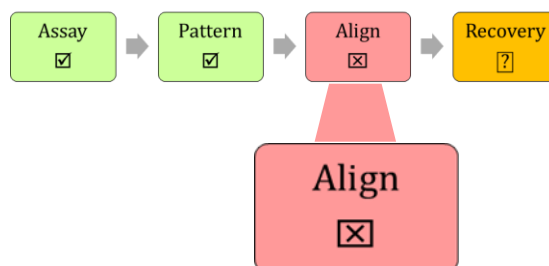
Figure 3.2 Graphical representation of the DiCAST process. (1) The array, loaded with the antibody library is reversibly bonded to the PDMS substrate to perform the assay. The PDMS seals the bottom of the array, effectively forming a micro well plate with millions of wells. (2) Incubation allows the clones to replicate and antibody is secreted, binding to the antigen coated on the PDMS substrate. (3) Post incubation the array is removed and stored while the PDMS substrate is analysed, to identify the positive clones. (4) The analysis provides the “map” with which the recovery system can locate the positive clones in the array and remove them into a 384 well plate for culturing

Linking the scanned image or map of the assay surface to the custom built recovery platform and software, allowed the realisation of a new disruptive antibody selection technology. This chapter describes some of the challenges in implementing this technology and the strategies to overcome those challenges.

3.2 Aligning Pattern on PDMS Surface to Micro-capillary Array

As described previously in Figure 3.1, the screening process performs a fluorescent linked immunosorbent assay (FLISA) within a sub-nanolitre micro-capillary array. Each cell can be spatially addressed in an individual capillary. The secreted antibody which is specific to the antigen is then detected on the removable PDMS assay surface. The assay protocol was developed and optimised within the research team by Dr. Paul Leonard and Ms. Valerie Fitzgerald, both of whom co-invented this new screening technology along with Dr. Ivan Dimov and Prof. Richard O’Kennedy (WO/2012/007537).

Once the antibody library is loaded, each capillary captures a single cell. Based on a specific cell dilution, according to a Poisson distribution, each capillary will receive only one cell. The subsequent FLISA will be highly specific for the antigen of interest, and the antibodies highlighted as positive need to be removed from the array. Translating the FLISA result, (Figure 3.1 d) where the individual fluorescent dots correspond to a particular micro-capillary within the array, is the challenge presented and addressed in this section.



The ability of the array to form a seal with the PDMS surface is crucial for the technology to function and any potential solution must not interfere with the planarity of that polished surface. With only 5 μm separating each capillary edge to edge, the resolution and accuracy of any potential solution had to be considered. The fundamental advantage of using the arrays was due to the density of the micro-capillaries, therefore maintaining the integrity of the bulk of micro-capillaries was a major design consideration.

Any implemented solution must be transferrable to the PDMS surface while remaining intact on the array for the duration of the process, so the resulting image of the PDMS can be correlated to the array.

Taking inspiration from the assay process, where each micro-capillary can provide a fluorescent dot on the PDMS surface, the concept of sacrificing a number of capillaries to transfer a specific pattern to the PDMS was devised and developed.

3.2.1 Concept Design and Considerations

To achieve the transfer of a pattern of specific capillaries, a strategy to block or sacrifice specific capillaries was designed. The main considerations in relation to implementing this strategy were:

- Minimising the number a sacrificed capillaries so as not to jeopardise the number of cells that can be screened at any time
- Maintain the planar surface of the array so as not to affect the sealing with the PDMS assay surface
- Ensure the blocked capillaries remain blocked for at least the duration of the assay process
- In tandem with mapping the locations identified from the PDMS surface, incorporation of a reference for orientation of the array was also required.

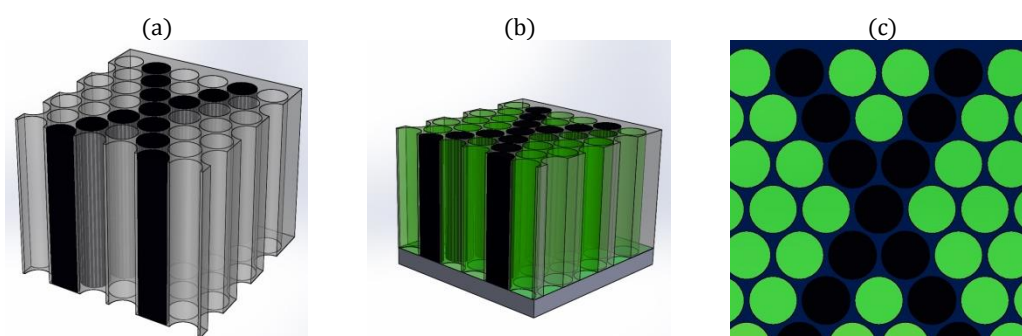


Figure 3.3 (a) A select pattern of capillaries are blocked. (b) The surrounding capillaries are then filled with a fluorescent control solution, similar to that use in the assay, and the array is sealed to the PDMS surface (c) Once the assay is complete and the array is removed from the PDMS surface, with the pattern of the blocked capillaries transferred to the PDMS.

It was envisaged that a particular pattern of capillaries in each corner of the array would be blocked or sealed, and while performing the assay a fluorescently labelled positive control would be added to the locations of these patterns. The capillaries that were intentionally blocked would not allow the fluorescent control pass through that capillary, meaning the resulting image on the PDMS surface would retain the outline of those blocked capillaries (Figure 3.1 c).

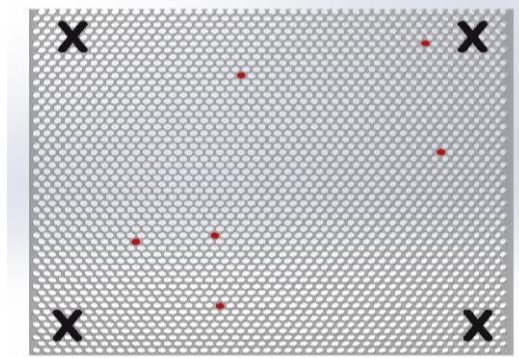


Figure 3.4 Reference marks are placed in each corner of the array. The capillaries of interest (highlighted red) can be located using the pixel coordinates from the scanned image. The recovery system then locates the capillary and removes its contents.

The patterns would serve two purposes. Firstly, they would provide a reference point in each of the corners of the array where individual capillaries within the array could then be triangulated. Secondly, the pattern should allow the user to readily identify the orientation of the array allowing no confusion once the array is uncoupled from the PDMS. It is possible that the array could become upturned, causing translations of the scanned PDMS image to the array to be incorrect and inverse to what they are intended to be. To accommodate this, a simple design inspired by a leading computer gaming console was utilised. By including, at the four points of a cross, a triangular arrow head to indicate the correct Y axis orientation, a square and circular arrowhead on the left and right extremes of the cross respectively, the orientation of the array at any point in time would be readily identifiable.

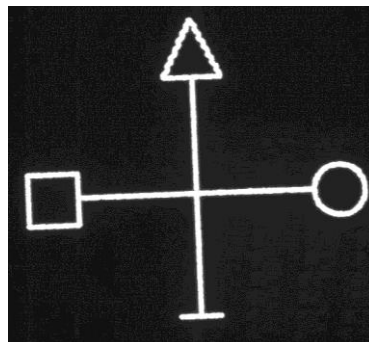


Figure 3.5 An example of an early design used to pattern arrays.

Maintaining the three different shapes in the correct orientation ensured the array was maintained in its correct orientation.

3.2.2 Experimental Approach

Owing to the μm scale dimensions of the capillaries involved, standard fabrication approaches were not suitable. In addition, with the 1.0 mm thick glass capillaries being particularly brittle and difficult to machine using traditional fabrication methods, photolithography was identified as a potential solution.

Photolithography is widely implemented as a fabrication method for microelectronic, microfluidic and MEMS devices (Becker & Gärtner 2008). A light sensitive polymer in liquid form is deposited onto a flat substrate, typically a circular silicon wafer or a glass substrate. Depending on the viscosity of the polymer, the height of the layer is controlled by depositing the material at the centre of the substrate and spinning at a pre-defined rpm. The speed relative to the viscosity provides a high degree of accuracy over the final height. Once the desired height is achieved, the polymer is exposed to a UV light through a patterned mask (Figure 3.6 b). The mask is typically a glass plate with a metallic coating on one side. The metallic coating is patterned to allow the UV light pass through and cure the photoresist polymer. After exposure the polymer becomes cross-linked and bonded to the silicon/ glass substrate. The remaining photoresist can be removed by immersion in photoresist developer solvent. The cross-linked polymer is resistant to the developer solvent, therefore remains intact on the substrate.

For this application we investigated filling capillaries with photoresist and subsequently curing a particular pattern. Photo-resist is easily loaded into the capillary due to its fluid nature until it is exposed to ultra-violet light, where the polymer becomes cross-linked and bonds to the glass capillary. Two approaches using photoresist were investigated.

3.2.2.1 Photolithographic Masking

The initial approach implemented a photomask to expose the desired pattern within the capillaries. SU8 3010 by MicroChem Corp., USA, was the photoresist used for this application. SU8 3010 is a negative photoresist, and as described in Figure 3.6, upon exposure a negative photoresist will become cross-linked. Specified for features of $< 20\ \mu\text{m}$ and coupled with its low viscosity of 340cSt, SU8 3010 was chosen. A drop of

photoresist was deposited in each corner of the micro-capillary array aligned with the locations of the patterns upon the photomask. With the array sealed by a block of degassed PDMS on one side, the photoresist was encouraged to penetrate the capillaries by taking advantage of the suction effect delivered by the PDMS when re-introduced to normal atmospheric conditions from a vacuum environment.

A glass slide coated with approximately 100 nm of gold was patterned as shown in Figure 3.7 (a). Using a 248 nm excimer laser with a 30 μm aperture, the pattern described was traced on the gold surface. The 30 μm aperture ablated a line 30 μm in width which was designed and drawn using AutoCAD.

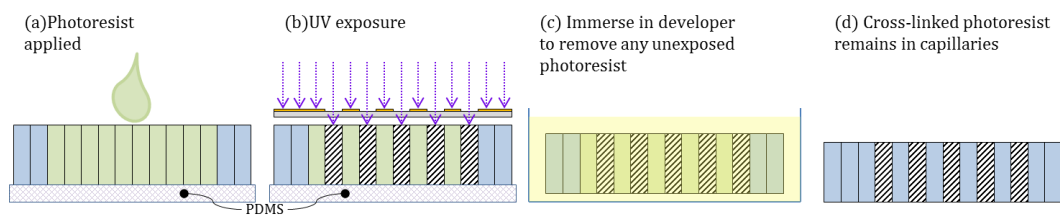


Figure 3.6 Photolithography process steps. (a) Photoresist is placed upon the array and penetrates the capillaries. (b) Custom fabricated gold photomask is positioned over the array and exposed to UV light source. (c) Following exposure the array is immersed in photoresist developer/solvent. At this point the photoresist that was exposed to the UV light is cross-linked, solidified and bonded to the glass capillary. The unexposed photoresist is “developed” away (d), leaving a replica of the pattern from the photomask in the capillaries.

By design, with a 30 μm aperture it was intended that the ablated feature on the mask would align with a single capillary on the array, due to each capillary having a 40 μm diameter.

However Figure 3.7 demonstrates that while the approach described can produce a defined pattern of capillaries, the resulting transfer of that pattern to the PDMS surface does not produce a well-defined pattern.

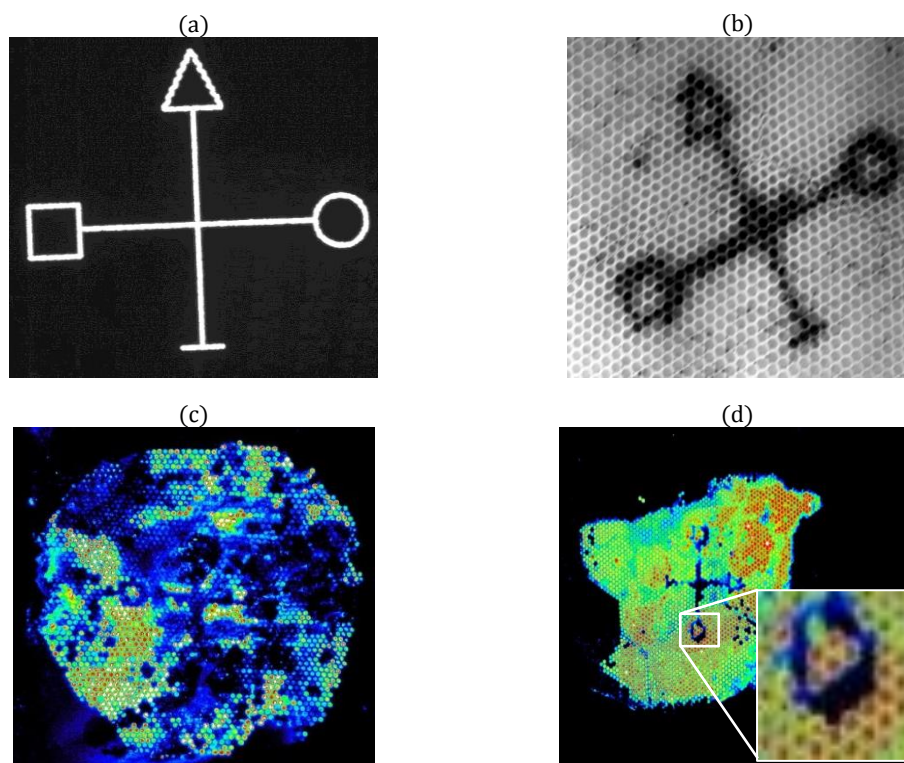


Figure 3.7 (a) Gold mask imaged under microscope. The dark portion of the image is the gold layer with the ablated crosshair allowing light to pass through from the light source below. (b) After UV exposure and developing, the cross-linked photoresist are visible within the capillaries. (c) The resulting fluorescent image with a vague outline of the pattern from the array.

The approach of adding a layer of photoresist to the surface of the array followed by curing that layer in a particular pattern proved successful to a point. The first drawback was the resulting modification to the planarity of the surface of the array. By adding even the slightest layer to the highly polished surface, in some cases the array was unable to seal with the PDMS surface and allowed leaking between the individual capillaries. The resulting pattern was unidentifiable and therefore unsuitable for the purpose of alignment.

Removal of uncured photoresist from capillaries outside of the desired pattern also proved troublesome. Due to the high aspect ratio of the capillary diameter to length, penetrating the full length of the capillary with photoresist developer was a difficult process and led to some capillaries remaining filled.

During the UV exposure it is also suggested that photoresist in adjacent capillaries was being exposed in some instances. Due to the glass capillaries, diffracted UV light that passed through the photomask was able to propagate through the walls of the capillaries, thus curing the photoresist in some of the adjacent capillaries meaning it could not be removed during developing.

3.2.2.2 Polymer Masking

To address the issue of photoresist being difficult to post process once added to the micro-capillaries, the approach was redesigned. It was proposed that only the capillaries that need to be filled receive photoresist. The addition of a polymer layer to the top surface of the array followed by ablating an opening in that layer that corresponded to the micro-capillary underneath meant that when the photoresist was added only that particular capillary was filled. By ablating a number of openings in a desired pattern it would be possible to accurately control the pores that receive the photoresist. Once cured, removal of the polymer mask would remove any excess photoresist, only leaving the pattern required.

Positive Fluorescent Alignment

The initial approach investigated here was to cut a square section of the polymer mask, while leaving a crosshair design intact within that bounding square. In doing so, the crosshair section would remain free of photoresist with the capillaries within the bounding square becoming filled with photoresist.

When translated to the PDMS the crosshair alignment mark in each corner would be presented as a dark bounding square with a highlighted alignment

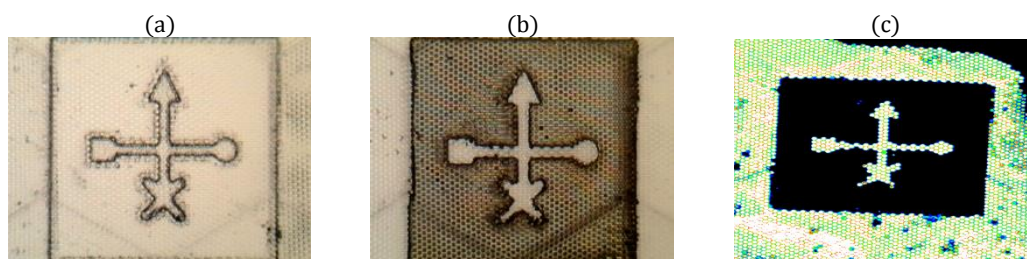


Figure 3.8 Positive fluorescent masking and resulting fluorescent transfer upon PDMS surface.

While this approach provided a very effective contrasting image where individual capillaries can be identified and located, sacrificing many capillaries was counterproductive to the high throughput nature of the antibody screening system. As described in Figure 3.8 each alignment sacrificed ~ 4000 capillaries with photoresist, not including the number of capillaries outside of the bounding square which were also filled with the control fluorescence. In the 23 mm x 23 mm array format there are some 260,000 micro-capillaries available. Using the design above, represented the sacrifice of at least 6.4% of available micro-capillaries within the array. To maximise the available area, an alternative and less wasteful design was required.

Negative Fluorescent Alignment

The negative of what was previously described was proposed as an alternative, similar to the photo masking approach, where the crosshair design was filled with photoresist. The resulting transfer to the PDMS is a dark crosshair with orientation highlighted with the fluorescent control.

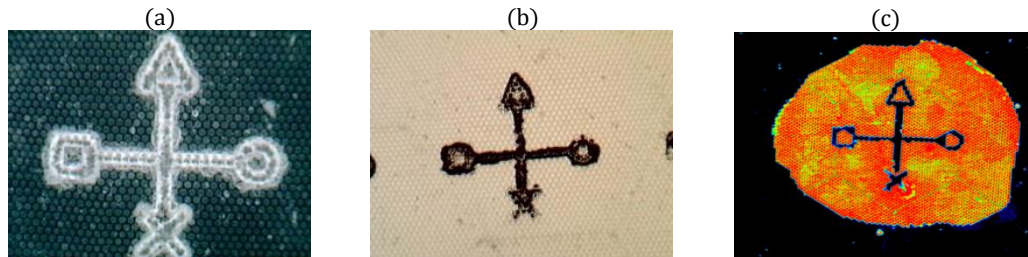


Figure 3.9 Negative fluorescent masking with resulting fluorescent transfer upon PDMS surface

Ablating a 50 μm trace in the polymer mask, similar again to the photomask approach, allowed access to at least one micro-capillary along the trace. By applying photoresist upon the now penetrated polymer mask, the photoresist flows into the available capillaries only, and is exposed to UV light for curing within the capillary. Each crosshair occupies or sacrifices ~ 250 micro-capillaries, representing a total loss of 0.04% micro-capillaries upon the array. From Figure 3.10, at this point in the project, addition of the control fluorescence was performed manually, resulting in unnecessary wastage in terms of capillaries required. As highlighted in Figure 3.10 d & e, if a more controlled or automated system was used to dispense the control onto the array; it would only necessitate the application of control to the inner portion of the shapes providing the orientation information. This again would reduce the number of micro- capillaries sacrificed.

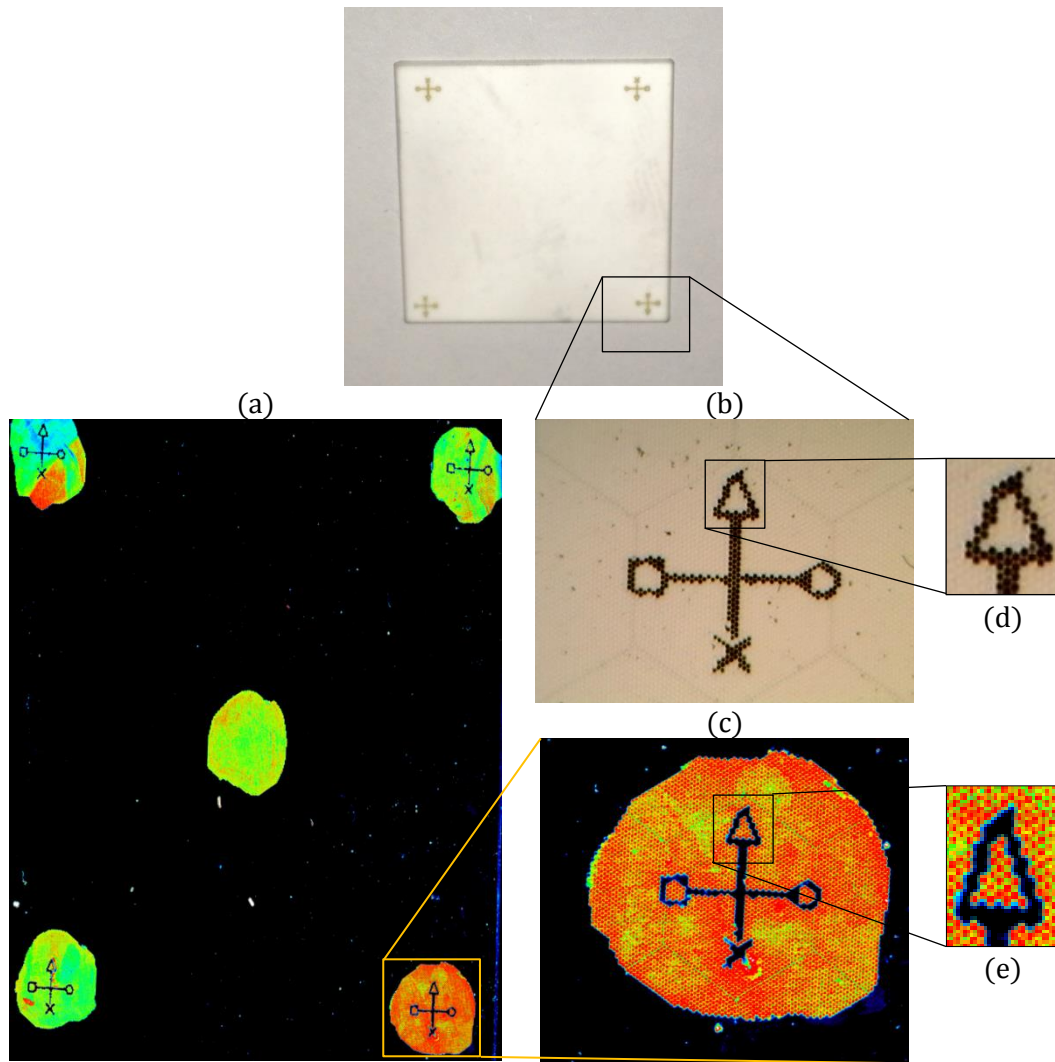


Figure 3.10 The finalised design and result of the chosen pattern. Top image of the physical array with 4 alignment marks in each corner. (a) The full 23 x 23 mm array pattern with alignment marks in each each corner. (b) Microscope image of the SU8 within the array with (c), the resulting fluorescent transfer on PDMS. (d,e) A magnified view of the features of the pattern with distinctly individual capillaries.

3.2.3 Results

The performance of the alignment marks were monitored over a number of patterning sequences to get an indication of the effectiveness, robustness and reproducibility. Presented in Figure 3.10 and Figure 3.11 are the data for array 204. The number of open capillaries described in Figure 3.11 is a count of the number of capillaries bound by each of the shapes at each node of the cross hair. It represents the number of capillaries that should permit the fluorescent control to transfer to the PDMS surface. As such, each pattern should replicate the same number of capillaries on the PDMS as is represented in Figure 3.10 (a), an actual microscope image of the array.

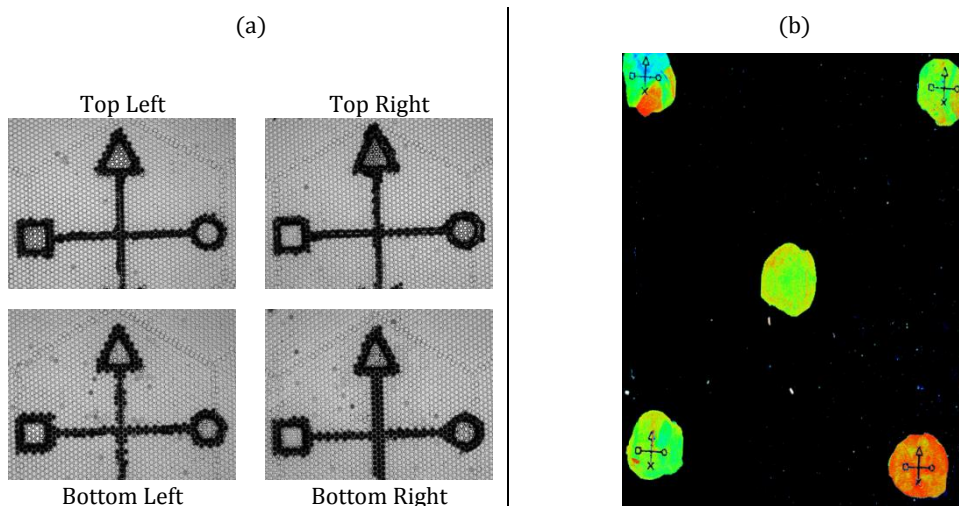


Figure 3.11 Array under microscope (a) showing the alignment marks in each corner and (b) the resulting fluorescent scanned image.

To be regarded as a successful alignment pattern, a specific pattern that transferred to the PDMS must be readily identifiable upon the actual array. After manual inspection of the fluorescent image, the recovery instrument and hardware were used to identify the corresponding specific pattern chosen on the physical array. With those criteria in mind, a measure of the reproducibility of the pattern produced from each array was taken by comparing the physical array to the transferred image on the PDMS surface as tabulated in Figure 3.12.

At present the loading of the control fluorescence and the application of the array to the PDMS surface is purely manual. As a result some errors occurred where the array did not completely seal to the array. From Figure 3.12, some experiments produced unusable results as a result of manual handling errors. In such cases the fluorescent image appears smudged and the identifiable marks unusable.

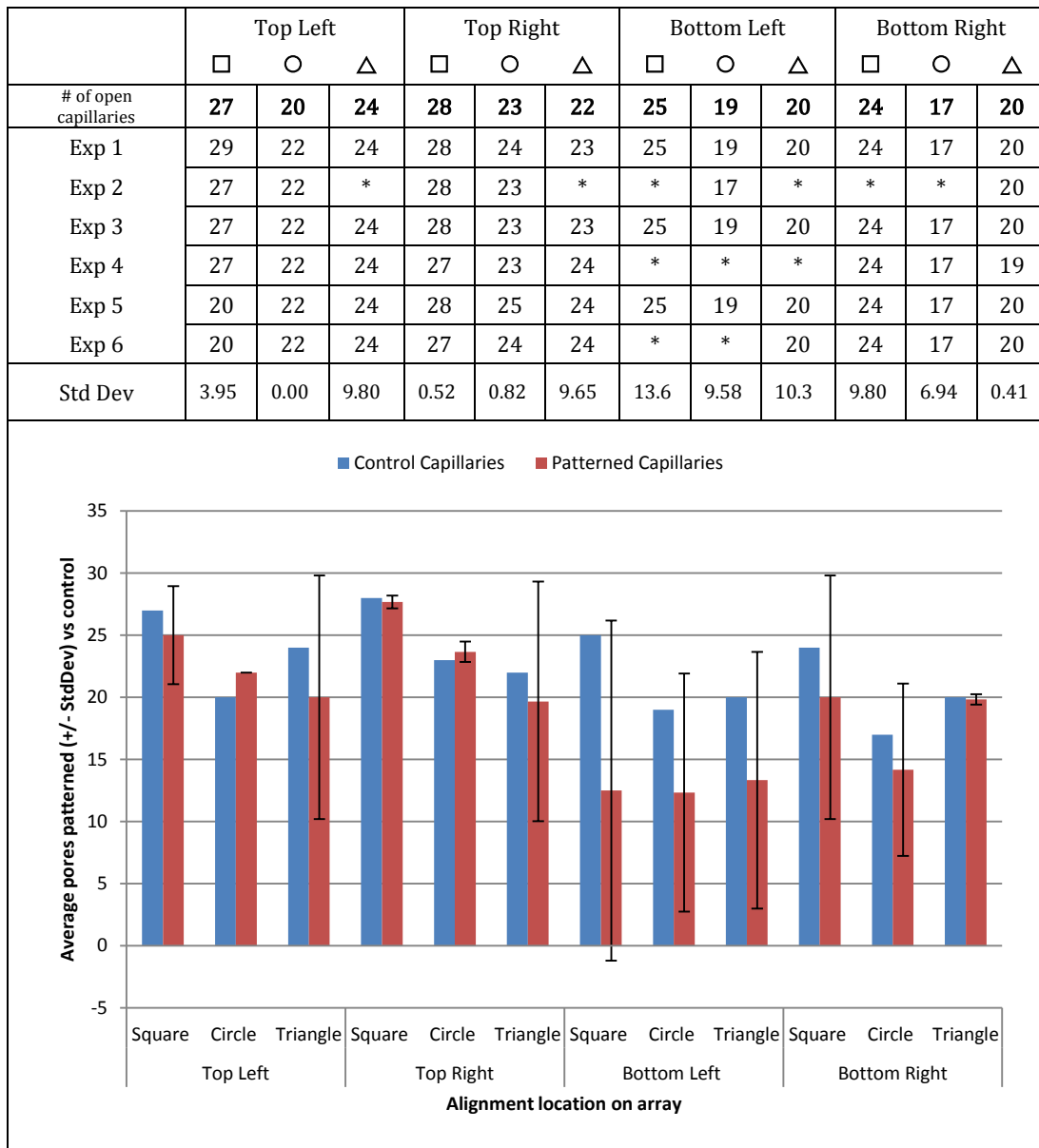


Figure 3.12 Reproducibility and stability data of alignment experiments. The graph and table above report the number of patterned capillaries within each shape at each corner of the array. (* feature not readable due to smearing of pattern on PDMS)

Taking each of the alignment orientation shapes as separate experiments, shows they perform robustly and reproducibly. It is proposed that any error introduced where the pattern does not transfer to the PDMS surface is a result of a handling error as the array is applied to the PDMS surface.

3.2.4 Discussion

Presented with the challenge of translating an identifiable and reproducible pattern from an almost random array of micro-capillaries, to an image which can be interrogated using machine vision software, described are the steps taken to achieve this by implementing common microfabrication techniques.

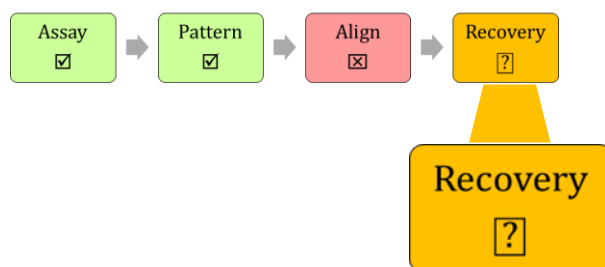
While initially successful, photoresist curing by using a photomask was somewhat uncontrollable in terms of the desired pattern. With diffraction through the walls of the glass capillaries cited as the main cause of curing in unwanted capillaries, the high level of control required to interrogate individual capillaries was not realised.

Lasing access holes corresponding to individual capillaries in a thin polymer layer which covered the entire array, allowed precise and accurate delivery of photoresist to the capillaries required. No excess photoresist penetrated the surrounding capillaries, with the removal of the polymer tape layer post-process removing all the unwanted excess photoresist.

Tracking the alignment marks over a number of experiments showed the photoresist to be stable over time. By observing the number of open capillaries bound by the different shape outlines, described in Figure 3.10, provided a baseline or control for the number of capillaries expected to be transferred during an experiment. The data presented in Figure 3.12 demonstrates the reproducibility of the process. However it also describes human error as being a cause of variation which would need to be addressed going forward. The manual nature of applying the array to the PDMS surface can introduce error and affect the sealing required. To address the error introduced by the manual application of the array to the PDMS surface would require the development of a high precision jig or high precision robotic system. Double movement of the array when placed in contact is the main source of error. With even the steadiest hand, precision of movement and control of movement cannot be guaranteed. As the overall DiCAST project was in the design and development phase, the focus was on developing a method of mapping the array to the recovery hardware. Even with this error present the system was able to develop, however for the DiCAST system to realise a commercial application a more robust system would be required. An array manipulation device would require resources that were beyond the scope of the project at the time of this work and should be developed to fully realise the reproducibility of this process.

The process described allowed the successful mapping of the physical array to the alignment software and subsequently allowed for the cherry picking of individual capillaries by the recovery hardware.

3.3 Capillary Recovery Challenge



Recovery of the identified capillaries for further analysis is the next challenge encountered. A method by which a single cell of interest can be removed from an individual micro-capillary and recovered into a standard 384 well plate is described. The initial concept, designed and fabricated by Mr. Barry O'Donnell, implements a thin polymer layer reversibly sealed the top of the array, sealing the capillaries. A CO₂ laser then ablates an opening in the polymer layer, at the location of a particular capillary as mapped from the scanned fluorescent image. As an opening is formed in the thin polymer layer, the laser shield gas of compressed N₂ is applied to the contents of that capillary. As illustrated in Figure 3.13, all adjacent capillaries remain undisturbed as only the capillary of interest was targeted. The contents, under the force of the compressed N₂, are collected below the array into a 384 well plate.

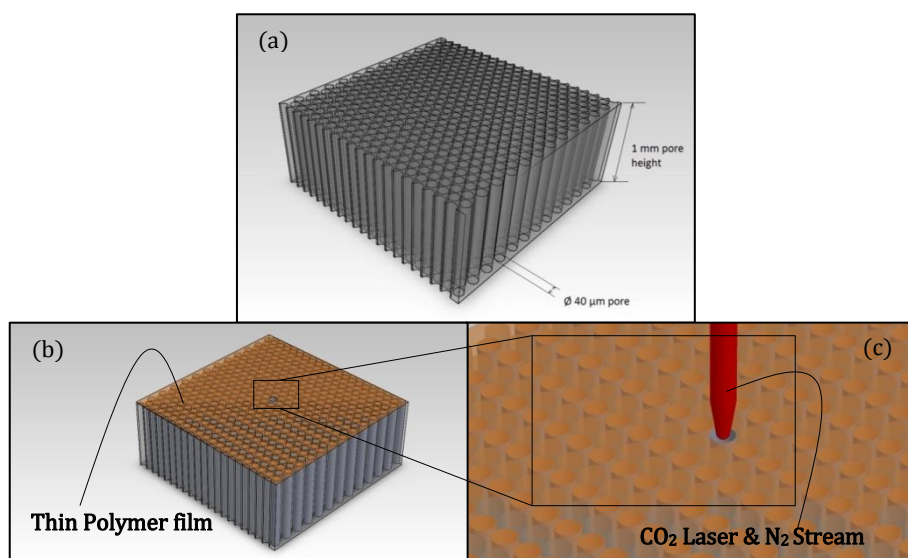


Figure 3.13 Laser ablation recovery method explained (a) The array is loaded with the library to be screened. The array is then placed on a PDMS substrate. (b) A thin polymer film is placed on the array to seal the contents during incubation and analysis. (c) Following analysis of the assay scan the locations of positive clones are identified. At the desired locations the CO₂ laser ablates a small opening. This allows a stream of N₂ to eject the contents of the capillary to the well plate below. As only individual capillaries are opened with each laser pulse only those contents are emptied into the well plate below.

The application of a laser in the process was identified as a possible cause of damage to the delicate contents of the capillary. Forces generated by a laser pulse (Tagawa et al. 2012), followed by a blast of turbulent compressed N_2 , were identified as potential sources of stress for mammalian cells in particular. Also, by removing the laser from the process would simplify the process and eliminate a huge portion of cost when building subsequent systems.

3.3.1 Micro-Air Jet

Due to the capillary forces acting on the contents of each micro-capillary, once the cell suspension is loaded it will remain within the capillary until an external force acts upon it. Taking advantage of this and removing the polymer lid from the array, implementing a micro-air jet to remove the contents of single capillaries was investigated. The micro-air jet concept was designed to be highly focused and capable of interrogating single capillaries without disturbing neighbouring capillaries.

This work involved the design and fabrication of a custom micro-air jet, and investigation thereafter of the removal of the contents from single micro-capillaries.

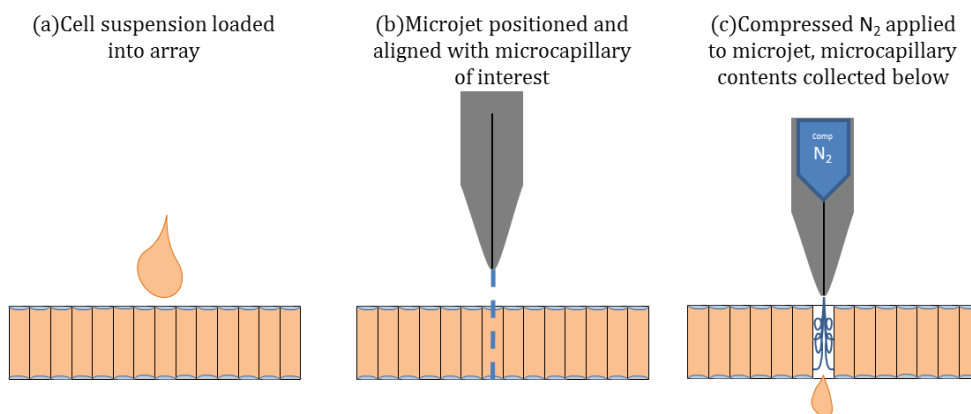


Figure 3.14 Demonstration of air jet removing contents of an individual micro-capillary.

3.3.1.1 Design and Fabrication

The micro jet was designed to deliver a jet of compressed gas, N_2 in this case, to the array. With this being one of the main considerations, the design had to consider any gas fittings required to couple the part to the compressed gas supply.

The main body of the device was fabricated with aluminium. 20 mm aluminium rod was turned on a lathe to produce the part as described in Figure 3.15 c. The function of this part in the device is to house the micro jet structure.

The internal diameter of the micro-jet was cast within the aluminium body. Suspending a 25 μm tungsten wire centrally through the core of the aluminium housing, PDMS was poured and cast around the wire. 25 μm diameter was selected for the jet orifice to interrogate a 40 μm capillary. By aligning the jet orifice with the 40 μm capillary and applying the compressed N_2 to the orifice, the resulting jet of compressed N_2 should eject the contents of the micro-capillary.

The PDMS was cast around a narrowing at the nozzle end of the housing. As shown by the section drawing in Figure 3.15 d, the PDMS illustrated in green is anchored either side of the narrow section. This was intended to allow the application of high pressure to the 25 μm opening in the PDMS and eliminating the chance of having the PDMS ejected from the aluminium housing. Once the PDMS was baked and allowed to cure, the 25 μm tungsten wire was removed to leave the 25 μm opening through the centre of the PDMS.

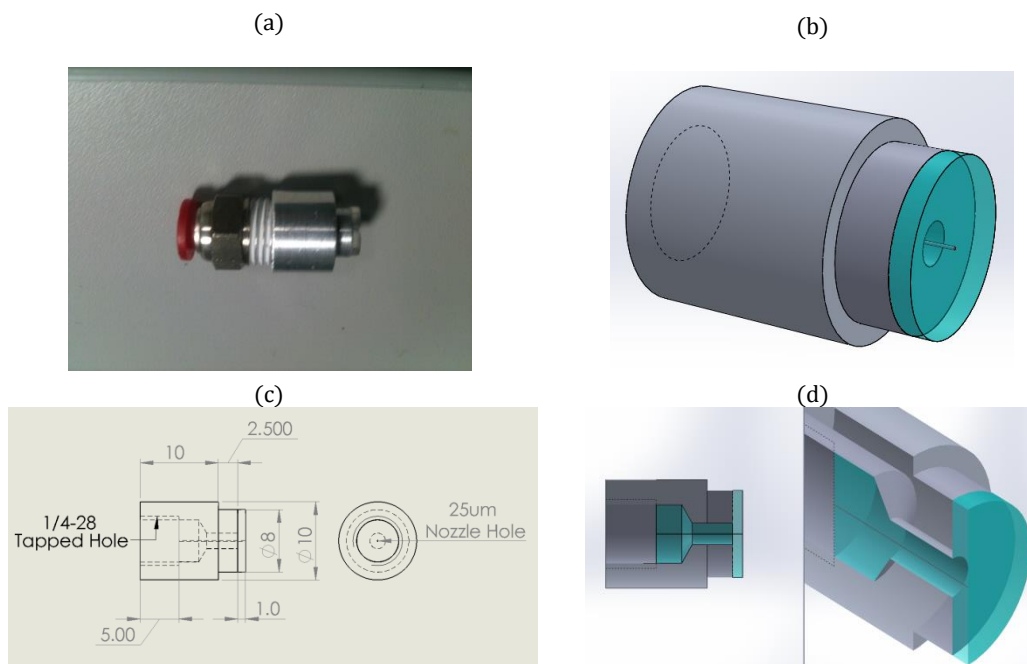


Figure 3.15 Micro-jet design. (a) Image of finished part with 6mm push fit pneumatic fitting attached. (b) 3D model of aluminium housing with PDMS depicted in blue. 25 μm orifice shown running along the centre line of the cylinder housing. (c) Schematic of aluminium housing with PDMS included for reference. (d) 3D cross section of the assembled aluminium and PDMS (25 μm opening not to scale), with PDMS depicted in green.

The open end of the aluminium housing was threaded to $\frac{1}{4}$ -28 UNF. This allowed the coupling of the 6mm push-fit pneumatic fitting, for connection to the compressed N_2 .

3.3.1.2 Proof of Concept Experimental Setup

For initial testing of the concept of using a micro-jet to remove the contents of a single micro-capillary, a simple experimental rig was set up. This included fabrication of a manifold to hold and position the micro-jet device described previously. The manifold was 3D printed with guide holes to run along the optical post. This permitted no movement in the horizontal plane, while allowing the micro-jet device to be moved in the vertical axis. From Figure 3.16, the array was placed below the 3D printed manifold, and manually aligned so that once lowered the micro-jet orifice was aligned within the bounds of the micro-capillary array.

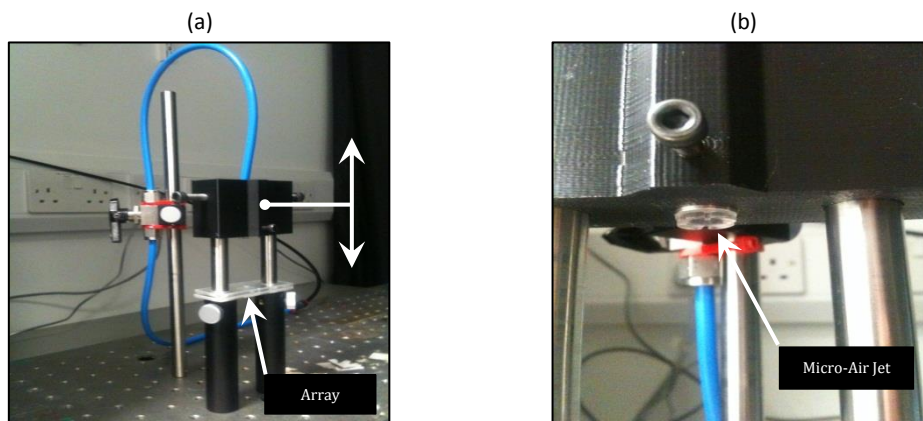


Figure 3.16 (a) The experimental setup allowed movement in the Z axis, guided vertically along two optical posts. A valve for engaging the compressed air with pneumatic tubing connected (blue). The array is placed on the surface below the air jet housing. (b) Shows the air-jet assembled within the 3D printed housing.

The manifold could be fixed at a certain position by 2 locking screws on each optical post. A locking screw was also used to lock the micro-jet device in position to avoid and unwanted movement. A manual gate valve was positioned inline on the 6 mm tubing, between the compressed gas regulator and the micro-jet device.

3.3.1.3 Results

Once the micro-jet was lowered into position and the micro-capillary array was manually positioned underneath, the gate valve was opened for ~ 2 seconds. The micro-jet was positioned manually, within several hundred microns of the array. After closing the valve the array could be repositioned, and the valve opened again.

to eject the contents of another micro-capillary. The array was imaged before and after ejection and the images were compared.

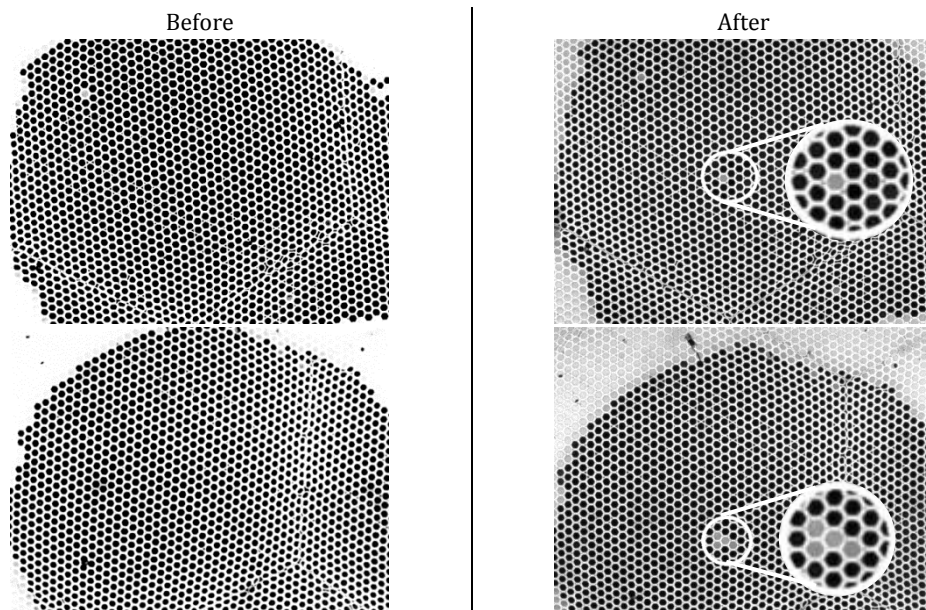


Figure 3.17 Food colouring loaded in an array, with before and after images following the interaction with the air jet. The images on top show single capillary evacuation. A cluster of 4 capillaries is shown to be evacuated possibly due to misalignment of the micro-jet to an individual capillary.

With the lack of control for positioning and alignment of the micro-jet the micro-capillaries, mixed results were achieved. While it was shown that the contents of single capillaries could be ejected while leaving the surrounding capillaries untouched, with misalignment, multiple capillaries were ejected in some instances. It is suggested if the micro-jet is misaligned and is applying the jet to the surface between two capillaries, it is likely that the contents of two or more capillaries, as a result of the deflection of the jet will be ejected or at least be disturbed. Also, due to the manual aspect of the movement and activation of the gate valve, some slight movements during the experiments contributed to some of the multiple capillary ejections.

By introducing increased level of control of movement of the micro-jet and activation of the compressed N_2 , an improvement in performance was expected.

3.3.2 Experimental Setup for Improved Control/ Accuracy

To improve on the accuracy of alignment and introduce some control on the movement of the micro-jet, a multi axis platform was sourced to control the micro-jet position and movement. With $0.025\ \mu\text{m}$ resolution the xyz adjustment meant the nozzle could be moved incrementally and reproducibly to investigate whether

numerous capillaries could be interrogated in sequence. All movements were performed via micrometre adjustment on each access and each access could be adjusted independently.

Keeping the array stationary, both the micro-jet and the microtiter plate below could be adjusted. A manual adjustment rig was fabricated for accurate movement of the microtiter plate below the array. The rig was set up for both a 96 and 384 well plates, with increments corresponding to each well location. Mounted upon the x and y axis of the translation stage, once a well position is selected the well plate moves with the micro-jet nozzle ensuring alignment between the micro jet, through the micro-capillary, and the well plate.

The addition of a fine adjustment regulator allowed greater control over the pressure applied to the micro-jet nozzle. Along with the addition of a digital pressure gauge, this allowed incremental adjustment of the pressure to investigate the effect of different pressures applied. A three port/two position (3/2) pneumatic spring loaded push button valve was also added to the circuit between the regulator and the nozzle. Upon activation of the valve, pressure was applied to the nozzle. Once released the valve closed and any back pressure or latent pressure remaining in the line between the valve and the nozzle was allowed to exhaust through the open port to atmosphere. This design element was included to release any back pressure on the nozzle opening to reduce the possibility of interfering with other capillaries during subsequent movement of the nozzle relative to the array.

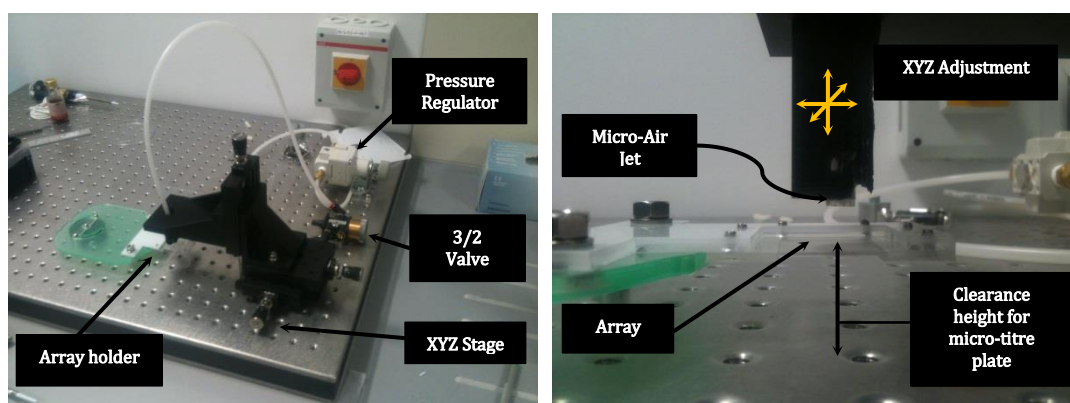


Figure 3.18 XYZ stage with fine adjustment pressure regulator and 3/2 valve. The set up shown was implemented to demonstrate the ability to interrogate individual capillaries in a particular pattern. Each axis was independently adjustable.

Figure 3.19 is the initial test carried out using the rig setup shown in Figure 3.18. By positioning the nozzle as close to the array as possible and activating the 3/2 valve, a capillary was emptied. From Figure 3.19 (a), after releasing the valve button, the

nozzle was moved in the horizontal plane in set increments of 200 μm . The valve was activated once again and the next capillary was evacuated. In Figure 3.19 (b) the nozzle was adjusted in two directions, again in set increments of 200 μm .

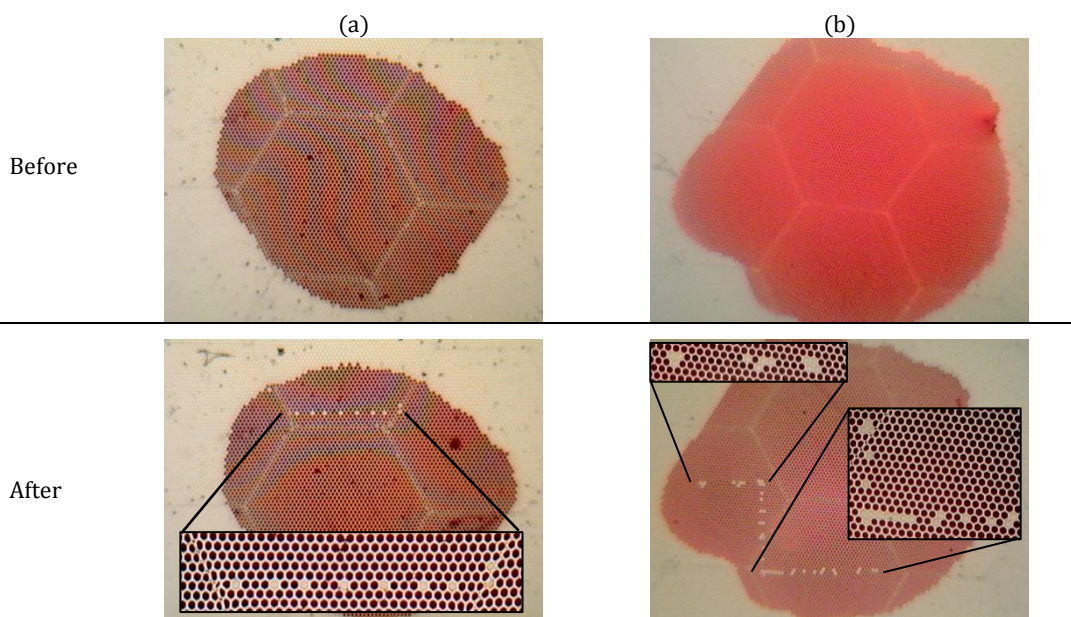


Figure 3.19 Demonstration of single capillary evacuation with improved control. Before and after images of arrays loaded with food colouring, demonstrating that with greater control and the ability to locate specific capillaries, it is possible to empty that capillary using a small jet of air.

With the manual nature of the position of the nozzle relative to each capillary some error is demonstrated, especially in relation to the post evacuation image of 3.19 (b). Where the nozzle becomes misaligned between two or possible more capillaries, multiple capillaries were evacuated.

For positioning of the well plate, a manual positioning stage was fabricated to adjust and position the well plate. The well plate position was adjustable relative to the tip of the nozzle, but once a position was chosen any movement of the micro-jet nozzle moved the well plate also. The manual stage was designed to accommodate each with increments for a 96-well plate or a 384-well plate. With the array held in a stationary position

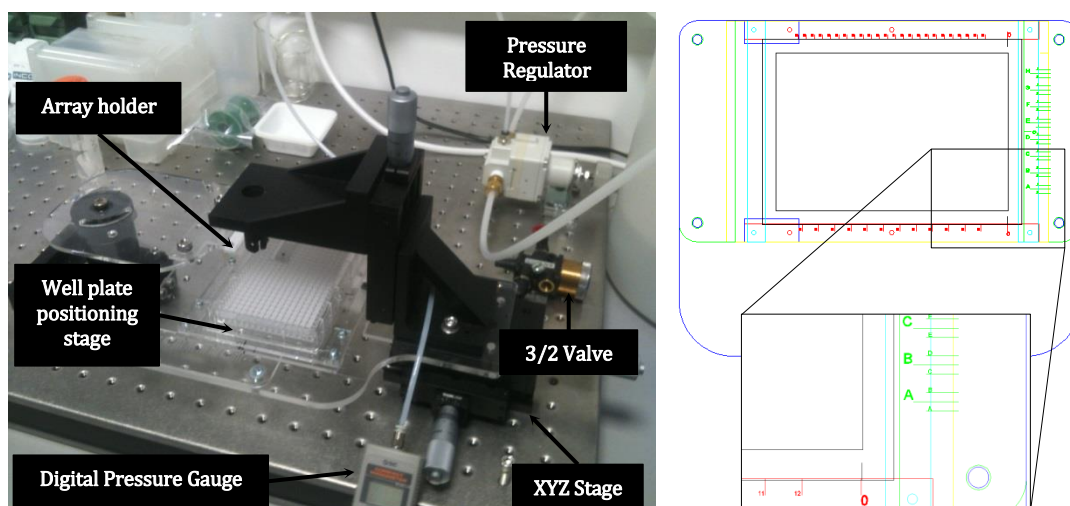


Figure 3.20 Image of the final pneumatic setup including a digital pressure gauge, and the manual x/y positioner for a microtiter plate showing (right) the alphabetical increments and numerical increments for 96 and 384-well plates.

3.3.2.1 Results:

Bacteria Cell Recoveries

With the proof of concept demonstrated, the challenge now was to load and array with bacteria cells and attempt to recover them using the micro-jet. Bacteria cells were chosen as the initial subject for experiments as they are more suitable for recovery. Bacteria cells are more robust against external forces, and even small numbers of recovered cells will propagate and grow if recovered into media. A 40 μm diameter capillary array was used for all the following experiments

Experiment 1

In this instance the array was loaded with two different concentrations of bacteria cells. The concentrations used were $2 \times 10^5/10 \mu\text{L}$ and $1 \times 10^5/10 \mu\text{L}$. 50 μL of each cell suspension was added at different locations within the array. 175 μL PBS was added to each well of the 96-well plate.

For the experiment described in Figure 3.21, a constant 6 bar pressure was applied to the micro-jet upon activation of the push button valve. Manually, each burst applied to the micro-jet was timed at ~ 5 seconds. A 100 μm increment in the X/Y plane was used to separate each recovery attempt.

A1	A2	A3	A4	A5	A6	A7	A8	A9	A10	A11	A12	
B1	B2	B3	B4	B5	B6	B7	B8	B9	B10	B11	B12	Non-Contact
C1	C2	C3	C4	C5	C6	C7	C8	C9	C10	C11	C12	
D1	D2	D3	D4	D5	D6	D7	D8	D9	D10	D11	D12	Non-Contact
E1	E2	E3	E4	E5	E6	E7	E8	E9	E10	E11	E12	
F1	F2	F3	F4	F5	F6	F7	F8	F9	F10	F11	F12	Non-Contact
G1	G2	G3	G4	G5	G6	G7	G8	G9	G10	G11	G12	
H1	H2	H3	H4	H5	H6	H7	H8	H9	H10	H11	H12	Non-Contact

Figure 3.21 Layout of 96-well plate for cell recoveries. Intended target wells are highlighted in blue, with the micro-jet/array interaction type highlighted in green for non-contact.

Once the experiment was complete the plate was removed and viewed under 10X magnification using an inverted microscope. No cells were observed in any of the wells

Experiment 2

For this experiment the micro jet was used both in contact and non-contact with the array. Each concentration of cells was interrogated with both methods. With the non-contact method, as described in the proof of concept section, the micro-jet was moved incrementally by 100 μm in the X/Y plane between each evacuation. The Z height was maintained throughout.

The contact method involved the micro-jet being lowered in the Z plane until in contact with the array. Once in contact the micro-jet was activated and the capillary below evacuated. The position at which the initial contact was made was recorded for subsequent contact evacuations. To move to the next position the micro-jet was retracted to a safe Z position before moving to seek the next capillary. Once repositioned above the next capillary the micro-jet was lowered to the previously recorded position to make contact with the array. This process was repeated as necessary for each recovery.

A 40 μm diameter capillary array was used for all the following experiments. In this instance the array was loaded with two different concentrations of bacteria cells. The concentrations used were $5 \times 10^5/50 \mu\text{L}$ and $7.75 \times 10^5/10 \mu\text{L}$. 50 μL of each cell suspension were added at different locations within the array. 200 μL PBS was added to each well of the 96-well plate.

A1	A2	A3	A4	A5	A6	A7	A8	A9	A10	A11	A12	
B1	B2	B3	B4	B5	B6	B7	B8	B9	B10	B11	B12	Non-Contact 5x10 ⁵ /50 μ L
C1	C2	C3	C4	C5	C6	C7	C8	C9	C10	C11	C12	
D1	D2	D3	D4	D5	D6	D7	D8	D9	D10	D11	D12	Non-Contact 7.75x10 ⁵ /10 μ L
E1	E2	E3	E4	E5	E6	E7	E8	E9	E10	E11	E12	
F1	F2	F3	F4	F5	F6	F7	F8	F9	F10	F11	F12	Contact 7.75x10 ⁵ /10 μ L
G1	G2	G3	G4	G5	G6	G7	G8	G9	G10	G11	G12	
H1	H2	H3	H4	H5	H6	H7	H8	H9	H10	H11	H12	Contact 5x10 ⁵ /50 μ L

Figure 3.22 Layout of 96-well plate for cell recoveries. Intended target wells are highlighted in blue, with the micro-jet/array interaction type highlighted in green for non-contact and yellow for contact. Cell concentrations are also outlined on the right.

For the experiment described in Figure 3.22, a constant 4 bar pressure was applied to the micro-jet upon activation of the push button valve. Similarly to experiment 1 previously, the plate was inspected using an inverted microscope at 10X magnification.

Once again no cells were observed in any well within the well plate.

Experiment 3

A 40 μ m diameter capillary array was used for all the following experiments. In this instance the array was loaded with two different concentrations of bacteria cells. The concentrations used were 2.5x10⁵/50 μ L and 5.0x10⁴/50 μ L. 50 μ L of each cell suspension were added at different locations within the array. 200 μ L PBS was added to each well of the 96-well plate.

This experiment was set up to look at the effects of varying the pressure applied to the micro-jet. A series of pressures were tested including 2, 3, 5 and 6 bar pressure. Contact and non-contact interaction with the array were also investigated for each cell concentration and each pressure. At each location pressure was applied to the micro-jet for ~5 sec

	1	2	3	4	5	6	7	8	9	10	11	12	Cell Conc.	Array Interaction
A		2bar		2bar		2bar		3bar		3bar		3bar	2.5x10 ⁵ /50 μ L	Non-Contact
B		2bar		2bar		2bar		3bar		3bar		3bar	5.0x10 ⁴ /50 μ L	
C		5bar		5bar		5bar		6bar		6bar		6bar	2.5x10 ⁵ /50 μ L	
D		5bar		5bar		5bar		6bar		6bar		6bar	5.0x10 ⁴ /50 μ L	
E		2bar		2bar		2bar		3bar		3bar		3bar	2.5x10 ⁵ /50 μ L	Contact
F		2bar		2bar		2bar		3bar		3bar		3bar	5.0x10 ⁴ /50 μ L	
G		5bar		5bar		5bar		6bar		6bar		6bar	2.5x10 ⁵ /50 μ L	
H		5bar		5bar		5bar		6bar		6bar		6bar	5.0x10 ⁴ /50 μ L	

Figure 3.23 Layout of 96-well plate for cell recoveries. Intended target wells are marked with the pressure applied to the micro-jet at that location, with the micro-jet/array interaction type highlighted in green for non-contact and yellow for contact.

Upon inspection, under 10X magnification, 2 cells were observed in wells A8 and G6.

Experiment 4:

Once again a 40 μ m diameter capillary array was used for the following experiment. In this instance the array was loaded with a single concentration of bacteria cells. The concentration used was 2.0x10⁴/50 μ L. 50 μ L of the cell suspension was added to the array. 200 μ L PBS was added to each well of the 96-well plate.

Here, the effects of changing the pulse applied to the micro-jet were investigated. This was done by manually adjusting the duration and number of pulses at each location. See Figure 3.24. All recovery attempts for this experiment were implemented with the micro-jet in contact with the array.

A1	A2	A3	A4	A5	A6	A7	A8	A9	A10	A11	A12	
B1	4bar	B3	4bar	B5	4bar	B7	4bar	B9	4bar	B11	4bar	Contact
C1	C2	C3	C4	C5	C6	C7	C8	C9	C10	C11	C12	
D1	5bar	D3	5bar	D5	5bar	D7	5bar	D9	5bar	D11	5bar	Contact
E1	E2	E3	E4	E5	E6	E7	E8	E9	E10	E11	E12	
F1	4bar	F3	4bar	F5	4bar	F7	4bar	F9	4bar	F11	4bar	Contact
G1	G2	G3	G4	G5	G6	G7	G8	G9	G10	G11	G12	
H1	5bar	H3	5bar	H5	5bar	H7	5bar	H9	5bar	H11	5bar	Contact

Figure 3.24 Layout of 96-well plate for cell recoveries. Intended target wells are highlighted in blue, with the micro-jet/array interaction type highlighted in yellow for contact.

The pulse was varied as follows:

- Row B: short on/off pulses of valve
- Row D: longer pulse, ~10 seconds
- Row F: 5X short on/off pulses at each location
- Row H: 2X ~5second pulse at each location

Following inspection of the plate post experiment, no cells were recorded as being present in any of the wells.

Investigation of recovery effectiveness

With less than favourable recoveries from the experiments reported it was planned to investigate the capture efficiency with the aim of quantifying the successful recovery of the contents of a micro-capillary.

To achieve this it was proposed to load the array with horse radish peroxidase (HRP), and attempt to recover the contents of single capillaries into tetramethylbenzidine substrate (TMB) loaded in a well plate below the array. When mixed with HRP, an enzymatic reaction causes a colour change in TMB. The intensity of the colour change can be measured to give an indication of the amount of HRP recovered.

Non-Contact Quantification Experiments

A1	A2	A3	A4	A5	A6	A7	A8	A9	A10	A11	A12
B1	B2	B3	B4	B5	B6	B7	B8	B9	B10	B11	B12
C1	C2	C3	C4	C5	C6	C7	C8	C9	C10	C11	C12
D1	D2	D3	D4	D5	D6	D7	D8	D9	D10	D11	D12
E1	E2	E3	E4	E5	E6	E7	E8	E9	E10	E11	E12
F1	F2	F3	F4	F5	F6	F7	F8	F9	F10	F11	F12
G1	G2	G3	G4	G5	G6	G7	G8	G9	G10	G11	G12
H1	H2	H3	H4	H5	H6	H7	H8	H9	H10	H11	H12

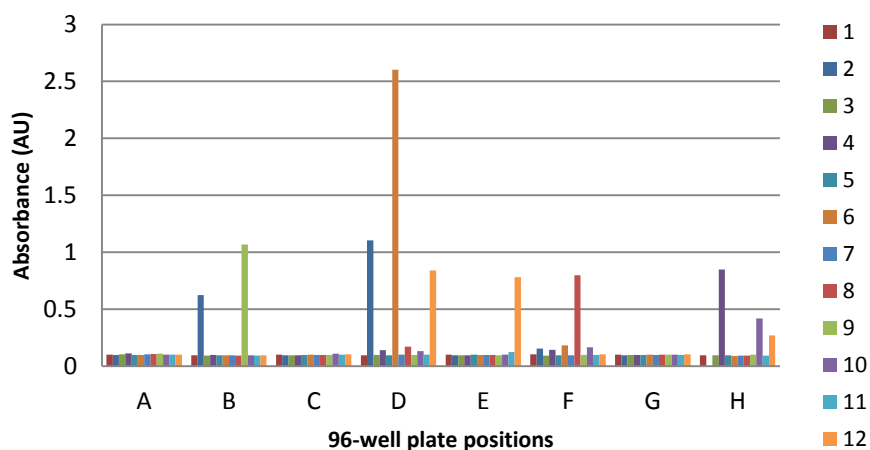


Figure 3.25 Recovery of HRP into 96-well plate with TMB. Above describes the layout of the 96-well plate into which each evacuated capillary was directed. All evacuations were under 4 bar pressure.

Figure 3.25 above shows the results for the application of 4 bar pressure to the micro jet with the table representing the location within the 96-well plate where the evacuated capillaries were directed. Each well contained 200 μ L of TMB. For every location the micro-jet was repositioned to interrogate a new capillary by adjusting 100 μ m in the X or Y plane, and the push button valve was activated for \sim 2 sec. The

tip of the nozzle did not make contact with the array for this experiment, maintaining a minimum distance between the tip and the array surface. The minimum distance was set manually by visual inspection.

Excluding position E12, each positive recovery was achieved at the desired well. 17 out of 24 intended wells show varying levels of recovery, demonstrating some loss of HRP during the evacuation of each capillary.

In an attempt to increase the recovery of the contents of the capillary the pressure applied to the nozzle was increased. A comparison of a low and high pressure was performed using the previous 4 bar and an increased 6 bar pressure. Using the same template as before, 24 wells were selected upon the 96-well plate into which a single shot from the micro-jet was directed. Once again the micro-jet was being aimed blindly, with the intention of capturing the minimum number of capillaries.

A1	A2	A3	A4	A5	A6	A7	A8	A9	A10	A11	A12
B1	B2	B3	B4	B5	B6	B7	B8	B9	B10	B11	B12
C1	C2	C3	C4	C5	C6	C7	C8	C9	C10	C11	C12
D1	D2	D3	D4	D5	D6	D7	D8	D9	D10	D11	D12
E1	E2	E3	E4	E5	E6	E7	E8	E9	E10	E11	E12
F1	F2	F3	F4	F5	F6	F7	F8	F9	F10	F11	F12
G1	G2	G3	G4	G5	G6	G7	G8	G9	G10	G11	G12
H1	H2	H3	H4	H5	H6	H7	H8	H9	H10	H11	H12

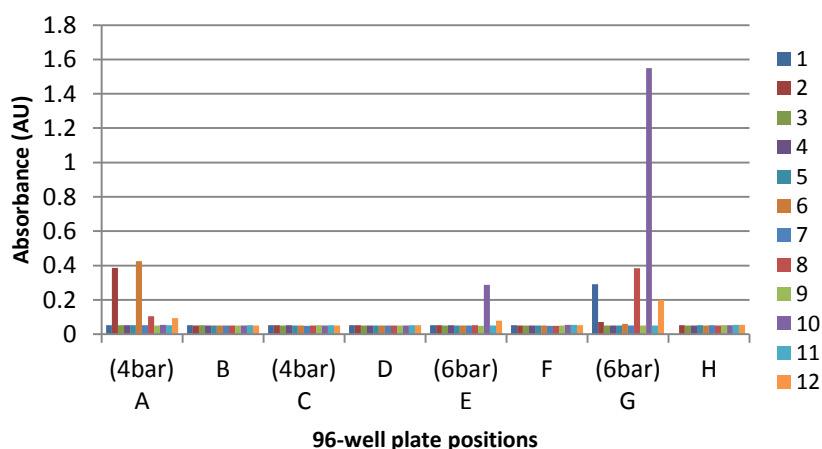


Figure 3.26 Recovery of HRP into 96-well plate with TMB. Rows A and C were subjected to 4 bar through the micro-jet with rows E and G having 6 bar applied. The results described were achieved with non-contact interaction with array

Similarly to the previous non-contact experiment, each well contained 200 μ L TMB. Each capillary recovery attempt was adjusted by 100 μ m increments.

The results shown in Figure 3.26 once again indicate that, while some wells do show recovery of HRP and were intended as target wells, only 11 of the 24 targets demonstrate recovery.

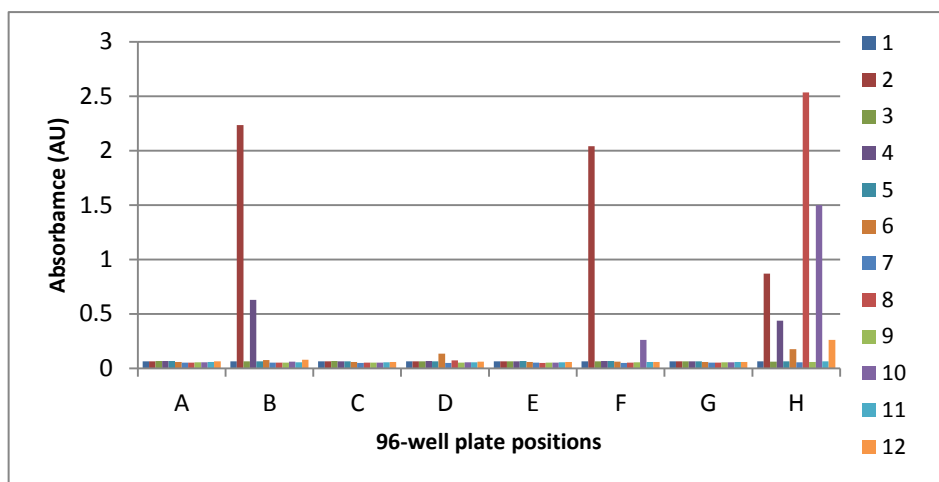


Figure 3.27 Non-contact recovery of HRP into 96-well plate containing TMB.

Contact Quantification Experiments

With the aim of trying to eliminate any loss of HRP during, the following experiment investigated interrogating each capillary with the micro-jet in contact with the array. The contact between the PDMS surface of the micro-jet and the array was intended to seal the jet orifice to the capillary of interest. Again, capillaries were chosen blindly at this point.

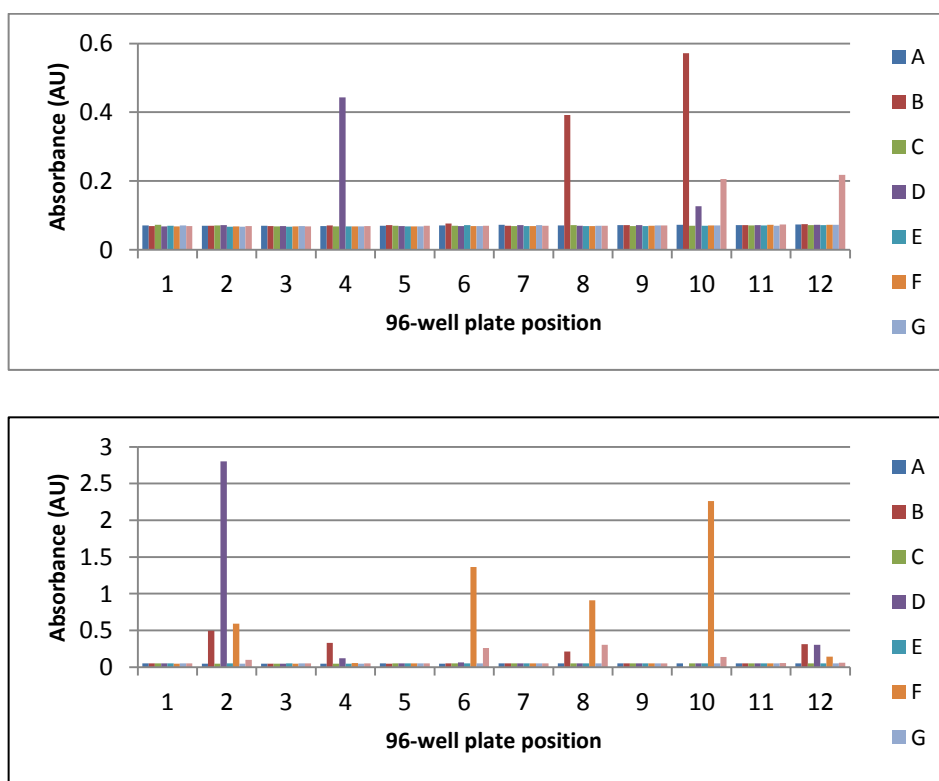


Figure 3.28 HRP recoveries into a 96-well plate

All HRP data show that, while emptying the capillaries of interest, reproducible and consistent recovery of the capillary contents is erratic.

Alignment of jet to capillaries factor, air jet evaporating contents, turbulence on under side of the array to be discussed

3.3.3 Discussion

Upon showing that a single capillary can be interrogated, the subsequent recovery of the contents proved elusive. Even with the primitive controls and equipment single capillary manipulation is possible.

The extremely sporadic results shown with the attempted cell recoveries demonstrates that, while the contents might well be forced out of the array, it does not continue in a linear trajectory for collection. Albeit they describe a liquid jet, Acero et al show that, with the aid of a co flowing fluid stream they can control and extend the focus of the resulting jet (Acero et al. 2012). A method such as this would be difficult to implement with gases, like compressed air and N₂ for example having similar densities. The similar densities would result in the diffusion of the two into one stream. The co-flowing stream would also interfere with the surrounding capillaries. Chang et al have reported that the surface tension on the underside of a nozzle, or in this case the underside of the array, can be significant and could cause the contents to spread along the bottom of the array (Chang et al. 2012).

It has also been hypothesised in the group that due to the extremely small volumes present, the contents could be diffused or vaporised under the jet of compressed N₂. The HRP recovery experiments would suggest that some of the contents of the targeted capillaries do in fact get collected in the well plate below, but as is evident with the low absorbance levels from graphs described in Section 3.3.2.1, the amount that does get collected varies greatly if collected at all.

While demonstrating that a jet of air can move the contents of the micro-capillary, albeit with little control, new approaches to achieve recovery were required and pursued. Section 3.4 continues to develop a recovery solution of the micro-capillary contents by trying to reduce or eliminate the variability that the air jet results present.

3.4 Micro-Liquid Jet

With the inconsistencies described by the air jet approach, a new concept was required. While the micro-jet concept was particularly simple in design, and compromise in simplicity and effectiveness was necessary. By selectively coupling a glass capillary to either side of the capillary of interest and passing a volume of liquid through that particular capillary, PBS in this case to maintain cell health, it was proposed that the capillary could be evacuated in a non-volatile way.

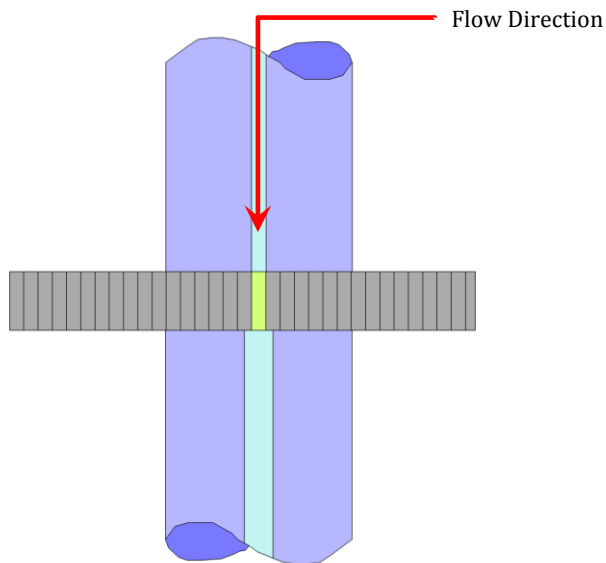


Figure 3.29 Concept of coupling a glass nozzle either side of the array and flowing a liquid through a selected capillary to retrieve its contents.

With the initial concept outlined troubleshooting of potential configurations that could be implemented was performed. In Table 3.1 each configuration is scored on different parameters that would impact its performance.

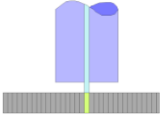
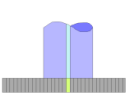
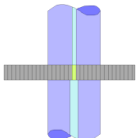
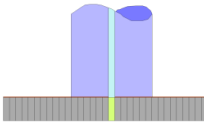
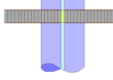
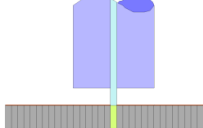
As was the case with the non-contact micro-jet, a non-contact liquid was the configuration that scored the best. Achieving the best score in all but two of the nine categories, the non-contact approach would require a very fine jet of liquid to travel through the capillary, removing the contents of that capillary in the process and continue to jet out the bottom side of the capillary into the well plate below. The intricacies of implementing such a system would prove difficult. Similarly, the contact jet would appear to be one of leading solutions with the second best score. However, as was the case with the micro-air jet, surface tension on the bottom surface of the array was identified as a possible pitfall.

The three least favourable options from the failure modes, effect and analysis involved some application of the laser process described previously when outlining

the capillary recovery challenge in Section 3.3 Capillary Recovery Challenge. Due the complexity of introducing the extra step of the lasing of holes in the polymer layer, all three options result with a poor score.

After considering all conditions, and with the main aim to recover the contents of a single capillary in the most robust way, the “collected contact jet” was chosen as the most suitable configuration. Some issues surrounding contamination of the two glass capillaries were identified, although with adequate cleaning protocols in place it was suggested contamination could be eliminated.

Table 3.1. Failure modes and effects analysis (FMEA) of potential liquid recovery configurations.

Score each consideration: 1= Good 2= Neutral 3= Bad		Non-Contact Jet	Contact Jet	Collected Contact Jet	Lasered Contact Jet	Lasered Collected Contact Jet	Lasered Non-Contact Jet
							
Considerations for effective single cell retrieval	% Liquid Loss	2	2	1	2	1	2
	Shear stress on pore contents	2	2	1	2	2	2
	Chance of contamination	1	2	3	1	1	1
	Throughput/ cycle time	1	2	2	3	3	3
	# of pores captured by jet	1	1	1	1	1	1
	ease of use/calibration effort	1	1	2	3	3	3
	simplicity of instrument	1	1	2	3	3	3
	reproducibility of instrument	1	1	2	2	2	2
	interference with alignment of the array through a cycle	1	3	3	3	3	2
Total Risk Score		11	15	17	20	19	19
Brief comments		Straight swap for the gas removal method. Quicker to adapt and make new instruments.	Solves problems of affecting adjacent capillaries but may need a new wash step and is slightly slower with additional movements and could interfere with the array alignment	Difficult to couple and align two tubes. Will likely affect the array alignment.	Likely to affect array alignment. Increased stress on contents of capillary due to laser.	Difficult to couple and align two tubes. Will likely affect the array alignment. Increased stress on contents of capillary due to laser.	More stress applied to the one open capillary? Reduces chance of contamination. Likely introduce additional clean up step of the excess liquid gathering on the tape.

3.4.1 Proof of Concept

To demonstrate the concept a simple rig was set up to couple two Tygon™ tubes either side of the array. The rig consisted of a top and bottom plate with two concentric holes of 2.4 mm diameter to match the outer diameter of the tubing. The parts were cut using a CO₂ laser and were made from 2 mm acrylic. The two plates were separated by a spacer by 2 mm to allow the array to be positioned between the two plates. The spacer was also cut from 2 mm acrylic using the CO₂ laser. The top tube was connected to a Hamilton 250 µl gastight syringe which was driven by a Harvard Apparatus Syringe pump. The bottom tube was directed to a waste container or well plate if necessary.

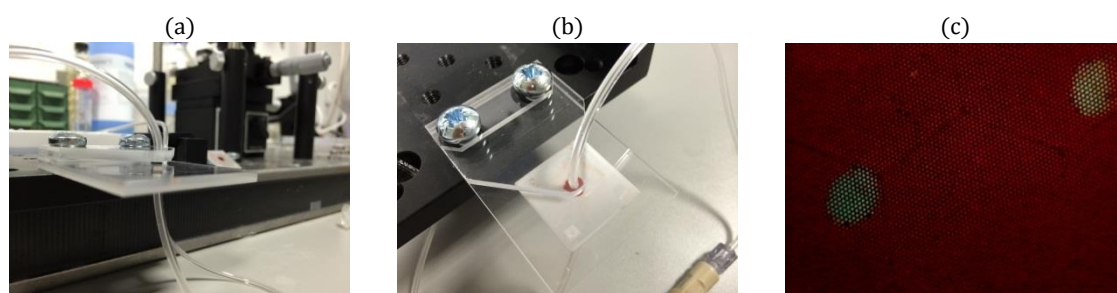


Figure 3.30 Proof of concept rig used to couple two tubes with the array. (a) shows a side profile of the two tubes aligned before the array is introduced. Image (b) shows the introduction of the array and (c) shows two separate recoveries from the array. Food colouring is used here to demonstrate the recovery of certain pores

From Figure 3.30 the recovery of a particular portion of capillaries is shown. The oval shape of the recovery is due to the manual application of force to each tube to seal with the array. This application of force deformed the normally circular inner diameter of the silicon Tygon™ tubing. However it can be seen that the shape is well defined which would indicate the water passed through the tubing followed the path intended by coupling the tubing to the array.

To further investigate the concept of coupling the array to two tubes either side, a new rig was designed. This second revision also used the 800 µm ID silicon tubing but removed the manual nature by which the tubing was coupled with the array.

The main design element with this concept is the screw thread feed wheel. The thread on either side of the wheel is opposite to each other i.e. one is a left hand thread while the opposite thread is the standard right hand thread. When the wheel is rotated, as shown in Figure 3.31(a), the jaws of the rig move in opposite directions. This results in the jaws moving in opposite direction, bringing the tubing together or apart.

The jaws were 3D printed, with the opening for the tubing designed to provide a friction fit. The tight tolerances allowed the tubing maintain its circular profile when pressure was applied during coupling with the array.

The feed wheel was turned on a lathe from 30 mm aluminium rod. The threads were hand cut using left and right hand M8 dies. The guide rod at the rear of the jaws acted as a guide to maintain the alignment. Due to the opposite threads the jaws tended to twist in opposite directions when the feed wheel was turned, thus requiring the need for the guide rod. The guide rod was machined using a lathe also, from 20mm aluminium rod.

The frame which all components were attached to was cut using a CO₂ laser. The material used was once again acrylic. The structure is formed in 3 sections, with the top and bottom section comprising 5 mm black acrylic. The middle spacer layer was cut from 6 mm clear acrylic, see Figure 3.31 (a) & (b).

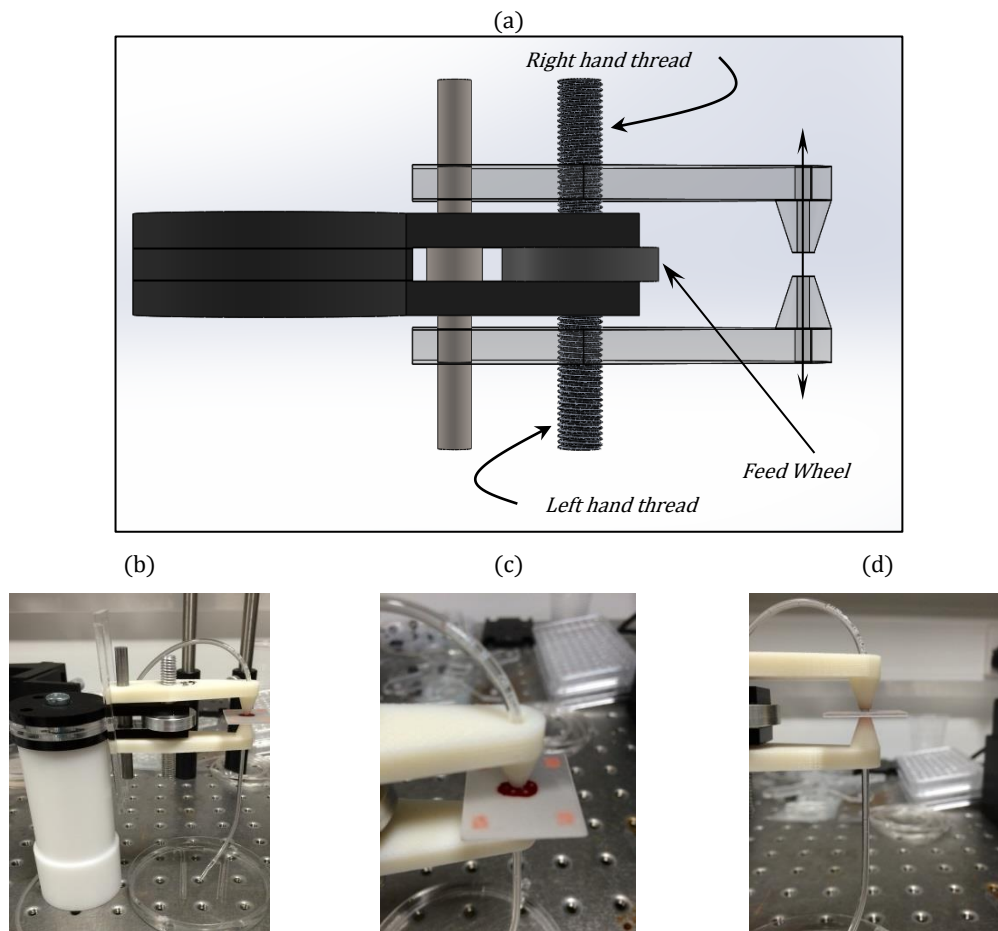


Figure 3.31 Revision of coupling mechanism for Tygon tubing to the array. (a) describes a 3D model of the apparatus with the jaws shown in wireframe for illustration. (b) demonstrates the assembled structure with the array in place between the jaws. (c) and (d) show close up images of the jaws in contact with the array.

The results of experiments using this improved experimental rig are presented in Figure 3.32 below.

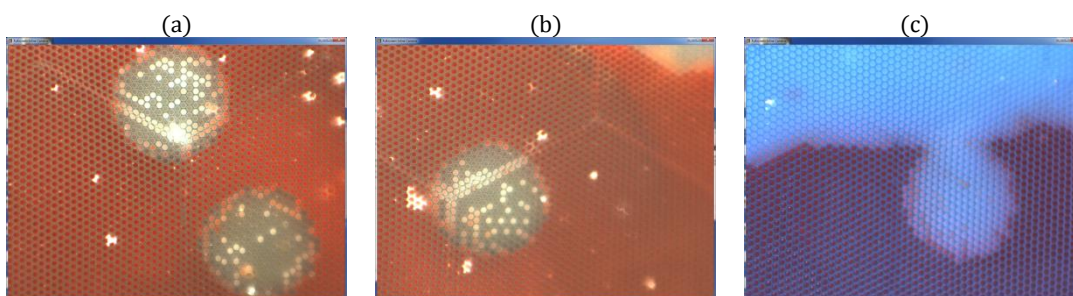


Figure 3.32 Results from testing with rig from Figure 3.30. All images show the ID has been maintained and that the capillaries encompassed within the ID are recovered.

Figure 3.32 demonstrates, using food colouring that the revised experimental rig allowed better control of the application of pressure to seal with the array. This resulted in good recovery of the food colouring. By flushing 100 μL of deionised water through the tubing and subsequently through the array, with a flow rate 200 $\mu\text{L}/\text{min}$, each of the experiments in Figure 3.32 show almost total clearance of the food colouring from the array. The waste was then collected in a petri dish below, with a diluted red colouring visible in the water.

3.4.2 HRP Recovery to Investigate Efficiency

To further look at the recovery efficiency, as before the array was loaded with HRP. Based on the area covered by the 800 μm ID of the tubing, 250 capillaries were targeted within the ID.

With each capillary holding 1.2 nL, 250 capillaries represents 300 nL. Based on this assumption a dilution of 300 nL in 100 μL was used as a control. A dilution in 10 μL was also used for comparison. To achieve this, 300 μL of HRP was added to 100 mL of deionised water and mixed, taking 100 μL of this mixture to provide the 300 nL/100 μL control. In Figure 3.33 the control dilutions of 300 nL/100 μL and 300 nL/10 μL are loaded in wells B2 and E2 respectively.

Wells B2-B6 and E2-E6 inclusive were initially loaded with 100 μL of TMB substrate before the addition of the controls. Wells B3-B6 inclusive were then loaded with a further 100 μL of deionised water that was passed through the tubing and the array. The same process was repeated for wells E3-E6, except with a 10 μL volume of deionised water.

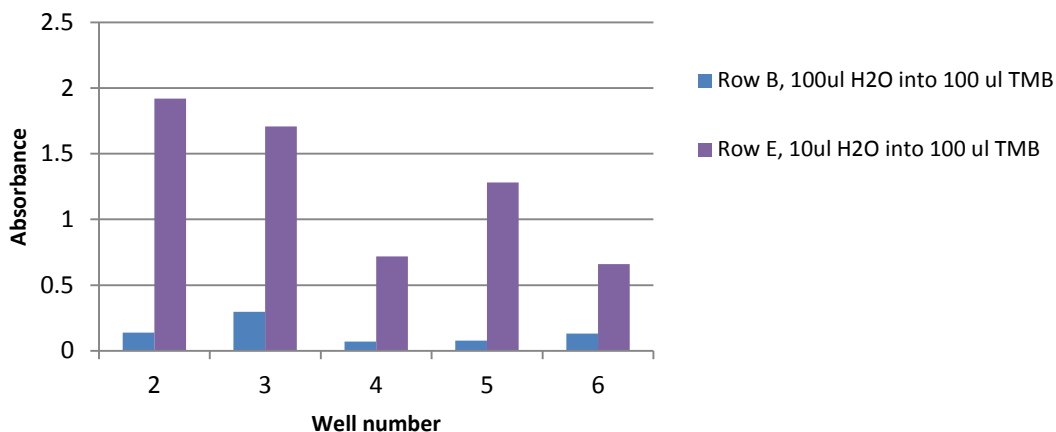


Figure 3.33 HRP recoveries with different dilutions. From the image opposite, well number 2 in both row B and E is a control. Wells 3-6 are actual recoveries of HRP from the array into the well plate. (rows G and H can be disregarded)

Glass Capillary Coupling with Array Design and Fabrication

With the concept demonstrated using a large ID tubing, the next challenge was to design a system capable of evacuating a single capillary. To that end, a device was designed using thick walled micro-bore tubing. With an outer diameter of 3 mm, inner diameters of 25 μm up to several hundred microns were available from Vitrocom Inc.

For this experiment the upper of the feed capillary had a 25 μm ID. A 20 mm section of the 300 mm rod supplied was cut with a ceramic grinding disk. Subsequently both ends were polished until flat and smooth, removing any scratches that occurred during machining.

The finished section was then inserted to the custom made aluminium sleeve. The sleeve had an ID of 3mm also, with a tight tolerance relative to the glass capillary. A thin layer of Araldite epoxy resin glue was applied to the outer surface of the capillary. Once the glue was applied the capillary was inserted into the aluminium sleeve.

The sleeve for the feed capillary had a counter bore hole at one end. The counter bore allowed a 10-32 UNF thread to be applied to this ID. The thread accommodated the fluidic

connections to couple the glass capillary to the syringe pump. As described in Methods 2.1.4, the HPLC fluidic connection tightens a flat bottomed flange onto the flat end of the glass capillary, creating a high pressure seal and a continuous fluidic path from the PEEK tubing to the glass capillary

For the collection capillary of 25, 75, 125, and 200 μm inner diameter were tested. All capillaries were tested by coupling the feed and collection capillary together and passing liquid through. The 200 μm capillary performed best thus was chosen for this experiment. The OD is the same at 3 mm with a 40 mm section length. The aluminium sleeve is almost identical, with the exception of the counter bore. The collection capillary remained open as it was directed to the well plate below. Therefore the fluidic connection is not required.



Figure 3.34 3D models describing how the concept will be assemble. The white part in both images was 3D printed with the aluminium sleeves and capillaries aligned concentrically. The array is intended to be placed between the two capillaries. The green objects modelled are standard HPLC 10-32 UNF threaded connectors.

Figure 3.34 describes the concept using 3D models. The physical objects are shown in Figure 3.35. The feed capillary can be seen in image (a) with the collection capillary shown in image (b). The fully assembled rig is then described in Figure 3.35 (c) and (d).

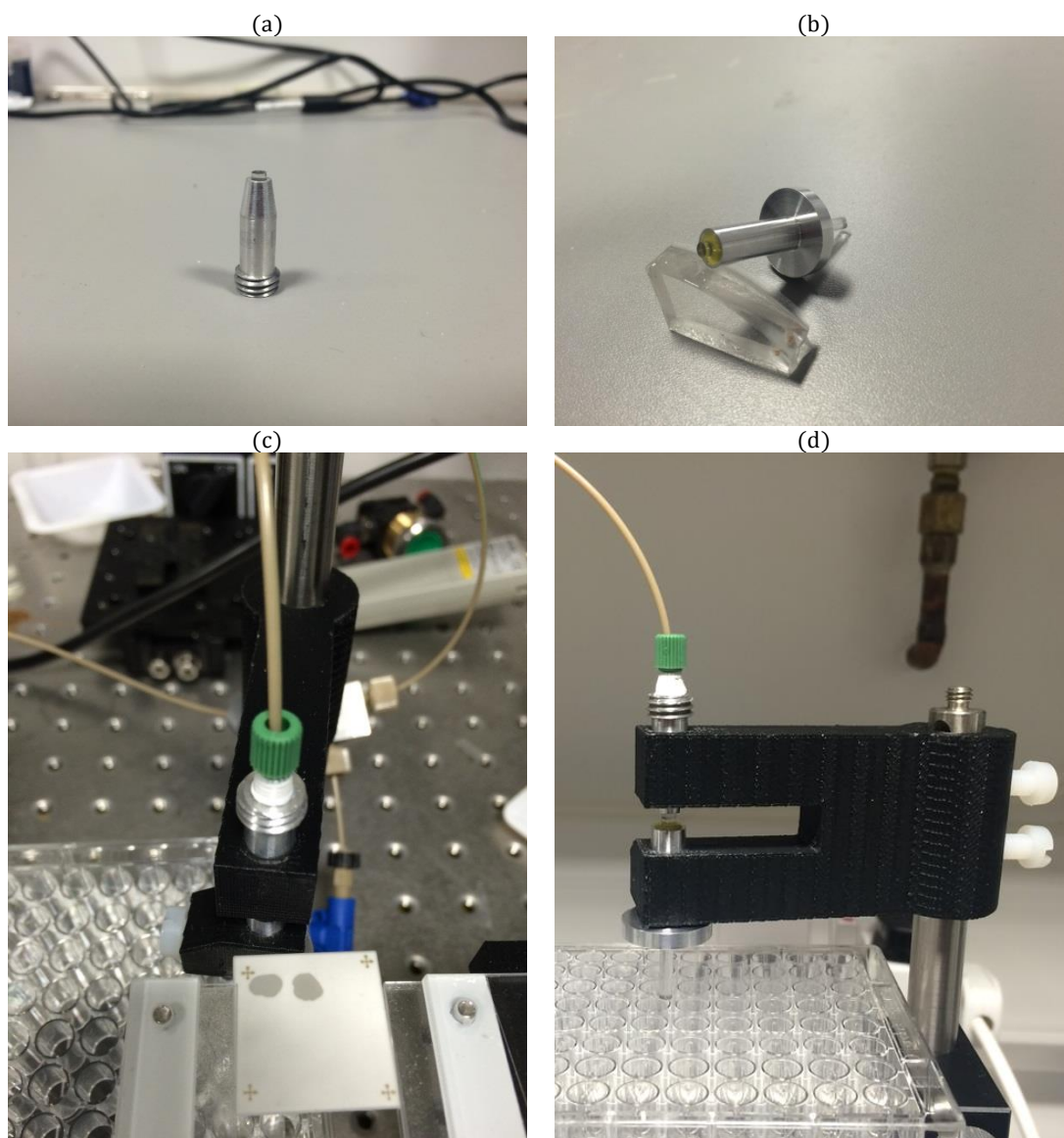


Figure 3.35 Images of liquid jet assembly. (a) Image of the feed capillary assembled within the aluminium sleeve. (b) Image of the collection capillary also assembled within its aluminium sleeve. The tip of both capillaries can be seen protruding from the sleeve. The open end of the collection capillary can be also seen protruding past the collar of the sleeve. (c) and (d) describe the assembled rig, with (c) including the array.

As was the case with the air jet previously described, a pressure relief valve was included to relieve any back pressure on the system. It was observed that as the syringe pump delivered the required volume and stopped pumping, the latent pressure would remain and liquid would continue to be ejected from the capillary. The back pressure was not adequate to form a jet with the liquid tending to seep from the capillary and gather on the array. By including a valve that released any build-up of pressure, reduced to seeping post recovery.

3.4.3 Glass Capillary Cell Recoveries

The results below show the recovery of cell from the array using the glass capillary concept from Figure 3.35. A cell concentration of 5×10^{-6} cells which according to a Poisson distribution should give ~ 5 cells per capillary. A 10 μL droplet of the cell suspension was pipetted onto the array in 2 different locations; see Figure 3.35 (c). The array was adjusted to align the first droplet of cell suspension with the glass capillaries. Once in position the array was lowered onto the collection capillary which remained fixed by means of a nylon retaining screw. The retaining screw tightened on the aluminium sleeve to maintain the position of the capillary.

The feed capillary was then lowered onto the array. In theory the feed capillary was coupled with a single capillary within the array and the collection capillary. A limitation of this system was the inability to accurately align the two capillaries with the array capillary. With both capillaries in contact with the array, while maintaining a downward force on the feed capillary, the syringe pump was activated. 200 μL of filtered PBS was passed through the feed capillary with a flow rate of 400 $\mu\text{L}/\text{min}$ and when aligned accurately, the PBS passed through the array and collection capillary and was collected in the well plate below.

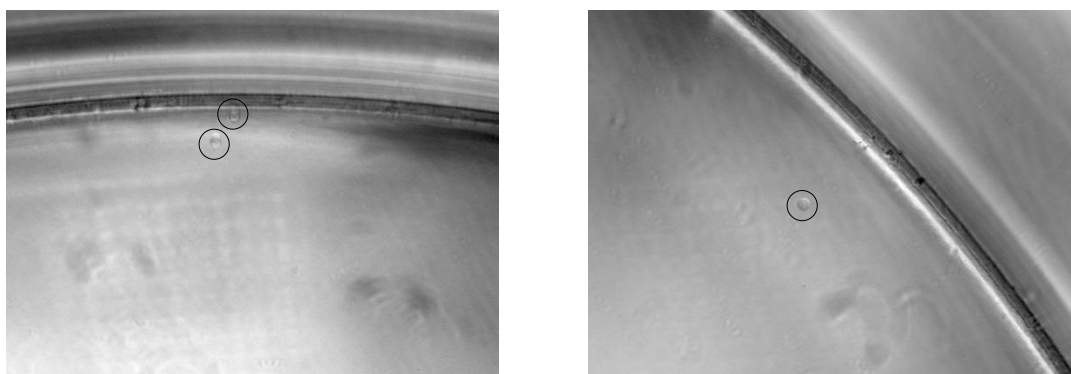


Figure 3.36 Cell recovery experiment 1 using micro-bore capillaries coupled to the array. A selection of the cells recovered are highlighted and amounted to 16 cells in total in the well. Images taken at 10X magnification.

The results shown in Figure 3.36 show the successful recovery of cells by coupling two glass capillaries to the array. 16 cells were recovered in this experiment.

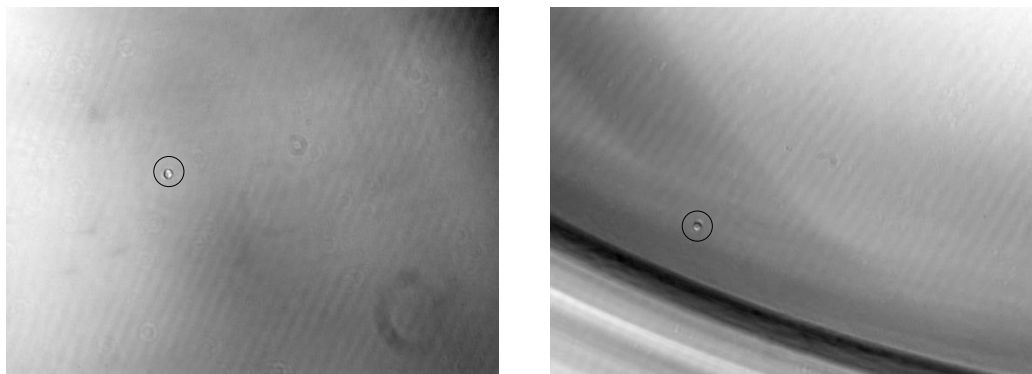


Figure 3.37 Cell recovery experiment 2 using micro-bore capillaries coupled to the array. A selection of the cells recovered are highlighted and amounted to 20 cells in total in the well. Images taken at 10X magnification.

Experiment two from Figure 3.37 also demonstrates successful recovery of viable cells from the array. 20 cells were counted in the well post recovery. Once again this is higher than the expected ~ 5 cells per capillary based on the Poisson distribution.

The excess number of cells recovered could be due to a number of factors. While the Poisson distribution suggests ~ 5 cells per capillary, the loading of the cell suspension into the array could introduce significant error. If the cell solution is not mixed well enough and the $10\ \mu\text{L}$ droplet to be placed on the array is drawn from a portion of the suspension with an artificially high concentration, the number of cell per capillary may be higher than expected.

It is also a possibility that due to the larger ID on the collection capillary, a number of the surrounding capillaries could be drawn into the well plate also. While the feed capillary should only target a single capillary due to its $25\ \mu\text{m}$ ID, the $200\ \mu\text{m}$ collection capillary will target at least 4 capillaries. As the liquid begins to flow through the collection capillary it is suggested that the surrounding capillaries could be evacuated also.

3.5 Discussion

The body of work reported here is part of a wider effort to improve and enable the DiCAST technology as described in the Introduction and Background. DiCAST has the potential to revolutionise antibody and drug discovery technology and as such truly is a disruptive technology. By being able to assay each ASC individually and recover each cell with a high degree of accuracy is seen as critical to its success.

As a concept the technology is simplistic. By placing each ASC within a “straw”, any potential targets would be identified and “blown” out of the straw. At 40 μm in diameter each and tightly packed into an array of hundreds of thousands of “straws”, recovery of the cells becomes a challenge. With the development of the alignment strategy, a method of mapping each capillary with high resolution accuracy was described. The permanent photoresist structure within the capillaries, allowed repeatable and reproducible results through which the assay surface could be mapped to the custom alignment software and recovery instrument. The alignment structures provided orientation and reference points to facilitate this mapping. The “map” could then translate each positive binding ASC from the assay surface to the capillary array, communicating with the recovery platform the precise location of each capillary to be recovered. The addition of the alignment structures facilitated the further development and realisation of the DiCAST platform.

The use of a laser as part of the recovery system was identified as a possible source of stress upon the cells with the array. Reported here are two alternatives that remove the need for the use of a laser, thus removing the potential stress on the cells, any safety implications associated with the use of lasers and reducing the potential footprint of the final instrument. The micro air-jet was developed as the first alternative approach. By moulding a 25 μm orifice in PDMS, and forcing compressed N_2 through the orifice a tiny jet of compressed N_2 was formed. Initial results show that individual capillaries can be targeted and interrogated without disturbing the neighbouring capillaries, but reproducible and reliable recovery proved elusive. With such small volumes, evaporation and surface tension are suggested as two phenomena that hinder the recovery of cells from the capillaries by such a method.

Following the discovery of the inconsistencies with the air-jet method, a liquid jet approach was investigated. Proof of concept experiments using large inner diameter tubing suggest the concept was feasible, demonstrating the recovery of bundles of adjacent capillaries. By designing and building a bespoke glass capillary recovery system,

it was demonstrated that by flowing a buffer solution through a single capillary and the contents of the capillary could be successfully collected. With similar inner diameters to that of the capillaries, the contents from an array were collected by coupling two glass capillaries to the array. The concept was based on reducing the stresses on the cells and removing the effects of evaporation and surface tension. As a result, the successful recovery of cells from within the capillaries was reported.

Taking advantage of the open ended micro capillaries, DiCAST promises the ability to grow and recover cells individually and in a non-competing environment. Providing this environment for analysing individual cells will lead to greater specificity and extremely high throughput of potentially millions of cells. By removing the need for traditional or more common single cell techniques such as micro-engraved micro-wells (Love et al. 2006; Frisk et al. 2011), micro fluidics (Grünberger et al. 2014; Zhu et al. 2012) and micro manipulators greatly increases the throughput of the DiCAST technology.

Through the development of the alignment structures and alternative recovery methods, this work has helped advance the possibilities of DiCAST becoming a revolutionary new antibody selection tool.

Chapter IV

Whole Blood Cellular Fraction Extraction with Active
Trapping (CLEAR)

4.1 Introduction

As discussed in Chapter 1, the work of this thesis comprises two elements (i) contribution to the DiCAST project already described in Chapter 4 and (ii) work which contributed to an Enterprise Ireland commercialisation fund project, MobiMate, which aimed to design a point-of-care fluorescence-based polymer microfluidic chip for detection of CRP, a marker for infectious disease, focusing initially on rheumatoid arthritis. The chip would take a blood sample, separate the plasma from the cellular constituents, direct the plasma to an assay region in the chip and perform a fluorescence-based assay which would be interrogated by a mobile phone. The main elements which are the focus of this thesis are (a) the development of the novel blood separation chip and associated microfabrication and microfluidics (b) the integration of the assay chamber based on sample flow and (c) initial work on the assay with optical detection using a laboratory-based instrument. Because of ineffective and significant delays often involved with blood testing procedures, the POC blood testing market has experienced a significant boom in recent years. The vision is to enable testing in decentralised or non- expert /healthcare professional settings. This facility for accurate, remote health monitoring and testing will eliminate the need for frequent and inconvenient visits to the hospital, reducing costs and improving quality of care. This is the main motivation behind this project.

4.2 SIMBAS Explained

The starting point for the development of the blood separation element of the chip was the SIMBAS concept (Dimov et al. 2011) which uses degas-driven flow, which was developed as a method of separating plasma from a whole blood sample and achieving this without the need for external pumping or power requirements. In this work, the SIMBAS concept was further improved and modified as described below, and the second part of this work explored how this concept could be used to integrate a fluorescence-based immunoassay, using a whole blood sample directly from a finger prick, onto a modified SIMBAS-based chip for a point-of-care application. By removing red and white blood cells in this way, signal to noise ratio (SNR) is improved and the dependence on large bench top laboratory equipment e.g. centrifuges, is removed. For a conventional assay, carried out in the laboratory, the blood components are normally separated using centrifugation. The stand-alone nature of degas driven flow, an integral part of the SIMBAS concept, removes the need for external pumping or actuation. The modified SIMBAS chip discussed in this Chapter is referred to here as CLEAR and is explained in the following sections.

4.2.1 Trench Filter Operation

SIMBAS employs a trench as the filter for separating cells from the whole blood sample. Figure 4.1 demonstrates the principle of operation of the SIMBAS platform, showing the inlet channel for sample introduction, the trench filter for separation and the outlet channel from the trench filter for extraction of separated plasma.

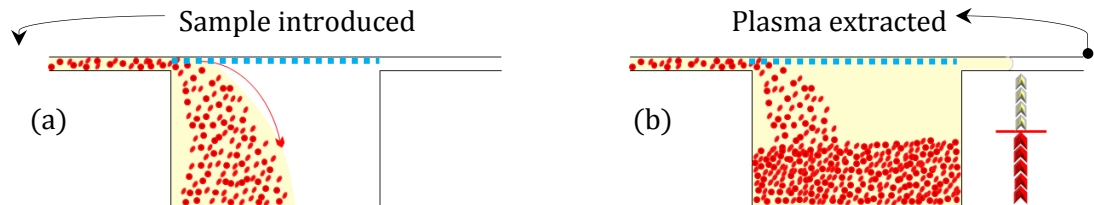


Figure 4.1 As the sample is introduced to the trench (a), the red blood cells (RBCs) tend to gravitate to the bottom of the trench. As the trench fills (b), the RBCs remain at the bottom of the trench and plasma occupies the top portion of the trench. Once the trench fills to the same height as the outlet, plasma is withdrawn, leaving behind the haematocrit portion of the whole blood sample. Blue dashed line shows location of hydrophobic coating on the top surface the trench filter which assists the sedimentation of the RBCs

By removing the chip from the low pressure of vacuum environment, the chip becomes active. As gas rushes back into the evacuated micro cavities of the porous PDMS, a negative pressure is generated in the channel of the chip to draw the sample through the channel network. Upon activation of the chip, a blood sample is placed on the chip. The sample is transported to the trench filter via the inlet channel. At this point the hydrophobic coating (e.g. what material?) on the top surface of the trench filter restricts the flow of the sample across the top surface of the trench filter, forcing the sample to the bottom of the trench. As the trench fills with the whole blood, the cells sediment to the bottom of the trench filter, under gravitational force. With the cells accumulated on the bottom surface of the trench, a plasma layer forms in the upper section of the trench. As the trench filter reaches capacity, the plasma layer that has formed is extracted via the outlet channel, with the cellular components of the sample remaining in the trench. Typical dimensions of the chip, as developed according to (Dimov et al. 2011), are 2 mm diameter x 2 mm depth with a channel of 50 μm x 250 μm .

4.2.2 Limitations of SIMBAS

Increase of the SNR for the assay is the main motivation for the removal of the cellular constituents from the whole blood sample. Also, removal of the large cellular components will reduce the likelihood of nonspecific binding or blocking of the capture sites, thus improving the assay signal further. Finally, in the case of a fluorescence-based assay, clear plasma forms a more favourable assay medium by minimising optical scattering and intrinsic fluorescence of the cellular constituents.

While SIMBAS achieves this, the possibility of re-suspension of the cellular constituents is a major limitation of the technology. Separation is dependent on the platform remaining stationary and in a horizontal orientation. Should the platform be disturbed or agitated during the process, the separated cellular constituents would become re-suspended, re-introducing them back into the plasma channel. These steps are illustrated below in Figure 4.2.

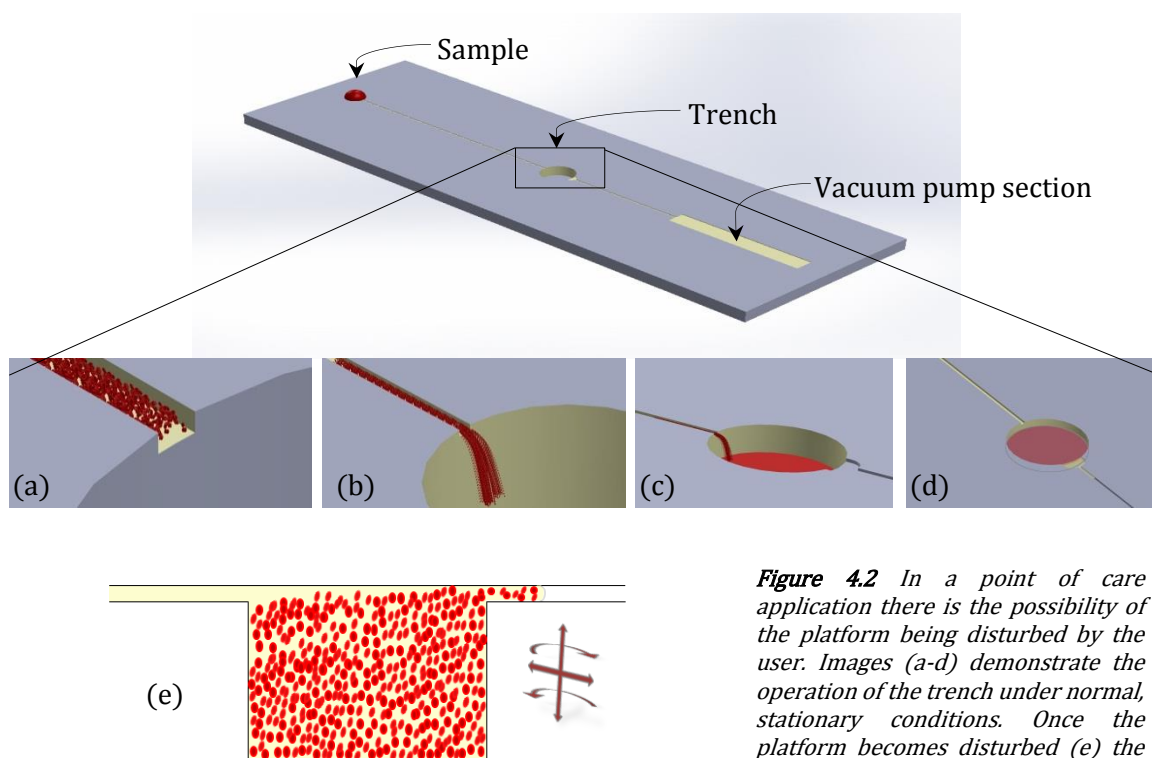


Figure 4.2 In a point of care application there is the possibility of the platform being disturbed by the user. Images (a-d) demonstrate the operation of the trench under normal, stationary conditions. Once the platform becomes disturbed (e) the cellular portion of the sample becomes re-suspended and can migrate to the plasma channel.

4.3 CLEAR Rationale and Implementation

For CLEAR, cellular fraction extraction using active trapping, it was required to remove the sedimented cells from the trench to eliminate the possibility of interference with the assay. To achieve this, a novel active trapping system was designed, which builds on SIMBAS by providing a more robust method of managing sample constituents following separation. Specifically, this new approach makes use of the existing SIMBAS separation mechanism, i.e. gravitational sedimentation, implemented using a trench, but includes an additional channel at the base of the trench which is pumped under degas driven flow also. This facilitates active removal of particles from the base of the trench to a reservoir and significantly reduces the likelihood of re-suspension following movement of the chip.

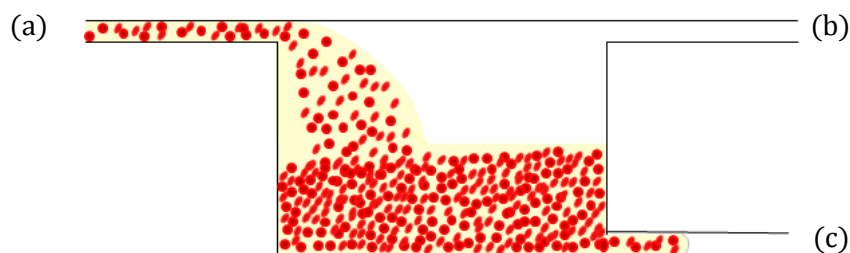


Figure 4.3 In the SIMBAS configuration, Figure 4.2 (e), the whole blood sample filled the trench from the bottom up. Once filled, the RBC's remained in the bottom of the trench and could be re-suspended if agitated. For CLEAR a channel was added (c) at the bottom of the trench to remove the RBC's to another location, removing the possibility of re-suspension into the plasma channel (b).

However, with SIMBAS filling the trench from the bottom up, inclusion of the cellular fraction extraction channel at the base of the trench (Figure 4.3) would inhibit the ability of the trench to fill to capacity. In this configuration, the cellular fraction extraction channel would encourage the emptying of the trench before the plasma reached the upper extraction channel.

4.3.1 Proof of Concept: Active Trapping of Beads Suspended in a Liquid Sample

Figure 4.4 shows a schematic representation of a micro-fluidic chip that was fabricated to demonstrate the CLEAR concept. This chip comprised of a sample inlet channel of 1 mm x 0.05 mm, a trench filter cylinder structure with 2 mm diameter and 2 mm height, and two outlet channels also 1 mm x 0.05 mm. The height of the channels is dictated by the thickness of the 0.05 mm PSA double sided tape. The two outlet channels were connected to a Harvard Apparatus Pico Plus syringe pump. A flow rate of 5 $\mu\text{l min}^{-1}$ flow rate was controlled by the pump. A suspension of 20 μm polystyrene beads in water was used as a sample for the chip.

Following introduction, the sample was transported to the trench filter and the beads were observed to sediment to the bottom of the trench filter. As the beads sedimented, they were sequestered to the outlet and away from the trench, reducing the likelihood of re-suspension into the top channel. Figure 4.4 shows a number of images obtained from the chip during these experiments. Figure 4.4(A) shows the beads at the bottom of the trench filter. Taken at 10X magnification this image is focused on the bottom surface of the trench showing sedimented beads. The channel leading to the outlet C can be seen at the right side of the image with direction of flow indicated by an arrow. With the water/beads suspension now separated, the water only portion is observed in Figure 4.4(B). Figure 4.4(C) shows the outlet with the collection of beads that the active channel had sequestered from the trench filter to the outlet. While carrying out this test, it was

observed that there was a tendency for the level of fluid in the chamber not to reach the top hence impeding the flow of plasma through the upper channel. This was the motivation for the inclusion of the sloped chamber in the final design.

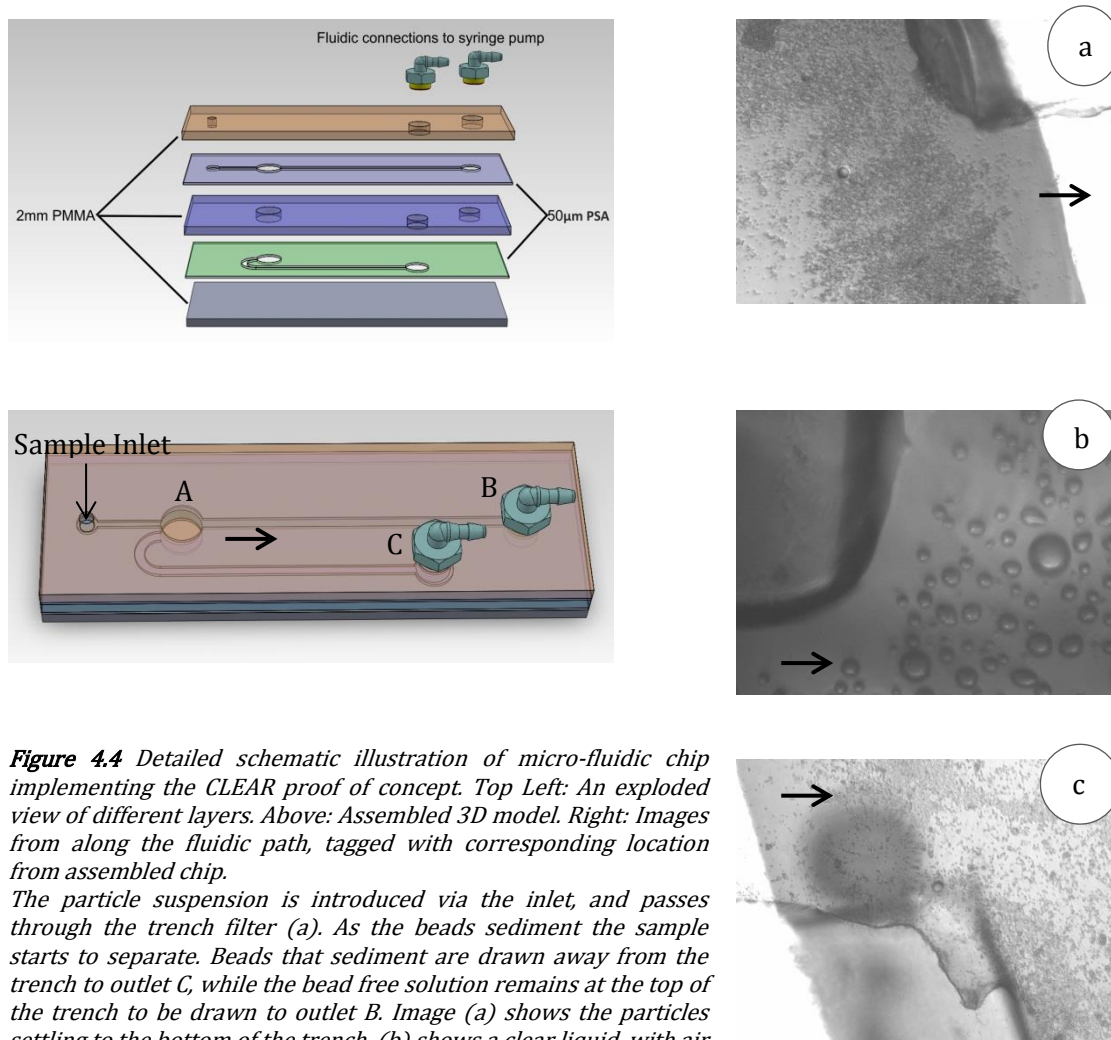


Figure 4.4 Detailed schematic illustration of micro-fluidic chip implementing the CLEAR proof of concept. Top Left: An exploded view of different layers. Above: Assembled 3D model. Right: Images from along the fluidic path, tagged with corresponding location from assembled chip.

The particle suspension is introduced via the inlet, and passes through the trench filter (a). As the beads sediment the sample starts to separate. Beads that sediment are drawn away from the trench to outlet C, while the bead free solution remains at the top of the trench to be drawn to outlet B. Image (a) shows the particles settling to the bottom of the trench, (b) shows a clear liquid, with air bubbles visible at corresponding outlet B while (c) shows the particle solution at corresponding outlet C.

4.3.2 Trench Modifications and Redesign

To overcome the possibility of the trench not reaching capacity before the plasma portion is extracted, the CLEAR platform included a redesigned trench incorporating a slope at the entrance. As the whole blood sample enters the trench filter the sloped surface allows for gradual filling of the trench. The sample remained in contact with both the sloped surface and the top surface of the trench. This allowed the trench to fill uniformly and encouraged a laminar flow profile through the trench. This resulted in the upper and lower extraction channels being presented with the sample simultaneously, by which time the cellular constituents should be sedimented and therefore separated. Figure 4.5 demonstrates the sloped trench principle, where a number of angled slopes were tested. Once the sample

reaches the end of the trench, the RBC's are sedimented and the plasma is drawn off the top of the trench. The RBC's are removed to a different location on chip so re-suspension cannot occur.

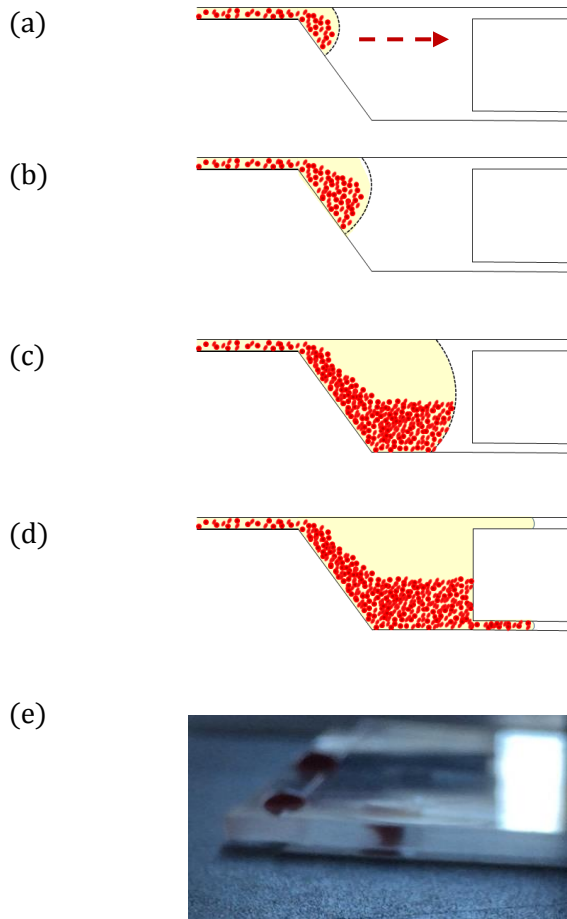


Figure 4.5 Modified trench schematic As the sample flows into the trench (a), the slope ensures that the sample maintains contact with the sloped surface of the trench and the top surface of the trench (b). As the sample continues to fill the trench the cellular components sediment (c), separating from the plasma. Finally, the sample is extracted from the trench (d) as separated plasma and the unwanted cellular components.

(Direction of flow - - - ->).

Image (e) is a side profile of a chip under flow, with the blood following the profile described in (a-d) above.

Another consideration for implementing a slope is the effect on the flow profile of the blood sample as it transitioned from the micro-channel to the larger macro-scale trench. It has been reported that where the blood flow encounters a large step within a blood vessel, e.g. in an aneurysm, the flow is disturbed and a recirculating effect is observed at the near portion of the step (Skilbeck et al. 2004; Charoenphol et al. 2012; Hall & Calt 2014; Chiu & Chien 2011). This recirculating and turbulent effect, it is proposed, would inhibit the sedimentation of the RBC's and hinder the successful extraction of plasma as a result.

4.4 CLEAR Dual-layer Fabrication

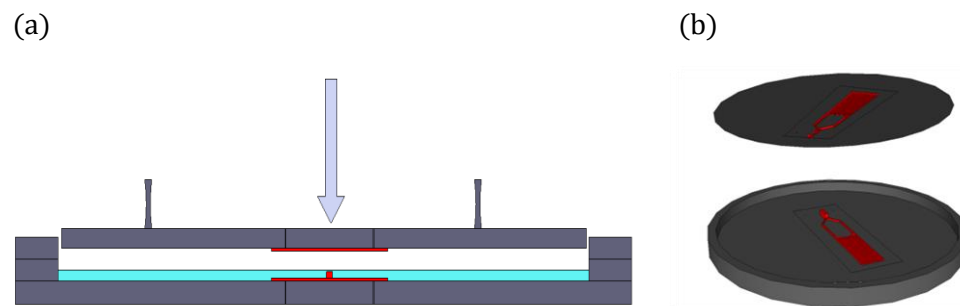
As described in Chapter 3: Methods, PDMS is typically moulded as a single layer, and where multiple layers are required numerous single layers are bonded together (Zhang et al. 2010; Wu et al. 2003; Wu & Lee 2013). Here is described a single step, two layer

fabrication process, whereby a dual layer micro-fluidic chip is fabricated in a single moulding step.

4.4.1 Preparing the Master

All channel structures were fabricated using a high precision double sided tape, ARcare® 92712 (Adhesives Research Inc), with an overall height of $48\text{ }\mu\text{m}$ ($\pm 2\text{ }\mu\text{m}$). The tape was easily configurable and highly reproducible in terms of a controlled height and shape for channel construction and allowed for rapid prototyping. In comparison to typical photolithography processes, every iteration of channel design would necessitate a new mask, and subsequently a new silicon wafer master, the ARcare® 92712 double sided tape provided a quick and cost effective alternative.

The channel structures were formed using a Graphtec RoboMaster Pro™ (Graphtec America Inc.), which uses a knife to trace a profile on the ARcare® 92712. The trace profile is designed and drawn using AutoCAD software, see Figure 4.8.



— PDMS — Channels and trench “via”

Figure 4.6 Schematic representation of the moulding process. (a) Demonstrates how the channels (shown in red) are connected by the trench. The bottom channels are applied within a vessel. A transparent lid is then applied, carrying the top channel structure. The transparent lid allows the top and bottom channels to be aligned via the trench. PDMS is then poured into the mould and baked

4.4.1.1 Pouring the Mould

A 10:1 mixture of Dow Corning Sylgard 184 (PDMS), was prepared (Dow Corning 2007). The resulting mixture was then degassed, by centrifugation at 3000 rpm for 3 minutes, before pouring into the mould.

As a result of the transparent acrylic lid, tiny air bubbles were observed when the PDMS was applied to the mould. Further degassing of the PDMS was required prior to baking because if allowed to remain, the air bubbles would expand during baking compromising the resulting channels.

At this point, the PDMS was baked at 65°C for > 4 hours. After baking, the mould was dismantled to remove the PDMS with resulting micro-fluidic channels now present. The channels were then inspected for any potential blockages and prepared for storage under vacuum until required for experiments. On occasion, some adhesive from the ARcare® 92712 remained within the PDMS channels and needed to be removed.

4.5 Optimisation of Flow Rate and Trench Dimensions

For the optimisation of the flow rate, the microfluidic platform was divided into two sections; the trench and channels post trench.

The trench dictated the volume of sample required for the chip to function as designed, but also was the structure within the platform where separation of the blood sample takes place. The channels post trench, including the degassed pump sections, dictated the flow rate and provided the capacity to receive and store the separated blood cells and plasma to avoid re-suspension or mixing of RBC's back into the plasma sample.

4.5.1 Trench Design

As illustrated in Figure 4.5, the CLEAR trench was designed to take on a rectangular cross section and include the addition of a slope at the front end of the trench. To investigate the hypothesis of the redesigned CLEAR trench a number of trench configurations were trialled.

The first key consideration looked at was the introduction of the trench and a number of angles were trialled, namely 40°, 50° and 60° slopes. Slopes less than 40° were too shallow and extended to far along the bottom surface of the trench, and therefore not investigated.

The next consideration for the design of the trench is the total length, along which sedimentation of the cellular components is allowed to occur and as a result separation is observed. Increasing the length of the trench ultimately increases the volume of the trench, thus increasing the volume of sample required to fill the trench. If the sample available is inadequate to fill the trench, the limited sample will not be able to travel along the trench as described in Figure 4.3. Due to its ambition as a point-of-care platform, CLEAR is designed with a volume similar to that taken via finger prick, limiting the sample volume to ~35 µl or less. It was necessary that the capacity of the trench was less than that of the total volume of sample added, to allow the trench to reach capacity, without introducing air to the system before separation was realised. Volumes of 10, 12, 15 and 18

μl were trialled, equating to trench lengths of 3.75, 4.25, 5.00 and 7.00 mm respectively. It should be noted that as the slope angle altered the volume of the trench was also altered. However, as the resulting volume did not drastically alter the volume, it was not deemed critical to the operation of the trench. In all cases the height and width of the trench were constant at 2mm each.

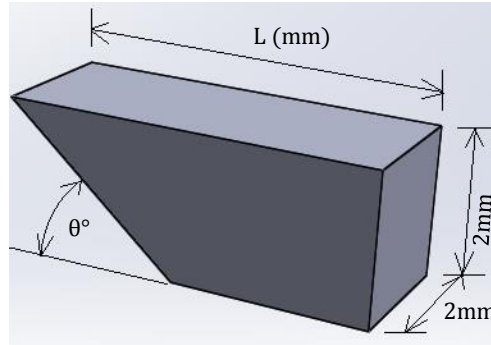


Figure 4.7 Illustration of the redesigned trench where alterations to the angle of the slope, θ , and the overall length, L , were investigated.

4.5.2 Degassed Pumped Section Considerations

The flow rate for the platform was controlled by the cross sectional area of the pump section at the end of the channels post trench. By increasing or decreasing the area available to the channel, the flow rate, could be increased or decreased respectively. Figure 4.8 illustrates the different cross-sections tested for the plasma channel at the top exit of the trench. The channel dimension in each case was 600 μm leading to a degas pump section of different cross sections. Channel (b) from Figure 4.8 was implemented for the RBC channel, varying only the plasma flow rate. While separation was the main motivation, the performance of the chip was also determined by the time taken to complete a sample draw. Here is where a compromise between trench volume and flow rate were required.

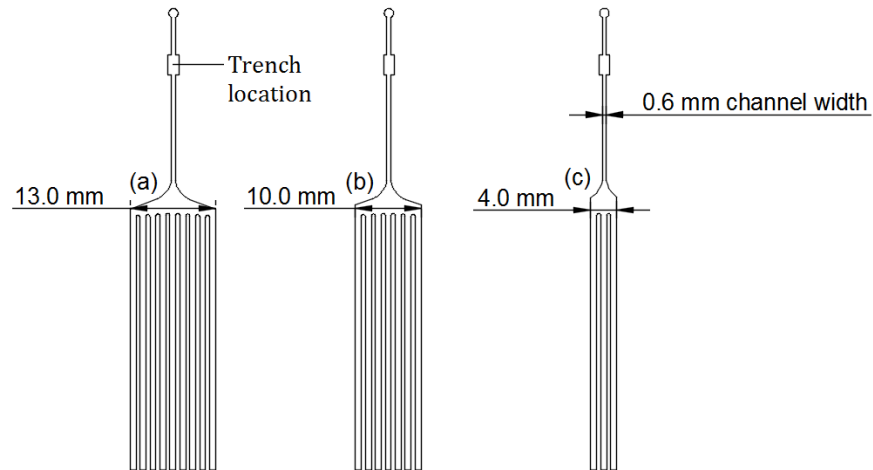


Figure 4.8 Three different channel dimensions used for the plasma extraction channel. In all cases the channel leading from the trench is $600\ \mu\text{m} \times 50\ \mu\text{m}$, with different degas pump sections adjusting the flow rate. (a) $13 \times 0.05\ \text{mm}$, (b) $10 \times 0.05\ \text{mm}$, (c) $4 \times 0.05\ \text{mm}$

When separation is observed and the presence of plasma within the top channel on the chip, the channel is no longer visible under the camera used during experiments, due to the change in refractive index at the interface of the Zeonor and the PDMS surfaces. As seen in the pre/post images in Figure 4.9 below, with no plasma present the channel outline is clearly visible and once the plasma fills the channel is no longer visible.

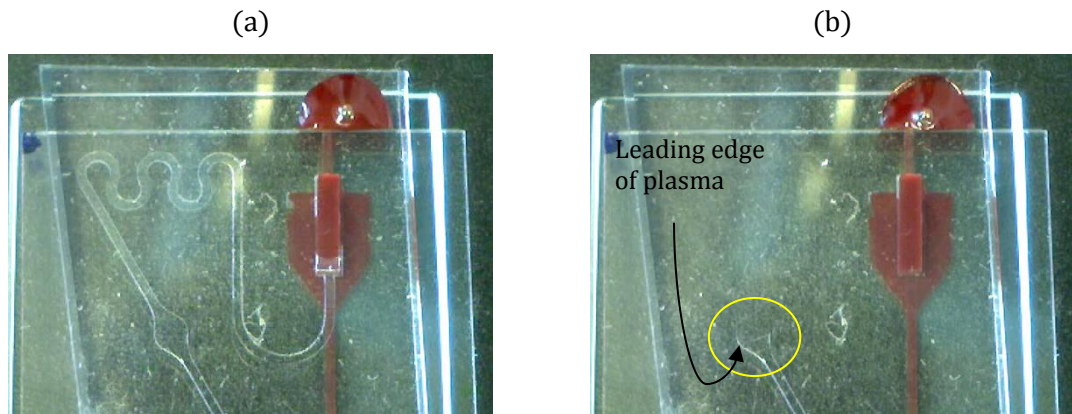


Figure 4.9 Image (a) shows the introduction of the whole blood sample with the trench almost filled. RBC's are actively being drawn away from the trench to avoid re-suspension. In image (b) the trench has filled and the plasma (meandering) channel is drawing separated plasma from the trench while RBC's continue to be segregated.

Upon completion the channels and the trenches have completely emptied. From Figure 4.10, the sample has passed fully through the trench and has move to the degas pump

section for storage and to ensure there is no chance of re-suspension of the cellular components back into the plasma portion of the sample.

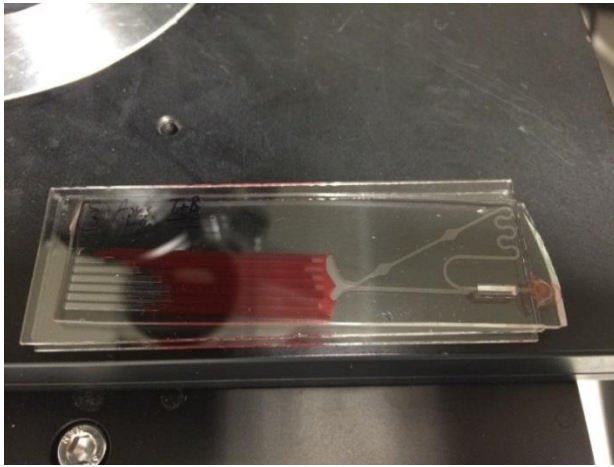


Figure 4.10 Image of chip post separation where the trench is completely emptied, with separate channel networks shown.

4.6 Quantification of RBC Separation

To quantify the effectiveness of the separation achieved, a selection of chips using the most suitable trench configuration as outlined in Figure 4.7 were tested. One blood sample was used for all chips. A cell concentration per mL was calculated using a hemocytometer to give an indication of the number of cells before separation was attempted. The blood sample was diluted to 1/1000 for the purpose of clarity while using the hemocytometer. The sample demonstrated normal levels of red blood cell concentration at 4.9×10^9 / mL.

The blood sample was then processed using four individual but identical CLEAR platforms. The separated plasma was removed from the chip for quantification of cell concentration / mL. A snapshot of the different chips showing the separate channels for RBC's and plasma are displayed in Figure 4.11. The resulting cell concentrations of the separated plasma compared with the whole blood concentration are plotted and shown in Figure 4.11.

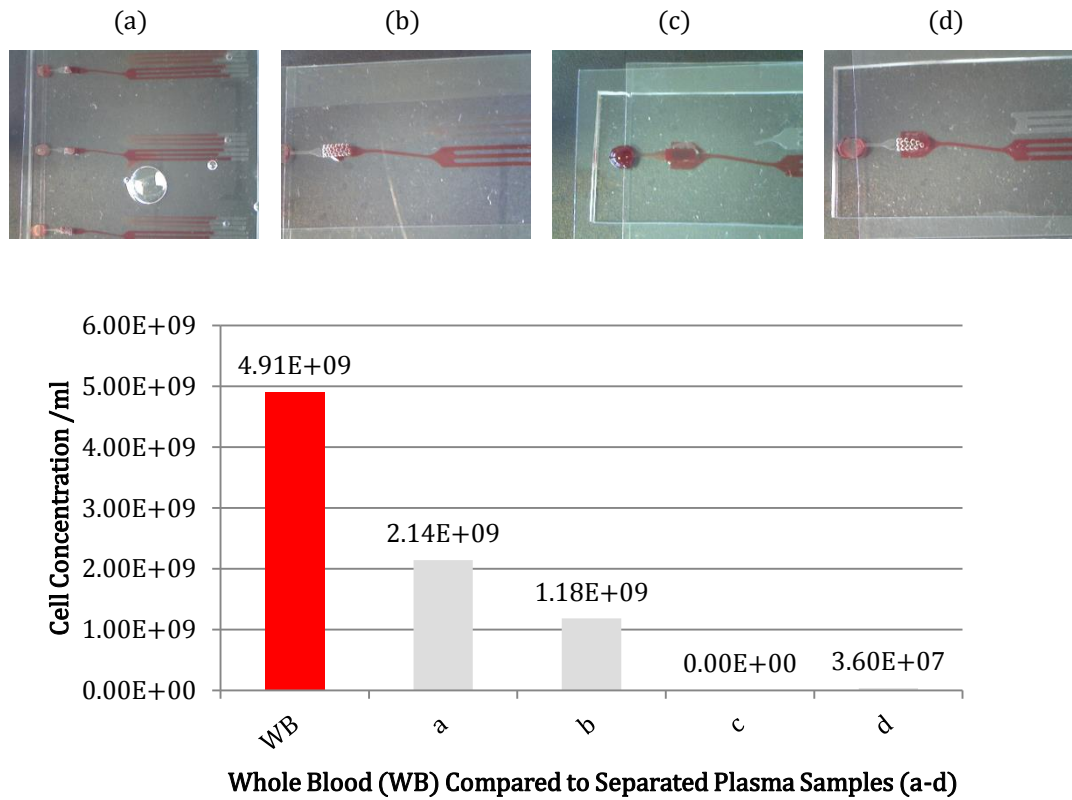


Figure 4.11 Separation efficiency of CLEAR.

Sample (a) performed the worst of all samples with sample (c) and (d) showing best performance.

4.7 Microfluidic Assay Application

The ultimate objective of the CLEAR project was to separate a whole blood sample, capturing the blood cells on chip whilst simultaneously performing an on chip immunoassay on the separated plasma to determine the C-reactive protein (CRP) levels in the sample. Dr Gemma Keegan (Zhang et al. 2015), Biomedical Diagnostics Institute, DCU, conducted all assay development and optimisation for eventual deployment on the CLEAR chip. In conjunction with Dr Keegan, we demonstrate the application of a fluorescence-linked immunosorbent assay (FLISA), under flow conditions, using a similar chip to that outlined in the separation sections previously. By adapting a standard FLISA to mimic the conditions of an assay under flow, Dr Keegan was able to correlate the assay result under flow and account for the hook effect discussed in following sections.

With time the largest constraint a compromise was reached to demonstrate the principle of a microfluidic FLISA using the CLEAR platform whereby elements of the assay were carried out off chip. The CRP assay was carried out under 'normal' traditional conditions in a 96 well plate to allow direct comparison and validation of the CRP assay before demonstrating the potential to perform the CRP assay under flow conditions on chip. Initially the assay was performed as a routine 2 step sandwich assay, which gave an indication of the dynamic range within which the assay was located and demonstrated that the antibodies were functioning as required. A single step sandwich assay was then performed, also in a 96 well plate, to demonstrate the assay could in fact be carried out without the need for multiple wash phases. Finally the assay was performed under flow, as a single step sandwich assay.

4.7.1 2-Step "Static" Sandwich Assay

As is normal practice for a sandwich FLISA performed in a 96 well plate, a combination of individual incubation, blocking and washing steps are performed. The protocol is optimised and developed to provide optimal conditions for antibody/ antigen interaction, to give the best signal possible. Capture antibody is given adequate time and incubated at ideal conditions to promote binding to the surface of the plate. Thorough washing is performed post incubation to remove any unbound proteins that might alter the eventual signal. To occupy any parts of the surface that did not bind with capture antibody, the surface is blocked and incubated again at ideal conditions. The plate is washed again. Antigen is added to bind to the available antibodies on the surface, again being allowed to incubate under ideal conditions. Again the plate is washed to remove any excess, unbound

antigen. At this point the secondary detection antibody is added, allowed to incubate and finally the plate is washed once more. Each step is controlled and optimised for the best results. Excellent results are achieved using this approach but the disadvantages are that it takes hours to achieve a result and requires a skilled personnel to perform the testing. Because of ineffective and significant delays often involved with blood testing procedures, the POC blood testing market has experienced a significant boom in recent years. The vision is to enable testing in decentralised or non- expert /healthcare professional settings. This facility for accurate, remote health monitoring and testing will eliminate the need for frequent and inconvenient visits to the hospital, reducing costs and improving quality of care. Here we aim to correlate a standard on-plate FLISA and a single-step FLISA under flow using the CLEAR degas driven chip.

The resulting assay curve is shown in Figure 4.12. The dynamic range obtained was 0.033–2.5 mg/L.

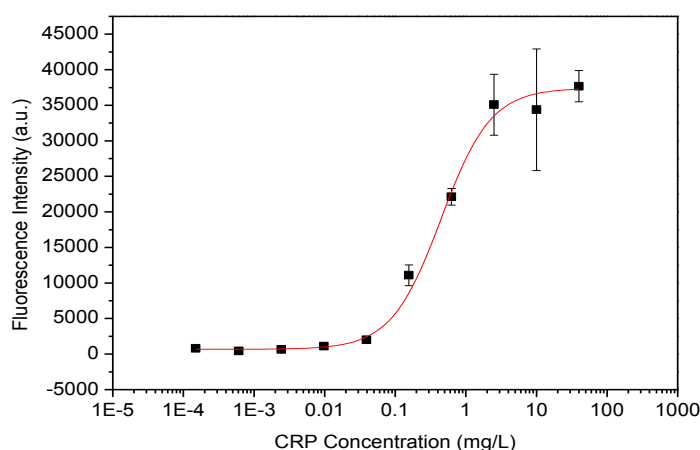


Figure 4.12 Two-step sandwich assay, with multiple wash steps and 1 hour incubation times

4.7.2 Single Step “Static” Sandwich Assay

The single-step assay here refers to the simultaneous addition of the antigen and detection antibody to the assay. The single step sandwich assay was performed in identical fashion to the 2-step assay, in all but one step. Following a modified single-step protocol, the CRP dilutions were pre-mixed with the DY647- α CRP detection antibody. CRP was prepared as $1/5$ dilutions of 50 μ g/mL, while 10 μ g/mL of DY647- α CRP was used.

CRP was successfully detected using the 1-step assay. Figure 4.13 shows that at higher concentrations of CRP the curve experiences a drop in fluorescent intensity, which is described as a “hook effect”.

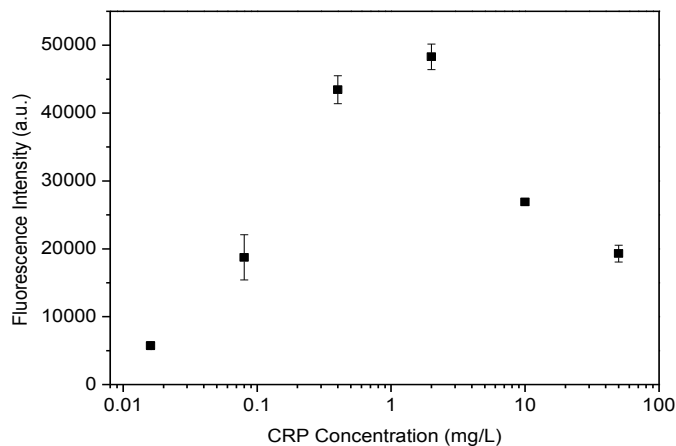
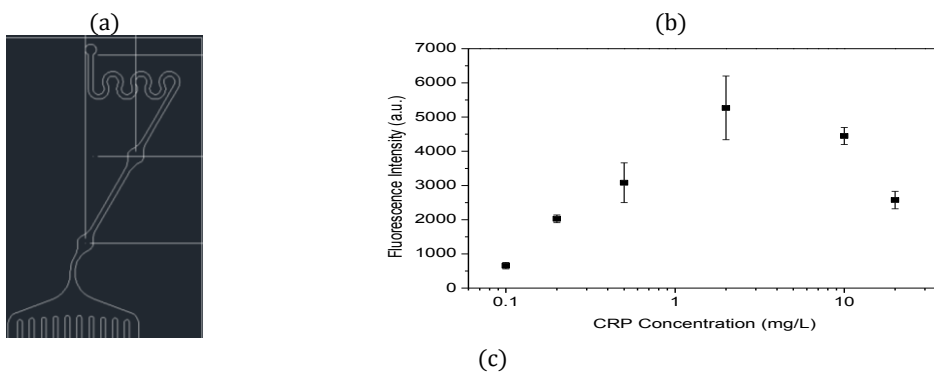


Figure 4.13 One-step sandwich assay, demonstrated on plate where the hook effect is also evident

4.7.3 Assay by Degas-Driven Flow – 1 Step Sandwich Assay

An assay performed under flow requires the protocols described previously in this section to be modified. The channel structures of the chip now hold and incubate the sample as it flows through. From Section 2.4, the chip comprises of the PDMS channels and a rigid substrate to seal the channels.



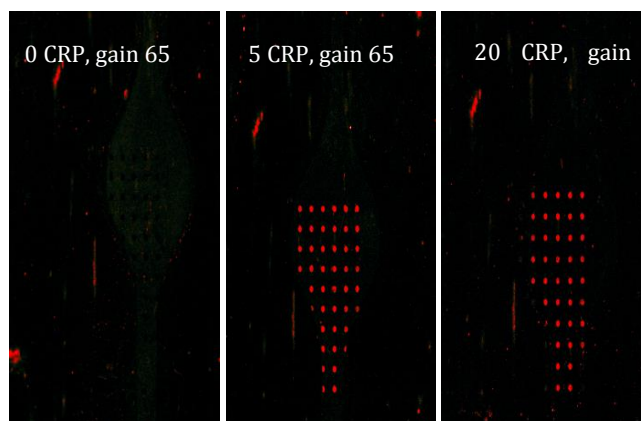


Figure 4.14 One-step sandwich FLISA, carried out under flow, incubation time ~10 mins. (a) Schematic of the degas flow chip with mixing meander and detection zones. (b) Resulting assay plot form experiment shown at (c), demonstrating a significant drop in signal at the higher CRP concentrations, or a hook effect

CRP was successfully detected under flow, but the hook effect reported in Figure 4.13 for the single step “static” ELISA, is again visible under “flow” conditions.

4.7.4 Possible Causes of Decreased Signal or “Hook Effect”

In the case of a standard FLISA protocol, the antigen and detection antibody are added to the 96 well plate separately, with a wash step in between. From Figure 4.15 (a), when the CRP is added to the assay it binds the capture antibody unimpeded. With increased concentrations of CRP, better coverage or a higher number of CRP can be expected. Therefore, the concentration of CRP determines the amount of bound detection antibody, resulting in increased signal with increased concentrations. At a point where there is total coverage, a saturation point is reached with no further increase in signal distinguishable.

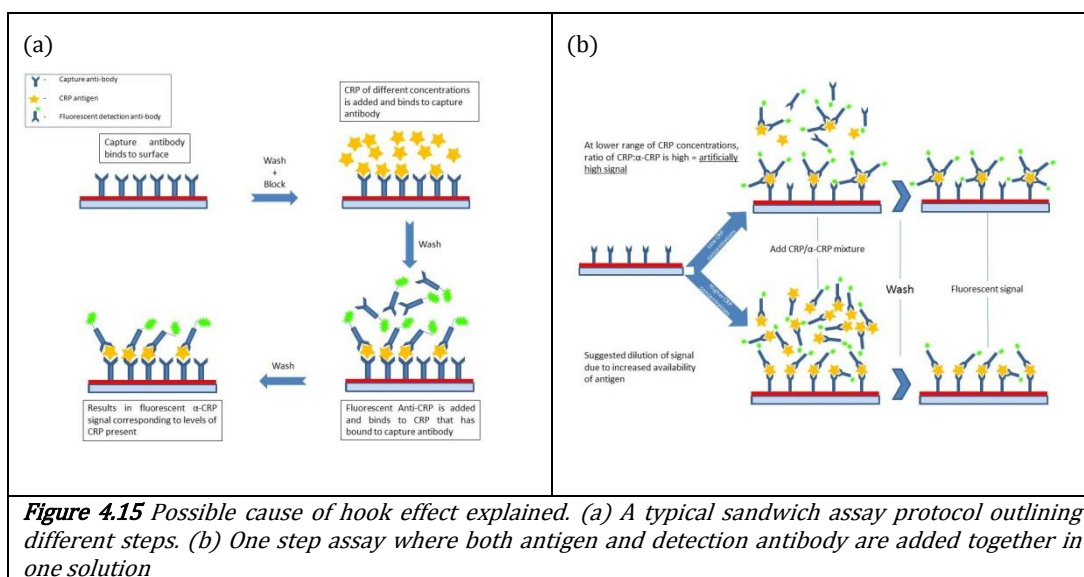


Figure 4.15 Possible cause of hook effect explained. (a) A typical sandwich assay protocol outlining different steps. (b) One step assay where both antigen and detection antibody are added together in one solution

In the case of the assay performed under flow, Figure 4.14 (b), the CRP/ α CRP solution is added as a single solution at the same time point. While in solution the CRP and α CRP can interact immediately.

At the lower concentration of CRP, the ratio of CRP: α CRP is high. With CRP's pentameric structure, multiple α CRP detection antibodies can bind the CRP antigen, thus restricting its ability to bind to the capture antibody on the surface. Even with a lower incidence of CRP binding, the signal is artificially increased as a result of numerous α CRP antibodies per CRP.

As the concentrations of CRP increase, the ratio of CRP: α CRP decreases, resulting in a reduction of the number of α CRP antibodies binding each CRP antigen. The result is a reduction in the overall signal irrespective of there being more CRP present.

To overcome or negate some of the potential loss of diffusion as a result of the flow conditions, the capture antibody concentration was increased from 5 μ g/mL to 200 μ g/mL. In doing so better coverage of the channel surface should be achieved thereby increasing the likelihood of binding the CRP as it flowed over the surface. In turn, the α CRP concentration was also increased, from 2.5 μ g/mL to 10 μ g/mL. This was the same concentration used in the single step plate assay. Due to costs associated with the fluorescent dye and detection antibodies, higher concentrations were not achievable within the projects budget. It is possible that if the α CRP detection antibody were increased the hook effect could be compensated for and negated.

4.7.5 Integrated 1 Step Microfluidic Assay

As stated previously the objective of the CLEAR concept is the implementation of a single step assay on-chip and under flow. Some preliminary experiments were carried to out investigate the feasibility of lyophilising, or drying, the detection antibody within the channel of the chip, whereby the detection antibody would then be re-suspended as the sample flowed over. The detection antibody would then bind to the CRP in solution, prior to encountering the capture antibody further along the microfluidic channel.

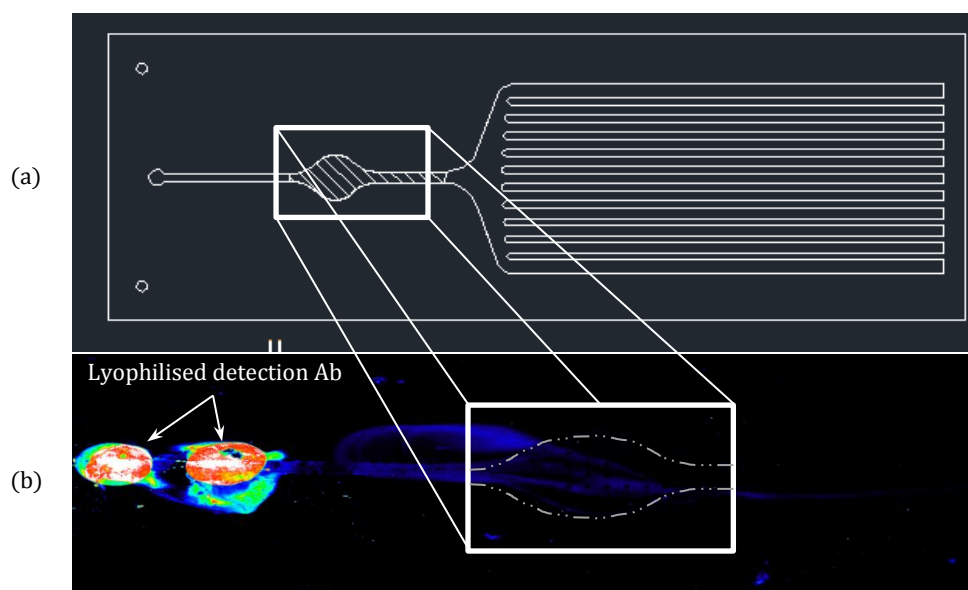


Figure 4.16 Initial test using a straight channel did not allow sufficient time for re-suspension of reagents. Image (b) shows the reagents lyophilised at the beginning of the channel with no signal detected at the detection antibody site, depicted in the hatched area in image (a)

Initial experiments with CRP spiked plasma, produced poor results. The straight channel did not provide sufficient time for re-suspension and diffusion at the assay site and limited binding occurred. See Figure 4.16. The lyophilised detection antibody can be seen on the left of the image 4.16 (b), with no binding occurring with the detection antibody at the location highlighted.

4.7.5.1 Re-suspension of Lyophilised Reagents

To aid re-suspension the channel was increased in length and a mixing region was added where the lyophilised labelled antibody was afforded time to re-suspend and diffuse in the plasma sample (Gervais & Delamarche 2009; Gervais et al. 2011). Once it reached the assay site, an increased signal was observed at the assay site. Comparing Figure 4.17 (b) with Figure 4.17 (b), a definite increase in signal is detected.

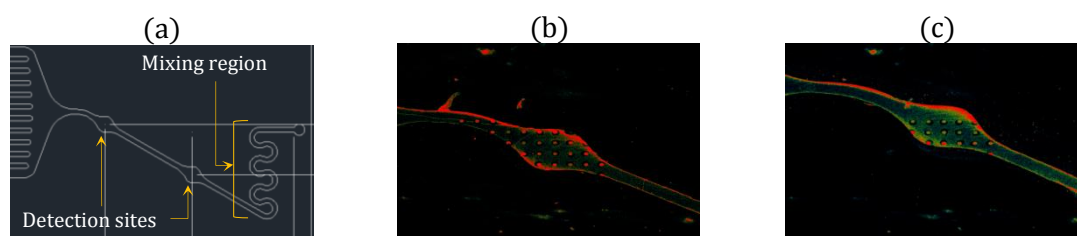


Figure 4.17 Schematic of the channel with increased channel length and mixing region (a)

Owing to the fact that the project reached its conclusion no further optimisation and experiments were performed. A single step CRP assay under flow was successfully demonstrated on chip and preliminary optimisation for resuspension of lyophilised detection antibody was performed. While the concept was demonstrated using CRP free

plasma spiked with CRP, it is proposed that a finger-prick of blood separated using the CLEAR platform would achieve the same result.

4.8 Discussion

Here we have demonstrated the successful transfer of a static FLISA CRP assay from a traditional 96 well plate format to a microfluidic chip with positive detection of CRP under flow conditions on-chip. In doing so we have reduced the time needed from several hours to a matter of minutes. Incubation is also performed in ~ 10 minutes and is carried out at room temperature.

The hook effect is problematic and reduces the effective range of the assay. However, by demonstrating its presence in the normal plate conditions points to the issue being one of a protocol adjustment as opposed to the difference of flow compared to the static assay. With further investigation of the ratio of CRP: α CRP, it is suggested that the hook effect could be compensated for and the range of the assay extended. By increasing the amount of α CRP, a more uniform coverage or binding to CRP is predicted across the different concentration points.

Also demonstrated is the potential for lyophilising α CRP within the channel. In doing so, the chip could be realised as a true point-of-care device. Only requiring the addition of the patients' finger-prick sample of whole blood, the resulting separated plasma now activates and re-suspends the lyophilised α CRP. Given sufficient time for re-suspension by increasing channel length and the mixing effect of a meandering channel, α CRP re-suspension was demonstrated.

4.9 Summary

It is hoped that the innovative design features of the CLEAR chip and the development work on the assay which has been reported in this chapter, demonstrates the potential of the concept for POC testing based on a pin-prick blood sample. It is unfortunate that time and project resource constraints have limited the progress that was achievable. Plans for future development of the concept are outlined in Chapter 5 of this thesis.

Chapter V

Conclusion and Future Work

Many results have been reported in this thesis with great potential. With the lifetime of the each project limiting the advancement of the respective technologies, much more work is needed to realise their full potential.

The DiCAST platform has the potential to revolutionise the antibody production market due to the possibility of extremely high throughput. Demonstrating the ability to screen possibly millions of cells, individually and in parallel was made possible by development of the alignment technique described in this work. However some issues remain with reproducibility and inter-user variability. With further development of a high precision array jig or robot, this variability could be addressed and removed.

The air jet concept of micro-capillary interrogation showed great promise as a proof of concept. It demonstrated a capability of evacuating individual micro-capillaries without disturbing the surrounding capillaries or their contents. Further characterisation of the fluid dynamics, of both the air-jet and the contents of the capillary when ejected, could determine the feasibility of further developing this approach to evacuate each capillary.

The air-jet nozzle, as reported here was fabricated in-house using a soft polymer. By redesigning and outsourcing the fabrication of the nozzle may also improve its performance. A highly toleranced, high precision focused glass nozzle could greatly improve performance.

Similarly, the liquid-jet demonstrated great promise as a proof of concept design. The ability to align nozzles either side of the array was possibly the greatest limiting factor with the device described here. The liquid-jet demonstrates a distinct advantage over the air-jet concept by the recovery of cells from the array which proved elusive for the air-jet. By using a similar medium to which the cells were suspended within, is suggested as a more favourable method of recovery. Any issues with evaporation are removed from the process and if the alignment issue can be rectified, the collection of the contents can be readily achieved.

Automation of the either the liquid or air-jet, is suggested as a logical next step to further remove any error by manual operation. With high precision control and adjustment of the jets coupled with a machine vision alignment system the concept could realise a much greater level of accuracy and control.

The CLEAR platform, as a point of care platform has the potential to be deployed into remote and low resource environments for the monitoring of some disease states such as

rheumatoid arthritis and early detection of others like cardio vascular disease. This body of work has demonstrated the effective removal of the large cellular components of a whole blood sample using a platform fabricated for a fraction of the cost of the equipment required in a laboratory setting. Removal of these components allows optical detection of biomarkers within the sample which can lead to early diagnosis and/or treatment of many common disease states. That the platform does not require any external power or actuation means it could be deployed in extremely low resource environments or simply at the point of care situation in a GP setting for instance.

To realise the potential of this application much work is required in terms of flow stability to ensure reproducible separation can be realised with each test. Characterisation of low pressure storage is required to investigate its effects on the device flow rate reproducibility.

At the outset, it was hoped this thesis would report the selection of a specific antibody using the DiCAST technology and subsequently detect and quantify its presence in a buffer with a known concentration, using the CLEAR device. It was envisaged that the combination of DiCAST and CLEAR could be demonstrated as a personalised medicine approach where the specific antigen response from a patient could be characterised using the DiCAST platform. This characterisation would then be used to tailor the chemistry placed upon the CLEAR platform, providing a highly specific and patient specific response. This concept is possibly a number of projects in their own right.

This body of work has successfully demonstrated many concepts to allow the development of potentially ground breaking disruptive technology. It is hoped that the work described here can be further developed as integral and necessary parts of the larger projects DiCAST and MobiMate.

Bibliography

- Acero, A.J. et al., 2012. Focusing liquid microjets with nozzles. *Journal of Micromechanics and Microengineering*, 22(6), p.65011. Available at: <http://stacks.iop.org/0960-1317/22/i=6/a=065011>.
- Adams, G.P. & Weiner, L.M., 2005. Monoclonal antibody therapy of cancer. *Nature biotechnology*, 23(9), pp.1147–57. Available at: <http://www.ncbi.nlm.nih.gov/pubmed/16151408> [Accessed March 10, 2013].
- Adhesives Research Inc, ArCare 92712.
- Barer, R. & Saunders-Singer, A., 1948. A new single-control micromanipulator. *Quarterly Journal of Microscopical* Available at: <http://jcs.biologists.org/content/s3-89/8/439.short> [Accessed December 8, 2015].
- Becker, H. & Gärtner, C., 2008. Polymer microfabrication technologies for microfluidic systems. *Analytical and Bioanalytical Chemistry*, 390(1), pp.89–111.
- Bernate, J.A. et al., 2013. Lab on a Chip. , (Vc), pp.1086–1092.
- Boder, E.T. & Wittrup, K.D., 1997. Yeast surface display for screening combinatorial polypeptide libraries. *Nature biotechnology*, 15(6), pp.553–7. Available at: <http://www.ncbi.nlm.nih.gov/pubmed/9181578> [Accessed May 6, 2015].
- Bradbury, A.R.M. et al., 2011. Beyond natural antibodies: the power of in vitro display technologies. *Nature biotechnology*, 29(3), pp.245–54. Available at: <http://www.pubmedcentral.nih.gov/articlerender.fcgi?artid=3057417&tool=pmcentrez&rendertype=abstract> [Accessed February 28, 2013].
- Burger, R. et al., 2015. An integrated centrifugo-opto-microfluidic platform for arraying, analysis, identification and manipulation of individual cells. *Lab on a Chip*. Available at: <http://pubs.rsc.org/en/content/articlehtml/2015/lc/c4lc01002g> [Accessed December 8, 2015].
- Burger, R. et al., 2012. Centrifugal microfluidics for cell analysis. *Current opinion in chemical biology*, 16(3-4), pp.409–14. Available at: <http://www.sciencedirect.com/science/article/pii/S1367593112000749> [Accessed November 26, 2015].
- Buss, N. a P.S. et al., 2012. Monoclonal antibody therapeutics: history and future. *Current opinion in pharmacology*, 12(5), pp.615–22. Available at:

- <http://www.ncbi.nlm.nih.gov/pubmed/22920732> [Accessed March 5, 2013].
- Carter, P., 2001. Improving the efficacy of antibody-based cancer therapies. *Nature reviews. Cancer*, 1(2), pp.118–29. Available at: <http://www.nature.com.dcu.idm.oclc.org/nrc/journal/v1/n2/full/nrc1101-118a.html> [Accessed October 26, 2015].
- Chang, B., Nave, G. & Jung, S., 2012. Drop formation from a wettable nozzle. *Communications in Nonlinear Science and Numerical Simulation*, 17(5), pp.2045–2051. Available at: <http://www.sciencedirect.com/science/article/pii/S1007570411004588> [Accessed October 4, 2015].
- Charoenphol, P. et al., 2012. Particle-cell dynamics in human blood flow: implications for vascular-targeted drug delivery. *Journal of biomechanics*, 45(16), pp.2822–8. Available at: <http://www.sciencedirect.com/science/article/pii/S0021929012005039> [Accessed April 20, 2015].
- Chiu, J.-J. & Chien, S., 2011. Effects of Disturbed Flow on Vascular Endothelium: Pathophysiological Basis and Clinical Perspectives. , pp.327–387.
- Conroy, P.J. et al., 2009. Antibody production, design and use for biosensor-based applications. *Seminars in cell & developmental biology*, 20(1), pp.10–26. Available at: <http://www.ncbi.nlm.nih.gov/pubmed/19429487> [Accessed February 27, 2013].
- Dimov, I.K. et al., 2011. Stand-alone self-powered integrated microfluidic blood analysis system (SIMBAS). *Lab on a chip*, 11(5), pp.845–50. Available at: <http://www.ncbi.nlm.nih.gov/pubmed/21152509> [Accessed November 2, 2012].
- Dow Corning, 2007. Product Information Sylgard ® 184 Silicone Elastomer. , p.3.
- Ehrlich, G., Berthold, W. & Bailon, P., 2000. Phage Display Technology. In P. Bailon et al., eds. *Affinity Chromatography SE - 18*. Methods in Molecular Biology. Humana Press, pp. 195–208.
- Fitzgerald, V. et al., 2015. Exploiting Highly Ordered Subnanoliter Volume Microcapillaries as Microtools for the Analysis of Antibody Producing Cells. , Mic.
- Frisk, T.W. et al., 2011. A silicon-glass microwell platform for high-resolution imaging and

- high-content screening with single cell resolution. *Biomedical microdevices*, 13(4), pp.683–93. Available at: <http://www.ncbi.nlm.nih.gov/pubmed/21465090> [Accessed November 16, 2012].
- Gai, S.A. & Wittrup, K.D., 2007. Yeast surface display for protein engineering and characterization. *Current opinion in structural biology*, 17(4), pp.467–73. Available at: <http://www.pubmedcentral.nih.gov/articlerender.fcgi?artid=4038029&tool=pmcentrez&rendertype=abstract> [Accessed November 9, 2015].
- George P. Smith, 1985. Filamentous Fusion Phage: Novel Expression Vectors that Display Cloned Antigens on the Virion Surface on JSTOR. *Science*, p.Vol. 228; pp. 1315–1317. Available at: http://www.jstor.org.dcu.idm.oclc.org/stable/1694587?seq=2#page_scan_tab_contents [Accessed November 24, 2015].
- Gervais, L. & Delamarche, E., 2009. Toward one-step point-of-care immunodiagnostics using capillary-driven microfluidics and PDMS substrates. *Lab on a chip*, 9(23), pp.3330–7. Available at: <http://www.ncbi.nlm.nih.gov/pubmed/19904397> [Accessed March 7, 2013].
- Gervais, L., Hitzbleck, M. & Delamarche, E., 2011. Capillary-driven multiparametric microfluidic chips for one-step immunoassays. *Biosensors and Bioelectronics*, 27(1), pp.64–70. Available at: <http://dx.doi.org/10.1016/j.bios.2011.06.016>.
- Godino, N. et al., 2012. Fabricating electrodes for amperometric detection in hybrid paper/polymer lab-on-a-chip devices. *Lab on a chip*, 12(18), pp.3281–4. Available at: <http://pubs.rsc.org/en/content/articlehtml/2012/lc/c2lc40223h> [Accessed December 12, 2015].
- Graphtec America Inc., Craft ROBO USER ' S MANUAL.
- Grünberger, A., Wiechert, W. & Kohlheyer, D., 2014. Single-cell microfluidics: opportunity for bioprocess development. *Current opinion in biotechnology*, 29, pp.15–23. Available at: <http://www.sciencedirect.com/science/article/pii/S0958166914000391> [Accessed November 23, 2015].
- Gubala, V. et al., 2012. Point of care diagnostics: status and future. *Analytical chemistry*,

- 84(2), pp.487–515. Available at: <http://www.ncbi.nlm.nih.gov/pubmed/22221172>.
- Haeberle, S. & Mark, D., 2012. Microfluidic platforms for lab-on-a-chip applications. *Microsystems and* Available at: http://link.springer.com/chapter/10.1007/978-3-642-18293-8_22 [Accessed December 12, 2015].
- Hall, C.L. & Calt, M., 2014. Computational Modeling of Thrombotic Microparticle Deposition in Nonparallel Flow Regimes. *Journal of Biomechanical Engineering*, 136(11), p.111002. Available at: <http://biomechanical.asmedigitalcollection.asme.org/article.aspx?doi=10.1115/1.4028134>.
- Hammers, C.M. & Stanley, J.R., 2014. Antibody phage display: technique and applications. *The Journal of investigative dermatology*, 134(2), p.e17. Available at: <http://dx.doi.org/10.1038/jid.2013.521> [Accessed July 15, 2014].
- Hansel, T.T. et al., 2010. The safety and side effects of monoclonal antibodies. *Nature reviews. Drug discovery*, 9(4), pp.325–38. Available at: <http://www.ncbi.nlm.nih.gov/pubmed/20305665> [Accessed March 2, 2013].
- Harrison, D.J. et al., 1992. Capillary electrophoresis and sample injection systems integrated on a planar glass chip. *Analytical Chemistry*, 64(17), pp.1926–1932. Available at: <http://dx.doi.org/10.1021/ac00041a030> [Accessed December 13, 2015].
- Hoogenboom, H.R. et al., 1998. Antibody phage display technology and its applications. *Immunotechnology*, 4(1), pp.1–20. Available at: <http://www.sciencedirect.com/science/article/pii/S1380293398000074> [Accessed November 5, 2015].
- Horlick, R.A. et al., 2013. Simultaneous Surface Display and Secretion of Proteins from Mammalian Cells Facilitate Efficient in Vitro Selection and Maturation of Antibodies. *The Journal of Biological Chemistry*, 288(27), pp.19861–19869.
- Hudson, P.J. & Souriau, C., 2003. Engineered antibodies. *Nature Medicine*, 9(1), pp.129–134. Available at: <http://www.nature.com.dcu.idm.oclc.org/nm/journal/v9/n1/full/nm0103-129.html> [Accessed October 15, 2015].

- Jönsson, C. et al., 2008. Silane-dextran chemistry on lateral flow polymer chips for immunoassays. *Lab on a chip*, 8(7), pp.1191–7. Available at: <http://pubs.rsc.org/en/content/articlehtml/2008/lc/b800297e> [Accessed December 12, 2015].
- Kersaudy-Kerhoas, M. et al., 2009. Hydrodynamic blood plasma separation in microfluidic channels. *Microfluidics and Nanofluidics*, 8(1), pp.105–114. Available at: <http://www.springerlink.com/index/10.1007/s10404-009-0450-5> [Accessed February 19, 2013].
- KÖHLER, G. & MILSTEIN, C., 1975. Continuous cultures of fused cells secreting antibody of predefined specificity. *Nature*, 256(5517), pp.495–497. Available at: <http://www.nature.com/nature/journal/v256/n5517/pdf/256495a0.pdf> [Accessed February 27, 2013].
- Kruif, J.D.E., Terstappent, L. & Boelt, E., 1995. Rapid selection of cell subpopulation-specific human monoclonal antibodies from a synthetic phage antibody library. , 92(April), pp.3938–3942.
- Lecault, V. et al., 2012. Microfluidic single cell analysis: from promise to practice. *Current opinion in chemical biology*, 16(3-4), pp.381–90. Available at: <http://www.sciencedirect.com/science/article/pii/S136759311200052X> [Accessed December 7, 2015].
- Lipman, N.S. et al., 2005. Monoclonal Versus Polyclonal Antibodies: Distinguishing Characteristics, Applications, and Information Resources. *ILAR Journal*, 46(3), pp.258–268. Available at: <http://ilarjournal.oxfordjournals.org/content/46/3/258.short> [Accessed October 26, 2015].
- Love, J.C. et al., 2006. A microengraving method for rapid selection of single cells producing antigen-specific antibodies. *Nature biotechnology*, 24(6), pp.703–7. Available at: <http://www.ncbi.nlm.nih.gov/pubmed/16699501> [Accessed February 28, 2013].
- Lu, Z.-J. et al., 2012. Frontier of therapeutic antibody discovery: The challenges and how to face them. *World journal of biological chemistry*, 3(12), pp.187–96. Available at: <http://www.pubmedcentral.nih.gov/articlerender.fcgi?artid=3531614&tool=pmcentrez&rendertype=abstract> [Accessed March 20, 2013].

- Mao, H. et al., 2010. Spatially addressed combinatorial protein libraries for recombinant antibody discovery and optimization. *Nature biotechnology*, 28(11), pp.1195–202. Available at: <http://www.nature.com.dcu.idm.oclc.org/nbt/journal/v28/n11/full/nbt.1694.html> [Accessed October 14, 2015].
- Martinez, A.W. et al., 2010. Diagnostics for the developing world: microfluidic paper-based analytical devices. *Analytical chemistry*, 82(1), pp.3–10. Available at: <http://dx.doi.org/10.1021/ac9013989> [Accessed June 6, 2015].
- Moffitt, J.R. et al., 2008. Recent Advances in Optical Tweezers. *Annual Review of Biochemistry*, 77(1), pp.205–228. Available at: <http://www.annualreviews.org/eprint/aq63mngayHAz5jqkstuN/full/10.1146/annurev.biochem.77.043007.090225> [Accessed October 5, 2015].
- Murphy, K., Travers, P. & Walport, M., 2008. *Janeway's Immunobiology*,
- Murphy, Kenneth; Janeway, Charles; Walport, Mark; Travers, P., 2012. *Janeway's Immunobiology (8th Ed.)*, New York: Garland Science.
- Sackmann, E.K., Fulton, A.L. & Beebe, D.J., 2014. The present and future role of microfluidics in biomedical research. *Nature*, 507(7491), pp.181–9. Available at: <http://dx.doi.org/10.1038/nature13118> [Accessed July 11, 2014].
- Sheehan, J. & Marasco, W.A., 2015. Phage and Yeast Display. *Microbiology spectrum*, 3(1), pp.AID-0028–2014. Available at: <http://www.asmscience.org/content/journal/microbiolspec/10.1128/microbiolspec.AID-0028-2014> [Accessed November 30, 2015].
- Shi, L., Pan, T. & Glowinski, R., 2012. Lateral migration and equilibrium shape and position of a single red blood cell in bounded Poiseuille flows. , 056308, pp.1–12.
- Sin, M.L. et al., 2011. System Integration - A Major Step toward Lab on a Chip. *Journal of biological engineering*, 5, p.6. Available at: <http://www.pubmedcentral.nih.gov/articlerender.fcgi?artid=3117764&tool=pmcentrez&rendertype=abstract> [Accessed November 7, 2015].
- Skilbeck, C. a. et al., 2004. Disturbed flow promotes deposition of leucocytes from flowing whole blood in a model of a damaged vessel wall. *British Journal of Haematology*,

126(3), pp.418–427.

Sun, M., Khan, Z.S. & Vanapalli, S. a, 2012. Blood plasma separation in a long two-phase plug flowing through disposable tubing. *Lab on a chip*, 12(24), pp.5225–30. Available at: <http://www.ncbi.nlm.nih.gov/pubmed/23114925> [Accessed November 20, 2012].

Tagawa, Y. et al., 2012. Highly Focused Supersonic Microjets. , 031002, pp.1–10.

Tansey, E.M. & Catterall, P.P., 1994. Monoclonal antibodies: a witness seminar in contemporary medical history. *Medical history*, 38(3), pp.322–7. Available at: <http://www.pubmedcentral.nih.gov/articlerender.fcgi?artid=1036884&tool=pmcentrez&rendertype=abstract> [Accessed September 10, 2015].

Wang, D. & Bodovitz, S., 2010. Single cell analysis: the new frontier in “omics”. *Trends in biotechnology*, 28(6), pp.281–90. Available at: <http://www.pubmedcentral.nih.gov/articlerender.fcgi?artid=2876223&tool=pmcentrez&rendertype=abstract> [Accessed December 2, 2015].

Weiner, L.M., Surana, R. & Wang, S., 2010. Monoclonal antibodies: versatile platforms for cancer immunotherapy. *Nature reviews. Immunology*, 10(5), pp.317–27. Available at: <http://www.pubmedcentral.nih.gov/articlerender.fcgi?artid=3508064&tool=pmcentrez&rendertype=abstract> [Accessed March 5, 2013].

Whitesides, G.M., 2006. The origins and the future of microfluidics. *Nature*, 442(7101), pp.368–73. Available at: <http://dx.doi.org/10.1038/nature05058> [Accessed July 10, 2014].

Wu, H. et al., 2003. Fabrication of complex three-dimensional microchannel systems in PDMS. *Journal of the American Chemical Society*, 125(2), pp.554–559.

Wu, W. & Lee, N.Y., 2013. Two-layer microdevice for parallel flow-through PCRs employing plastic syringes for semi-automated sample injection and a single heater for amplification: Toward process simplification and system miniaturization. *Sensors and Actuators B: Chemical*, 181, pp.756–765. Available at: <http://linkinghub.elsevier.com/retrieve/pii/S0925400513001883> [Accessed April 4, 2013].

Yager, P., Domingo, G.J. & Gerdes, J., 2008. Point-of-care diagnostics for global health.

- Annual review of biomedical engineering*, 10, pp.107–44. Available at: <http://www.annualreviews.org/doi/full/10.1146/annurev.bioeng.10.061807.160524> [Accessed December 8, 2015].
- Yin, H. & Marshall, D., 2012a. Microfluidics for single cell analysis. *Current opinion in biotechnology*, 23(1), pp.110–9. Available at: <http://www.sciencedirect.com/science/article/pii/S0958166911007130> [Accessed September 23, 2015].
- Yin, H. & Marshall, D., 2012b. Microfluidics for single cell analysis. *Current opinion in biotechnology*, 23(1), pp.110–9. Available at: <http://www.ncbi.nlm.nih.gov/pubmed/22133547> [Accessed October 26, 2012].
- Zeng, X., Shen, Z. & Mernaugh, R., 2012. Recombinant antibodies and their use in biosensors. *Analytical and bioanalytical chemistry*, 402(10), pp.3027–38. Available at: <http://www.ncbi.nlm.nih.gov/pubmed/22159424> [Accessed March 7, 2013].
- Zhang, M. et al., 2010. A simple method for fabricating multi-layer PDMS structures for 3D microfluidic chips. *Lab on a chip*, 10(9), pp.1199–1203.
- Zhang, Y. et al., 2015. Highly sensitive C-reactive protein (CRP) assay using metal-enhanced fluorescence (MEF). *Journal of Nanoparticle Research*, 17(7), p.326. Available at: <http://link.springer.com/10.1007/s11051-015-3128-9>.
- Zhu, Z. et al., 2012. Microfluidic single-cell cultivation chip with controllable immobilization and selective release of yeast cells. *Lab on a chip*, 12(5), pp.906–15. Available at: <http://www.ncbi.nlm.nih.gov/pubmed/22193373> [Accessed November 7, 2012].